Simplified Modelling of Pollutant Transport in Naturally-layered Aquifers

Amjad Ali

Institute of Natural & Mathematical Sciences

Massey University

A thesis submitted for the degree of

PhilosophiæDoctor (PhD)

2015 February

Abstract

Chemical species such as tracers or dissolved pollutants flow along with the slow-moving water as it makes its way through the complex porous structure of the aquifer; during this process they are dispersed in different directions. The rate of dispersion depends on the geometric characteristics of the porous structure and speed of the fluid.

Generally, groundwater systems have layered structures determined by different events in the geological processes that formed them. The layers in a system have different physical properties, and their thicknesses are not uniform. This naturally layered structure is used here to advantage by discretizing them into almost horizontal layers, where each may have different geometrical characteristics such as thickness permeability, dispersivitiy, porosity, etc. The system of advection-dispersion equations that model the fluid and species transport then have coefficients that depend mainly on depth, but with a layer composition that may change with horizontal distance.

The mean dynamic pressure (or mean hydraulic head) may be assumed constant vertically at each horizontal point if it is not in the vicinity of a well or where there is very small vertical flow. In the vicinity of recharge or pumping wells, the mean dynamic pressures or hydraulic heads for each sub-layer of the aquifer may be allowed to have different values for each different sub-layer. Steady-state fluid flow is considered in this thesis in both confined and phreatic (unconfined) aquifers.

This thesis work is dedicated to my father, Farman Ali, who has been a constant source of support and encouragement during the challenges of graduate school and life. I am truly thankful for having you in my life. This work is also dedicated to my mother, Ghulam Sughra, who has always loved me unconditionally and whose good examples have taught me to work hard for the things that I aspire to achieve.

Acknowledgements

First and foremost I offer my sincerest gratitude to my supervisors, Robert McKibbin and Winston L. Sweatman, who have supported me thoughout my thesis with their patience and knowledge whilst allowing me the room to work in my own way.

Next, I would like to thank Higher Education Commission of Pakistan for providing me with a doctoral scholarship, and Massey University for providing me the opportunity to work in a wonderful learning environment.

I am delighted to extend my gratitude to the people who have contributed their time and knowledge during my postgraduate study at Massey: Graeme Wake, Mick Roberts, Shaun Cooper and Carlo Laing. Special thanks to my fellow PhD students who have been with me during my PhD study.

I would also like to thank my Mum and Dad, Sughra and Farman, for the support they provided me through my entire life and in particular, my wife, Sumaira for supporting me throughout my studies at the University.

Contents

Nomenclature

$\bar{c}$	average concentration of pollutant in the fluid averaged over sub-layer thickness [kg m^{-3}]
$\mathbf{D}$	three-dimensional tensor coefficient of mechanical dispersion of a dissolved pollutant while it flows in the porous media [m^2 s^{-1}]
D	scalar coefficient of mechanical dispersion of a dissolved pollutant while it flows in the porous media [m^2 s^{-1}]
F	steady rate of fluid recharge in or pumping out of a sub-layer of the aquifer (F has dimensions of [m s^{-1}] when thickness varies in one horizontal direction and of [m^2 s^{-1}] when thickness varies in both horizontal directions)
f	mass flux function in a sub-layer of the aquifer or fluid recharge flux function in or pumping flux function out of a sub-layer of the aquifer (if f is used for mass flux of a chemical, it has dimensions of [kg m^{-3} s^{-1}] and if it is used for fluid flux it has dimensions of [s^{-1}])
g	gravitational acceleration [m s^{-2}]
H	hydraulic head [m]
$\bar{H}$	mean hydraulic head averaged over the sub-layer thickness [m]
h	thickness of the sub-layer or the aquifer [m]
$\mathbf{K}$	permeability tensor of the porous media [m^2]
K	isotropic permeability of the porous media [m^2]

$\bar{K}$ mean (weighted) isotropic permeability of the aquifer averaged over the aquifer thickness, i.e., $\bar{K} = (\sum h_i K_i)/h$ [m^2]

M steady mass flux of fluid in or out of a sub-layer of the aquifer [kg m^{-3} s^{-1}]

P dynamic pressure of the fluid [kg m^{-1} s^{-2}]

$\bar{P}$ mean dynamic pressure of the fluid averaged over the sub-layer thickness [kg m^{-1} s^{-2}]

p absolute pressure of the fluid [kg m^{-1} s^{-2}]

Q instantaneous flow of mass in a sub-layer of the aquifer (Q has dimensions of [kg m^{-2}] when thickness varies in one horizontal direction and of [kg m^{-1}] when thickness varies in both horizontal directions)

$\mathbf{q}$ total horizontal volume flux $\mathbf{q} = (q_x, q_y)$ through the whole aquifer [m^2 s^{-1}]

q steady mass or volume flux of fluid or a chemical in a sub-layer of the aquifer (if q is used for mass flux of a chemical, it has dimensions of [kg m^{-2} s^{-1}] when thickness varies in one horizontal direction and [kg m^{-1} s^{-1}] when thickness varies in both horizontal directions and if q is used for the fluid flux, it has dimensions of [m s^{-1}] when thickness varies in one horizontal direction and [m^2 s^{-1}] when thickness varies in both horizontal directions)

r the fluid flux normal to the layer interface from the lower sub-layer to the upper sub-layer [m s^{-1}]

$\mathbf{u}$ Darcy velocity vector of fluid $\mathbf{u} = (u, v, w)$ in the porous media [m s^{-1}]

$\bar{\mathbf{u}}$ average two-dimensional horizontal Darcy velocity vector of fluid $\bar{\mathbf{u}} = (\bar{u}, \bar{v})$ in the porous media averaged over sub-layer thickness [m s^{-1}]

z height above datum [m]

Greek Symbols

α dispersivity of the porous medium [m]

δ	Dirac delta function
κ	hydraulic conductivity [m s^{-1}]
μ	dynamic viscosity of the fluid [kg m^{-1} s^{-1}]
ρ	density of the fluid [kg m^{-3}]
τ	interlayer dispersive transfer coefficient [m s^{-1}]
Φ	the function Φ_i for the ith interface level between the sub-layers (starting from bottom) is defined by $\Phi_i(x, y, z) = z - z_i(x, y)$, where z_i is the interface level between the $i-1$th and the ith sub-layers [m]
ϕ	porosity of the porous media [-]
ψ	the two-dimensional stream function [m^3 s^{-1}]

Subscripts

atm	atmospheric
d	downstream
I	injection
L	longitudinal
P	pollutant
R	remediating agent
ret	retention
s	curve along phreatic surface
st	stream
T	transverse
t	top
tot	total
u	upstream
V	volume
W	withdrawal
x, y, z	principal directions of Cartesian coordinate system

1

Introduction

The study of groundwater flow and mass transport in porous media has become increasingly popular in recent times. This is because of growing concern about management of groundwater resources and making decisions about how to keep these resources free of hazardous chemicals. These chemicals get introduced into the groundwater systems by wastes from factories, excessive fertiliser applications, sea water intrusion, and other human activities. Authorities in the Canterbury region of New Zealand, have shown their concern over excessive nitrogen and phosphorous application as fertiliser which is making groundwater a health hazard [28, 31]. In a report, United Nations Environment Programme (UNEP) has summarised the types and sources of contaminants [1]. They have also pointed out the potential risks that these contaminants can cause for the global environment and human life.

This thesis deals with the mathematical modelling of fluid flow, pollutants transport and remediation of pollutants while they are being transported in confined[1] and phreatic[2] aquifers. An extensive amount of research has been done in this field, being one of the most burning issues across the globe for a long time (for example, [9, 11, 13]). Although there are various simulation software packages based on mathematical models that are used to simulate the single and multiphase fluid flow and transport in porous

[1] Confined aquifers are those which are bounded from above and below by an impermeable dirt/rock layer that prevents water from seeping into the aquifer from the ground surface located directly above. Instead, water seeps into confined aquifers from farther away where the impermeable layer does not exist.

[2] Phreatic or unconfined aquifers are those into which water seeps from the ground surface directly above the aquifer.

media (for example TOUGH [26], PoreFlow [27]), they require a huge amount of data input which is very expensive to gather and need a huge amount of computational time to do full-scale simulations.

This study focuses on development of simplified models without taking the risk of introducing large errors. Computational errors are introduced in the results, if the assumptions made in the development of each model are violated. Generally groundwater aquifers are composed of layered structures possibly due to historical events such as floods, lava flows, winds, and volcanic ash dispersal. A natural layered structure, probably formed by submarine sedimentation is shown in Figure 1.1. This study focuses on the assumption that the physical properties of aquifers are the same vertically in each layer but they may vary horizontally. Then, partial differential equations (PDE's) for vertically averaged fluid flow and contaminants transport may be written for each sub-layer of the aquifer. Thus a complete three-dimensional model can be reduced to a horizontal two-dimensional model for each sub-layer where these PDE's are for values at the vertical midpoints of each sub-layer. Though an extensive amount of work has been done in the field of modelling transport in porous media, the concept of natural layering discretization is new. Some work has already been published using this concept ([24], [25], [3], [2], [4], [6], and [5]).

Suppose a pollutant (or tracer) enters into a layer at a specific point of the aquifer. The concentration of this pollutant will be high at this point and at the time it enters the permeable matrix. Suppose there is a point in the layer where its thickness decreases; the flow speed of water should also increase here to conserve mass and momentum, and hence the concentration of the pollutant is not simply time-dependent.

When a tracer is injected from Well A into layer 2 of the aquifer shown in Figure 1.2, it dissolves in water and is carried with the underground water flow. As it moves farther from Well A, its concentration decreases depending on time and distance from Well A. But as the layer thickness changes, the speed of fluid may change. This will depend on the thickness of the surrounding layers. The concentration of the pollutant will vary laterally because of advection by the fluid, mechanical dispersion by the porous matrix, and layer transfer across the layer interfaces. All of these aspects will depend on the physical parameters of the matrix system i.e., layer thicknesses, porosities, permeabilities and dispersivities, as well as background pressure gradient, etc.

Figure 1.1: A photograph of limestone cliffs (near the 12 Apostles), situated along the Great Ocean Road, approximately 275 km west of Melbourne, Victoria on the coastline of the Southern Ocean. The layered structure of the limestone cliffs can be seen clearly.

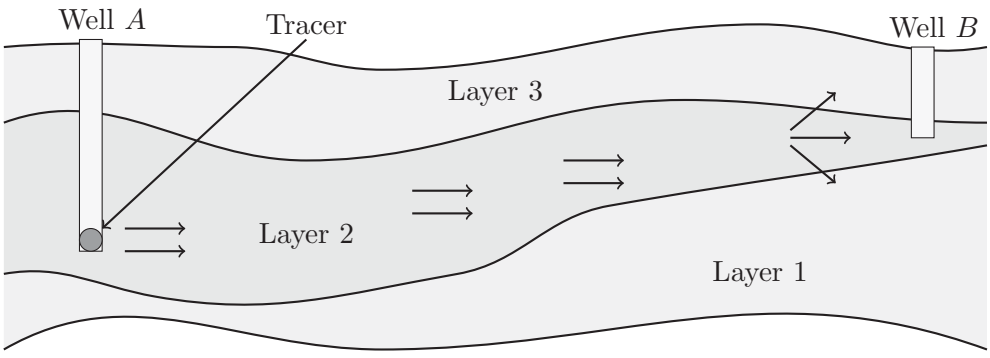

Figure 1.2: Schematic of layered structure of a typical aquifer.

This thesis is arranged into seven chapters with the current chapter being the introduction of the document.

In Chapter 2, some background of the study is discussed. Darcy's law, Dupuit

approximation and some other literature is reviewed. Dynamic viscosity[1] of groundwater changes with its temperature. A relationship between groundwater temperature and its dynamic viscosity is shown. Mechanical dispersion coefficient is discussed and its dependence on the fluid velocity and hydrodynamic dispersivity[2] is also explained. Permeability[3] of porous medium is also discussed.

Chapter 3 examines fluid flow models in confined aquifers. The confined aquifers which do not have significant vertical flow, either because of injection or withdrawal wells in one of the sub-layers or because of extreme slopes of sub-layer interfaces, are modelled first. It is proved, in this case, that vertical variations in the dynamic pressure are of the order of the square of the interlayer slopes. For the cases when the interlayer slope is extreme or if there is significant vertical flow because of recharge or pumping in one of the sub-layers, the dynamic pressure has large vertical variations. Therefore, dynamic pressure is assumed to have different values in each sub-layer.

Chapter 4 focuses on the fluid flow modelling in phreatic aquifers. Prediction of phreatic surface[4] with known boundary conditions is modelled in this chapter. The pressure at the phreatic surface is equal to atmospheric pressure and the slope of the phreatic surface indicates the direction of groundwater movement. It is convenient to use hydraulic head[5] instead of dynamic pressure in phreatic or unconfined aquifers. Again, for the cases where vertical flow in the phreatic aquifer is not significant, the variations in the value of hydraulic head are small and hence hydraulic head is assumed to have value equal to that of mean hydraulic head at each horizontal point. When there is vertical flow either because of extreme interlayer slopes or recharge or pumping in one of the sub-layers, the hydraulic head is assumed to have different values in each sub-layer of the unconfined aquifer.

In Chapter 5, tracer or pollutant transport is modelled for both the confined and unconfined aquifers. In addition to advection of the chemical along the slow varying sub-layer thicknesses, it disperses horizontally and into the neighbouring sub-layers. It advects along the fluid into the neighbouring sub-layers. A procedure is devised to deal

[1]The dynamic viscosity of a fluid is a measure of its resistance to shearing flows.

[2]Dispersivity is an empirical measure of porous medium which quantifies how much contaminants stray away from the main path of groundwater flow.

[3]Permeability is a measure of porous medium that how easy it is for fluids to pass through it.

[4]Phreatic surface is the location where pore water has pressure equal to atmospheric pressure.

[5]Hydraulic head or piezometric head is height of the water table above a geodetic datum.

with the cases where sub-layers appear or disappear. Analytic solutions are possible in some simple cases. Release of the tracer or pollutant into the aquifer can either be a point or distributed source. A comparison of model results to a data set is also presented in this chapter.

Chapter 6 presents models for the remediation of pollutants with a remediating agent. These models are for in situ chemical oxidation (ISCO) remediation strategy. The reaction between the pollutant and the remediating agent is assumed to be of second order. The scale of molecular diffusion is much smaller than that of mechanical dispersion. Since, both molecular diffusion and mechanical dispersion contribute in the dispersion coefficient, therefore, the values of dispersion coefficients for flow of both the chemicals in the porous material are almost the same. An example to devise a strategy for optimum remediation is also presented.

Chapter 7 is devoted to a summary and results of this thesis. Limitations of model and further research areas are also discussed.

Throughout this PhD research work, a three-dimensional Cartesian coordinate system XYZ is used where the positive z-axis is aligned vertically upwards as shown in Figure 1.3.

The thesis focuses on both transient and steady pollutant transport superimposed on steady fluid flow. The storage properties of the aquifers e.g., storativity[1], specific storage[2] are, therefore, not so important in this study. The porous structure is assumed to be non-deformable, so that, the physical properties like porosity and permeability are constant with time. Moreover, the contaminants are soluble and are not adsorbed in the permeable matrix to change its properties over the time. The scale of modelling is large, so that, the effects that are dominant on the smaller scale, e.g., wettability[3], capillary action[4], etc. are negligible.

[1]Storativity or the storage coefficient is the volume of water released from storage per unit decline in hydraulic head in the aquifer, per unit area of the aquifer.

[2]The mass (or volumetric) specific storage is the mass (or volume) of water that a portion of an aquifer releases from storage, per unit mass (or volume) of aquifer, per unit change in hydraulic head, while remaining fully saturated.

[3]Wettability is the ability of a solid surface to maintain contact with a liquid by reducing the surface tension of the liquid such that it spreads over the surface and wets it.

[4]Capillary action is the tendency of a liquid to rise in narrow tubes or to be drawn into small openings.

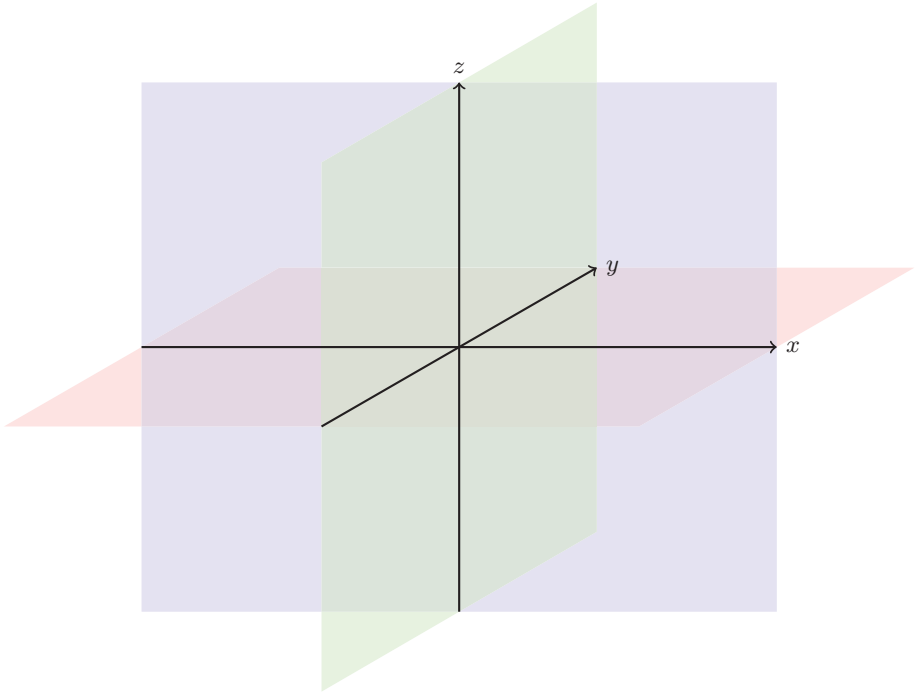

Figure 1.3: Cartesian coordinate system.

Some of the one-dimensional fluid flow and transport models are solved by direct integration in each sub-layer. Almost all of the two-dimensional and some of the one-dimensional models are solved numerically. Boundary value fluid flow problems are solved by iterative *relaxation methods* on *finite difference* discretizations of differential equations and are further compared to the solutions obtained by *finite element* methods. All the numerical solutions of transport problems are found by finite difference methods. The author has written his own codes for both the finite difference and the finite element methods and generated his own meshings for finite element methods.

2

Background

Groundwater aquifers are porous structures with highly heterogeneous physical properties. At microscopic level, the physical properties of aquifers are not continuous and the full detail of the solid boundaries of the microscopic pores (in which groundwater flows) is unknown and too complex to state. Hence, modelling mass flow is not possible at microscopic level. Modelling of fluid flow and mass transport can, however, be done by using a continuum approach at macroscopic level. In a continuum approach, a sample volume of porous structure is considered and geometrical properties of the porous media are averaged on that volume to get average properties of porous media representative to the centre of the sample volume. If the sample volume is different, the average values of physical characteristics of the porous media at the same centre point will be different. If the sample volume is smallest of the ones that yield, more or less, consistent geometrical characteristics of the porous media at their centre points, then this volume is called Representative Elementary Volume (REV). All the physical characteristics of the groundwater aquifers mentioned in this thesis are macroscopic and averaged over an REV.

Henry Darcy, in 1856, performed some experiments on fluid flow in the ground at the fountains of the city of Dijon, France [11, 12]. He investigated flow of water in porous media and presented his conclusions as the famous Darcy's law [16]. By Darcy's law, the specific discharge or the Darcy velocity[1] of an isothermal, single-phase fluid in a rigid porous structure is proportional to the negative of pressure gradient. In

[1]Darcy velocity is volume of water flowing per unit time through a unit cross-sectional area normal to the direction of flow

mathematical notation, it can be expressed in a three-dimensional Cartesian coordinate system (where the z-axis is aligned vertically upwards) as

$$\mathbf{u} = -\frac{1}{\mu}\mathbf{K} \cdot \nabla \left(p + \rho g z\right) = \frac{1}{\mu}\mathbf{K} \cdot \left(-\nabla P\right), \tag{2.1}$$

where $\mathbf{u}(x, y, z) = (u, v, w)$ is the Darcy velocity $\left[\text{m s}^{-1}\right]$ of the fluid, μ is the dynamic viscosity of the fluid $\left[\text{kg m}^{-1}\text{s}^{-1}\right]$, $\mathbf{K}$ is the permeability of the porous matrix $\left[\text{m}^2\right]$ and is, in general, a second order symmetric tensor, p is the absolute pressure $\left[\text{kg m}^{-1}\ \text{s}^{-2}\right]$, ρ is the fluid density $\left[\text{kg m}^{-3}\right]$ and g is the gravitational acceleration $\left[\text{m s}^{-2}\right]$. The dynamic pressure P can be expressed in terms of absolute pressure as

$$P(x, y, z) = p(x, y, z) - p_0 + \rho g z, \tag{2.2}$$

where p_0 is a datum pressure. If the permeability is assumed to be isotropic then Darcy's law takes the form

$$\mathbf{u} = \frac{K}{\mu}\left(-\nabla P\right). \tag{2.3}$$

Darcy's law is equivalent to a conservation of momentum equation and represents a balance between driving pressure gradient and viscous resistance when inertial effects are negligible. Conservation of mass is expressed by the equation

$$\frac{\partial}{\partial t}\left(\rho\phi\right) + \nabla \cdot \left(\rho\mathbf{u}\right) = 0, \tag{2.4}$$

where ϕ is the effective porosity[1] $[-]$ of the aquifer. If the fluid is isothermal and incompressible and the porous structure does not deform with time, then the conservation of mass equation becomes

$$\nabla \cdot \mathbf{u} = 0, \tag{2.5}$$

that is, the Darcy velocity $\mathbf{u}$ is a solenoidal or incompressible vector and can therefore be expressed as the curl of some other vector field.

Darcy's law laid the foundation for the study of fluid flows in underground porous structures. According to Darcy's law, the Darcy velocity of the fluid is proportional to the permeability of the porous matrix and the negative of the pressure gradient in the direction of the fluid flow, and inversely proportional to the dynamic viscosity of the fluid.

[1]Effective porosity is a measure of void interconnected spaces in a porous material that may be occupied by groundwater. It is the fraction of void interconnected volume to the total volume of porous material in an REV.

The permeability of the porous medium may be approximated by certain physical properties of the medium. Typical values of the permeability for various types of porous structures range from 10^{-7} [m^2] (well sorted gravel) to 10^{-21} [m^2] (breccia, granite) [11]. The dynamic viscosity of liquid water changes with temperature. Water at a temperature of 20 [°C] has a dynamic viscosity of 1.002×10^{-3} [Pa s]; its viscosity at temperatures from 0 [°C] to 150 [°C] is plotted in Figure 2.1 [21]. The total porosity[1] ϕ_{tot} is usually measured by calculating volume of solids after drying the sample from porous media at high temperatures and dividing this volume by the total volume of the sample. The effective porosity ϕ and the total porosity ϕ_{tot} are then related to each other as

$$\phi = \phi_{tot} - \phi_{ret}, \tag{2.6}$$

where ϕ_{ret} is the field capacity or the specific retention. The ϕ_{ret} is usually measured by calculating the ratio of the residual water contents in an REV after all the drainage due to gravity has stopped.

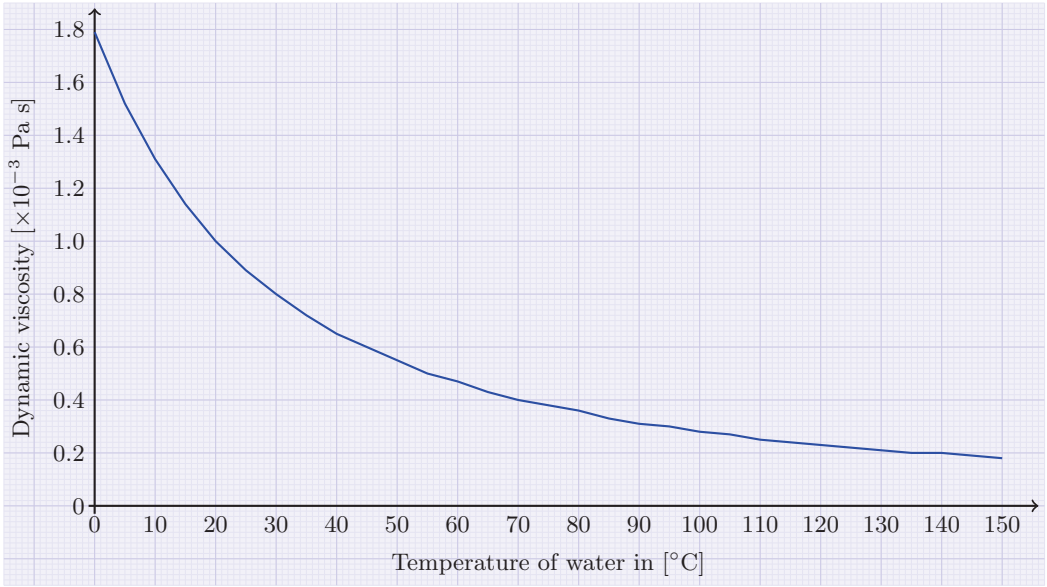

Figure 2.1: Dynamic viscosity of liquid water at various temperatures.

Thus, for a very high pressure gradient of 1 [Pa m^{-1}], the specific discharge of the water at 20 [°C] (with not much contaminant in it) in porous structures may vary from

[1] Total porosity is the ratio of pores volume to the total volume in an REV.

10^{-4} [m s^{-1}] (approx. 10 [m day^{-1}]) for a well sorted gravel to 10^{-18} [m s^{-1}] (approx. 10^{-12} [m day^{-1}]) for almost impervious granite. This means that movement (Darcy velocity) of the fluid in groundwater aquifers is usually very slow.

Groundwater aquifers are generally composed of different sedimentary layers which may have different physical properties (and hence permeabilities). Furthermore, these aquifers may be confined from the top or below, phreatic (unconfined) at the top, or leaky from the top or below. For modelling purposes, only two types of aquifers, the confined and the unconfined are considered; the leaky aquifers are just the ones with a semi-permeable sub-layer in the middle.

When modelling the fluid flow in a phreatic aquifer, one needs to predict the phreatic surface level that may be time-dependent or independent. In most groundwater flows, the slope of phreatic surfaces is in the range 0.001 to 0.01, which is very small [13]. The pressure at the phreatic surface is close to atmospheric.

If a curve s is imagined along the phreatic surface within a vertical two-dimensional xz-plane, the Darcy velocity $\mathbf{u}_s$ at each point of this curve is in a direction tangent to this curve and is given by

$$\mathbf{u}_s = -\frac{K\rho g}{\mu}\frac{\mathrm{d}z_t}{\mathrm{d}s}, \tag{2.7}$$

where z_t [m] is phreatic surface measured above a datum level and it also serves as the hydraulic head $H(x, y, z, t)$ [m] of the phreatic aquifer. The hydraulic head and the dynamic pressure $P(x, y, z, t)$ are related as

$$P = \rho g(H - z), \tag{2.8}$$

where z is the elevation at the piezometer bottom above the datum level. Dupuit [17] suggested that due to the small slope of the phreatic surface, the derivative $\mathrm{d}z_t/\mathrm{d}s$ may be replaced by $\mathrm{d}z_t/\mathrm{d}x$ for this xz-plane, that is, fluid flow is considered close to horizontal. This assumption works very well for most of the practical cases except where the slope of the phreatic surface is too high (i.e., especially in the vicinity of sources and sinks). Dupuit assumption can be used close to injection or withdrawal wells if the slope of water table there is small.

While modelling pollutant transport in aquifers, another important aspect to be taken into account is dispersion. Solutes disperse in all directions while passing through

the complex porous structures. By Fick's law, the mass flux due to dispersion is

$$\frac{\partial}{\partial x_i}\left(D_{ij}\frac{\partial c}{\partial x_j}\right), \tag{2.9}$$

where indices i, j represent coordinate axis directions, c represents the concentration of the solute and D_{ij} [$\mathrm{m}^2\ \mathrm{s}^{-1}$] represents the dispersion coefficient in the ij direction.

The dispersion coefficient can be shown to be a second rank tensor (see [24] and [25], for example). The coefficient of dispersion is the sum of the coefficient of mechanical dispersion and the coefficient of the molecular diffusion of the solute molecules in water [8]. The coefficient of molecular diffusion is a scalar and its magnitude is usually very small compared to the coefficient of mechanical dispersion. The effect of molecular diffusion only becomes significant when a tracer or pollutant is convected by fluid while passing through narrow fractures [19]. The dispersion is suggested to be proportional to the fluid velocity with coefficients α_L [m] in the longitudinal direction and α_T [m] in the direction transverse to the fluid velocity [13]. The coefficients α_L and α_T are also called longitudinal and transverse dispersivities of the porous structure. The entries of the symmetric tensor $\mathbf{D}$ are, therefore

$$D_{ij} = \alpha_T|v|\delta_{ij} + \frac{(\alpha_L - \alpha_T)v_i v_j}{|v|}, \tag{2.10}$$

where v_i and v_j are components of fluid velocity in directions i and j, respectively and $|v|$ is scalar magnitude of the velocity vector. Usually, α_L is much larger than α_T [30]. The coefficient of transverse dispersion α_T is mainly due to molecular diffusion caused by the concentration gradient of the pollutant between adjacent streamlines across the velocity vector. If the x-axis of the Cartesian coordinate system shown in Figure 1.3 is aligned with the direction of fluid flow, the off-diagonal entries of the symmetric tensor $\mathbf{D}$ are zero.

Simple fluid and transport models developed historically have been solved by transformation techniques and Green functions etc. The more complicated models have been solved by numerical techniques such as finite difference, finite element and finite volume methods.

The determination of dispersivity for large-scale heterogeneous aquifers is generally a challenge. The dispersivity in a large-scale groundwater system can be evaluated, for example, by geochemical method when the solutes are conservative or non-reactive and

non-sorptive [32]. The dispersivity at laboratory-scale experiments can fairly efficiently be determined for the conservative single or multi-component solute transport [14].

Short articles have already been published at different stages of the development of this model. The flow of fluid and transport of contaminants in confined and rigid aquifers where the thicknesses of the sub-layers are uniformly constant have been explored in [24]. There, the vertical flow of the isothermal and incompressible fluid is assumed to be very small and there are no sources or sinks to cause significant inter-layer vertical flow.

In the more general case when thicknesses of the sub-layers of the confined aquifers are varying, the fluid flow and the tracer or contaminant transport model is formulated in [25]. Fluid flowing in a layer may enter into neighbouring layers with a rate that depends on the difference of permeabilities and thicknesses of the two layers. Again, the vertical flow was assumed negligible.

The model was extended to include fluid flow and tracer transport in the phreatic aquifers in [3] and [2] by maintaining the assumption of no significant vertical flow. The difficulty of implementing numerical procedures when a sub-layer of the aquifer appears or disappears laterally (e.g. a lens) has been explored in [4]. It was found that by allowing the sub-layer with partial appearance to continue across the lateral extent of the aquifer with a very small thickness does not affect the total results. The remediation of hazardous contaminants in groundwater by introducing strong oxidizers into the aquifer was discussed in [6]. There, a simple model based on the natural layering of the aquifer was used to model the flow of the introduced remediation agent in the groundwater while the pollution degradation takes place.

In all these models, vertical flow was assumed to be very small. In cases where there are recharge wells or pumping wells, vertical or interlayer flow is not purely based on the difference in permeabilities and thicknesses of the sub-layers. The mean dynamic pressure may not then be assumed constant throughout the thickness of the aquifer. Illustrations from the previous models and the newer work when each sub-layer of the aquifer has a different mean dynamic pressure or hydraulic head from those above or below have been discussed in [5].

3

Fluid Flow Model for a Confined Aquifer

This chapter discusses mathematical modelling of steady fluid flows in three types of confined aquifers, each representing an extra level of difficulty from the previous one:

1. flow in a confined aquifer with no pumping or recharge well,
2. flow in a confined aquifer with a pumping or recharge well across the whole aquifer thickness, and
3. flow in a confined aquifer where a pumping or recharge well is in one of the sedimentary sub-layers.

The development process of mathematical models for each case are discussed in detail here.

3.1 Fluid flow in absence of wells

The Darcy velocity within an isotropic porous medium in a Cartesian coordinate system (x, y, z), where z is vertical, is given by the famous Darcy's law:

$$\mathbf{u}(x, y, z) = \frac{K}{\mu} \left(-\nabla p + \rho \mathbf{g}\right) = \frac{K}{\mu} \left(-\nabla P\right), \tag{3.1}$$

where K [m^2] is the permeability of the porous structure, μ [$\mathrm{kg\ m^{-1}\ s^{-1}}$] is the dynamic viscosity of the fluid, p [$\mathrm{kg\ m^{-1}\ s^{-2}}$] is the absolute pressure in the fluid, ρ [$\mathrm{kg\ m^{-3}}$] is

the fluid density, $\mathbf{g} = (0, 0, -g)$ [m s^{-2}] is the gravitational acceleration, and P is the fluid dynamic pressure given by $P(x, y, z) = p(x, y, z) - p_0 + \rho g z$, where p_0 is a datum pressure. From mass conservation, the Darcy velocity $\mathbf{u} = (u, v, w)$ of an incompressible and isothermal fluid in a rigid porous media is a solenoidal vector, i.e., $\nabla \cdot \mathbf{u} = 0$.

Suppose that the fluid is flowing in a confined aquifer composed of N sedimentary layers, which may have matrix properties that are different from each other. Within a layer the matrix properties are assumed to be similar at different heights although they may vary slowly in the horizontal directions. The thicknesses of the layers may also vary with horizontal position (x, y). The layer interface levels at horizontal position (x, y) are denoted by $z_0(x, y), z_1(x, y), z_2(x, y), \ldots, z_N(x, y)$, with $z_0(x, y)$ and $z_N(x, y)$ being the impervious bottom and top boundaries of the aquifer, respectively. Then the thickness of the ith layer is $h_i(x, y) = z_i(x, y) - z_{i-1}(x, y)$, $1 \leq i \leq N$.

If the component of the Darcy velocity in the x-direction at point (x, y, z) of the ith layer of the aquifer is denoted $u(x, y, z)$, then the averaged horizontal speed of the fluid in the x-direction in the ith layer is

$$\bar{u}_i(x, y) = \frac{1}{h_i(x, y)} \int_{z_{i-1}(x,y)}^{z_i(x,y)} u(x, y, z) dz,$$

at point (x, y) on the XY-plane.The total volume flux q_{x_i} per unit width of the ith layer in the x-direction is

$$q_{x_i} = h_i(x, y)\bar{u}_i(x, y) = \int_{z_{i-1}(x,y)}^{z_i(x,y)} u(x, y, z) dz. \tag{3.2}$$

Similarly, the total volume flux q_{y_i} in the y-direction through the ith layer can be written in terms of y-component v of the Darcy velocity. The horizontal (two-dimensional) total volume flux vector through the ith layer is then
$\mathbf{q}_i(x, y) = (q_{x_i}(x, y), q_{y_i}(x, y))$, and the total horizontal volume flux vector through the whole aquifer is

$$\mathbf{q}(x, y) = (q_x(x, y), q_y(x, y)) = \sum_{i=1}^{N} (q_{x_i}(x, y), q_{y_i}(x, y)) . \tag{3.3}$$

By applying the general form of the Leibniz integral rule and also continuity requirements of the fluid flux across the layer interfaces, it can be shown that

$$\nabla \cdot \mathbf{q} = \mathbf{u}_0 \cdot \nabla \Phi_0 - \mathbf{u}_N \cdot \nabla \Phi_N = 0. \tag{3.4}$$

Here, $\mathbf{u}_0$ and $\mathbf{u}_N$ are the fluid specific discharges at z_0 and z_N, respectively. The functions Φ_0 and Φ_N are defined by $\Phi_0(x,y,z) = z - z_0(x,y)$ and $\Phi_N(x,y,z) = z - z_N(x,y)$, respectively. Note that the bottom and top boundaries of the confined aquifer system at z_0 and z_N are assumed to be impervious. Therefore the fluid velocity $\mathbf{u}$ is parallel to these boundaries.

The (two-dimensional) divergence of the horizontal volume flux through the ith layer $\mathbf{q}_i = \langle q_{x_i}, q_{y_i} \rangle$ is

$$\nabla \cdot \mathbf{q}_i = \mathbf{u}_{i-1} \cdot \nabla \Phi_{i-1} - \mathbf{u}_i \cdot \nabla \Phi_i = r_{i-1}(x,y) - r_i(x,y); \qquad 1 \leq i \leq N. \tag{3.5}$$

Here, $r_i = \mathbf{u}_i \cdot \nabla \Phi_i$ is the component of the fluid flux normal to the layer interface from the ith layer to the $i+1$th layer. The normal interface fluxes $r_0(x,y)$ and $r_N(x,y)$ are zero, because the bottom and the top boundaries of the aquifer are impervious. The averaged dynamic pressure in the ith layer over the layer thickness $\bar{P}_i$ is defined by

$$h_i(x,y)\bar{P}_i(x,y) = \int_{z_{i-1}(x,y)}^{z_i(x,y)} P(x,y,z)dz.$$

Taking the partial derivative with respect to x and using Darcy's law for the x-component of the fluid specific discharge, it can be shown that

$$h_i \frac{\partial \bar{P}_i}{\partial x} = -\frac{\mu}{K_i} h_i \bar{u}_i + (P_i - \bar{P}_i)\frac{\partial z_i}{\partial x} - (P_{i-1} - \bar{P}_i)\frac{\partial z_{i-1}}{\partial x}, \tag{3.6}$$

where $P_i = P\left(x, y, z_i(x,y)\right)$ is the dynamic pressure at the layer interface. Similarly, in the y-direction

$$h_i \frac{\partial \bar{P}_i}{\partial y} = -\frac{\mu}{K_i} h_i \bar{v}_i + (P_i - \bar{P}_i)\frac{\partial z_i}{\partial y} - (P_{i-1} - \bar{P}_i)\frac{\partial z_{i-1}}{\partial y}. \tag{3.7}$$

The vertical component of the Darcy velocity in layer i averaged over the layer thickness is

$$\bar{w}_i = \frac{1}{h_i}\int_{z_{i-1}}^{z_i} w(x,y,z)dz.$$

Then the vertical volume flux through the ith layer of the aquifer is

$$q_{z_i} = h_i \bar{w}_i = \int_{z_{i-1}}^{z_i} w(x,y,z)dz = \int_{z_{i-1}}^{z_i} \frac{K_i}{\mu}\left(-\frac{\partial P}{\partial z}\right)dz = \frac{K_i}{\mu}\left(P_{i-1} - P_i\right). \tag{3.8}$$

Rearranging the mass conservation equation $\nabla \cdot \mathbf{u} = 0$, we have

$$\frac{\partial w}{\partial z} = -\left(\frac{\partial u}{\partial x} + \frac{\partial v}{\partial y}\right). \tag{3.9}$$

If horizontal variations in pressure in the ith layer are $O(\Delta P_i)$, then the horizontal components of fluid velocity in the ith layer (and mean horizontal fluid velocities $\bar{u}_i$, $\bar{v}_i$ in each layer) are of order $(K_i \Delta P_i)/(\mu L)$, where L is the order of the lateral extent of the aquifer. If the thickness of the ith layer of the aquifer is $O(H_i)$, then horizontal gradients of the ith layer interfaces are $O(\epsilon_i)$, where $\epsilon_i = H_i/L << 1$ and (3.9) shows that w_i (and $\bar{w}_i$) is $O\left(\left(\epsilon_i K_i \Delta P_i\right)/\left(\mu L\right)\right)$. Also, (3.8) shows that vertical variations in P in the ith layer are $O\left(\left(\mu H_i \epsilon_i K_i \Delta P_i\right)/\left(K_i \mu L\right)\right) = O\left(\epsilon_i^2 \Delta P_i\right)$. Thus, the latter two terms of both (3.6) and (3.7) are a factor $O\left(\epsilon_i^2\right)$ smaller than the corresponding first right-hand terms, and they may be neglected for small ϵ_i. The mean dynamic pressure over whole aquifer thickness is then $\bar{P} = \left(\sum_{i=1}^{N} h_i \bar{P}_i\right)/h$, where $h(x,y) = \sum_{i=1}^{N} h_i(x,y)$. Thus, the last two terms on the right hand side of (3.6) and (3.7) are $O\left(\epsilon_i^3 \Delta P_i\right)$. If ϵ_i is small, the last two terms of both (3.6) and (3.7) are smaller than the first terms on the right hand side of both equations by $O\left(\epsilon_i^2\right)$, and therefore, may be neglected. The mean dynamic pressure over the whole aquifer thickness is then $\bar{P} = \left(\sum_{i=1}^{N} h_i \bar{P}_i\right)/h$, where $h(x,y) = \sum_{i=1}^{N} h_i(x,y)$.

The continuity requirement for P at the layer interfaces implies that vertical variations in $\bar{P}_i$ are $O\left(\sum_{i=1}^{N} \epsilon_i^2 \Delta P_i\right)$. Thus, a variation of 10% in slopes of the layer interfaces, will introduce vertical variations of the order of 1% in the dynamic pressure in that layer. So, to a good approximation, $\bar{P}_i$ in (3.6) and (3.7) may be replaced with $\bar{P}$, and therefore

$$\frac{\partial \bar{P}}{\partial x} = -\frac{\mu}{K_i}\bar{u}_i, \qquad \frac{\partial \bar{P}}{\partial y} = -\frac{\mu}{K_i}\bar{v}_i. \tag{3.10}$$

The mean horizontal velocity $\bar{\mathbf{u}}_i = (\bar{u}_i, \bar{v}_i)$ in the ith sub-layer may then be written as

$$\bar{\mathbf{u}}_i = -\frac{K_i(x,y)}{\mu}\left(\frac{\partial \bar{P}}{\partial x}, \frac{\partial \bar{P}}{\partial y}\right). \tag{3.11}$$

Using (3.2) and (3.11) in (3.3), it is found that

$$\mathbf{q}(x,y) = -\frac{\sum_{i=1}^{N} h_i(x,y) K_i(x,y)}{\mu}\left(\frac{\partial \bar{P}}{\partial x}, \frac{\partial \bar{P}}{\partial y}\right). \tag{3.12}$$

Now, using (3.12) in (3.11) and the result in (3.2), the layer total volume fluxes can be written as

$$\mathbf{q}_i = \frac{h_i(x,y) K_i(x,y)}{\sum_{j=1}^{N} h_j(x,y) K_j(x,y)}\mathbf{q}. \tag{3.13}$$

If the horizontal components of the fluid velocity averaged over the whole aquifer system thickness in the x and y-directions are denoted by $\bar{u}(x,y)$ and $\bar{v}(x,y)$ respectively, then (3.4) gives

$$\frac{\partial}{\partial x}\left(h(x,y)\bar{u}(x,y)\right)+\frac{\partial}{\partial y}\left(h(x,y)\bar{v}(x,y)\right)=0, \tag{3.14}$$

where (3.14) suggests defining a stream function $\psi(x,y)$ [$\mathrm{m}^3\ \mathrm{s}^{-1}$] throughout the thickness of the aquifer by

$$h(x,y)\bar{u}(x,y)=\frac{\partial\psi}{\partial y}, \qquad h(x,y)\bar{v}(x,y)=-\frac{\partial\psi}{\partial x}. \tag{3.15}$$

Using the condition of irrotationality of the fluid, $\partial\bar{u}/\partial y-\partial\bar{v}/\partial x=0$, it can be shown that

$$\frac{\partial}{\partial x}\left(\frac{1}{h}\frac{\partial\psi}{\partial x}\right)+\frac{\partial}{\partial y}\left(\frac{1}{h}\frac{\partial\psi}{\partial y}\right)=0. \tag{3.16}$$

Also, using (3.12), (3.4) can be re-written as

$$\frac{\partial}{\partial x}\left(-\sum_{i=1}^{N}\left(h_iK_i\right)\frac{\partial\bar{P}}{\partial x}\right)+\frac{\partial}{\partial y}\left(-\sum_{i=1}^{N}\left(h_iK_i\right)\frac{\partial\bar{P}}{\partial y}\right)=0. \tag{3.17}$$

Defining vertically averaged permeability $\bar{K}$ throughout the aquifer at each planar point (x,y) as $\bar{K}(x,y)=\left(\sum_{i=1}^{N}h_iK_i\right)/h$, equation (3.17) becomes

$$\frac{\partial}{\partial x}\left(-h\bar{K}\frac{\partial\bar{P}}{\partial x}\right)+\frac{\partial}{\partial y}\left(-h\bar{K}\frac{\partial\bar{P}}{\partial y}\right)=0. \tag{3.18}$$

3.1.1 Illustration

For suitable boundary conditions, the mean dynamic pressure and the stream function can be found for an aquifer by solving (3.16) and (3.18) numerically (here, a finite-difference scheme is used). A simple example is used for illustration. A homogeneous aquifer lies in the rectangular region $0\le x\le 100$ [m], $0\le y\le 80$ [m], with the thickness profile $h(x,y)=1+0.5\cos\left(\pi x/25\right)\cos\left(\pi y/20\right)$ [m]. The boundary conditions are taken to be

$$\psi(x,0)=0,\quad \psi(x,80)=10,\quad \frac{\partial\psi(0,y)}{\partial x}=\frac{\partial\psi(100,y)}{\partial x}=0, \qquad \text{and}$$
$$\bar{P}(0,y)=20,\quad \bar{P}(100,y)=0,\quad \frac{\partial\bar{P}(x,0)}{\partial y}=\frac{\partial\bar{P}(x,80)}{\partial y}=0.$$

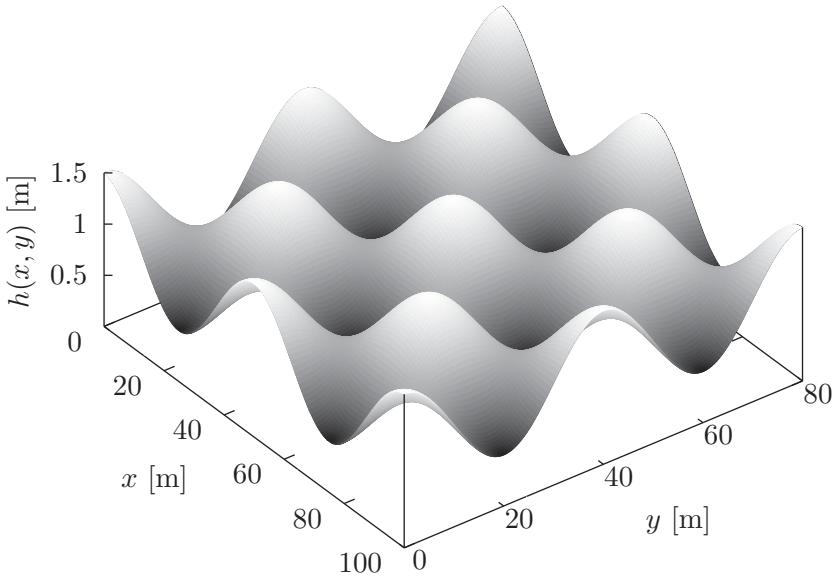

Figure 3.1: Thickness profile of the aquifer. Note that the bottom surface of the aquifer, here shown parallel to the XY-plane, need not be planar; this is just a special case of the thickness profile.

The stream function ψ and the dynamic pressure $\bar{P}$ are in SI units. The thickness profile is shown in Figure 3.1 and the isobars and streamlines are plotted in Figure 3.2. The streamlines (blue) are perpendicular to the isobars (red) depicting the fact that fluid flows in a direction opposite to the dynamic pressure gradient (in a direction where pressure drops the most) but not in a direction where the dynamic pressure is constant (isobar). One can note that the streamlines are spread apart in the narrower regions of the aquifer but the isobars are closer to each other, meaning that the fluid spreads while passing through such regions of smaller thickness and it speeds up there because of higher dynamic pressure gradient.

3.2 Flow in presence of recharge or pumping well across the aquifer thickness

Suppose the aquifer is being recharged steadily with rate M_I [kg m^{-3} s^{-1}] and the fluid is being pumped out of the aquifer with a constant rate M_W [kg m^{-3} s^{-1}], then

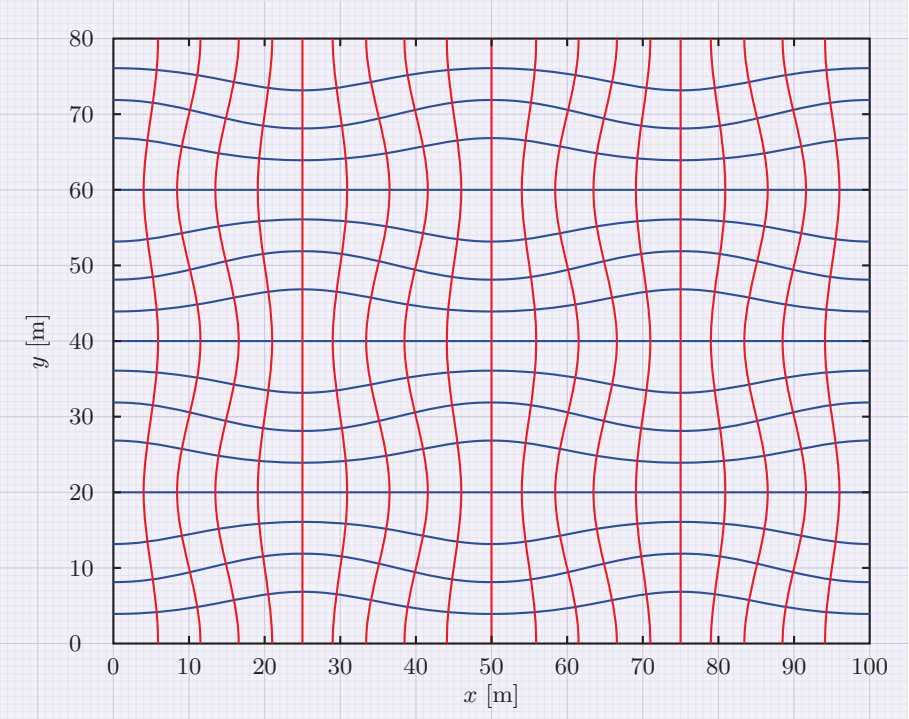

Figure 3.2: Streamlines (blue) and isobars (red). Note that streamlines and isobars are orthogonal wherever they intersect. The streamlines and isobars are contoured at equally spaced linear scale.

the conservation of mass equation for incompressible and isothermal fluid in a non-deformable porous media takes the form

$$\rho \nabla \cdot \mathbf{u} = M_I - M_W. \tag{3.19}$$

Mass fluxes M_I and M_W in (3.19) may be replaced with volume fluxes $f_I = M_I/\rho$ and $f_W = M_W/\rho$ $[(\mathrm{m}^3\ \mathrm{s}^{-1})\ \mathrm{m}^{-3} = \mathrm{s}^{-1}]$, respectively. Considering the divergence of total volume flux $\mathbf{q}(x, y)$ per unit width of the aquifer and using similar assumptions as in the section 3.1, it turns out that

$$\nabla \cdot \mathbf{q}(x, y) = (f_I(x, y) - f_W(x, y))\, h(x, y). \tag{3.20}$$

Then, using (3.12) it is simple to show that

$$\frac{\partial}{\partial x}\left(-h\bar{K}\frac{\partial \bar{P}}{\partial x}\right) + \frac{\partial}{\partial y}\left(-h\bar{K}\frac{\partial \bar{P}}{\partial y}\right) = \mu h\,(f_I - f_W)\,. \tag{3.21}$$

3.2.1 Illustration: analytic solution of a very special case

Consider a homogeneous aquifer with permeability K, with thickness h varying in only one horizontal direction x and with a steady source at $x = x_0$ of strength F_I [$(\mathrm{m}^3\ \mathrm{s}^{-1})\ \mathrm{m}^{-2} = \mathrm{m\ s}^{-1}$]. The dynamic viscosity μ of the fluid stays constant over time and space.

The governing differential equation for $\bar{P}(x)$ in this case can be written as

$$\frac{d}{dx}\left(-h\frac{d\bar{P}}{dx}\right) = \frac{\mu h}{K}F_I\delta(x - x_0). \tag{3.22}$$

This linear DE can easily be solved analytically and its solution is a piecewise function with a discontinuity in the derivative of $hd\bar{P}/dx$ at $x = x_0$. If x_u and x_d are the upstream and the downstream boundaries, respectively, than the solution is

$$\bar{P}(x) = \begin{cases} \bar{P}_u - \dfrac{\bar{P}_u - \bar{P}_d - \frac{\mu h_0 F_I}{K}\int_{x_0}^{x_d}\frac{d\xi}{h(\xi)}}{\int_{x_u}^{x_d}\frac{d\xi}{h(\xi)}}\int_{x_u}^{x}\frac{d\xi}{h(\xi)} & \text{for } \ x < x_0 \\ \bar{P}_u - \frac{\mu h_0 F_I}{K}\int_{x_0}^{x}\frac{d\xi}{h(\xi)} - \dfrac{\bar{P}_u - \bar{P}_d - \frac{\mu h_0 F_I}{K}\int_{x_0}^{x_d}\frac{d\xi}{h(\xi)}}{\int_{x_u}^{x_d}\frac{d\xi}{h(\xi)}}\int_{x_u}^{x}\frac{d\xi}{h(\xi)} & \text{for } \ x \geq x_0 \end{cases} \tag{3.23}$$

In the case of an aquifer with constant thickness, $\bar{P}(x)$ becomes a piecewise linear function with a discontinuity in its derivative at x_0. Consider a homogeneous aquifer, with varying thickness $h(x) = 2 + \cos(\pi x/2.5)$ [m]. If mean dynamic pressures at upstream and downstream are $P_u = 20$ and $P_d = 0$ [Pa], respectively and if the aquifer is being recharged with $F_I = 0.0864$ [$(\mathrm{m}^3\ \mathrm{day}^{-1})\ \mathrm{m}^{-2} = \mathrm{m\ day}^{-1}$] at $x = x_0$, then the pressure distribution along the length of the aquifer is as shown in Figure 3.3.

The permeability of the homogeneous aquifer is $K = 10^{-9}$ [m^2] and the dynamic viscosity of the fluid is taken as $\mu = 1.002 \times 10^{-3}$ [$\mathrm{kg\ m}^{-1}\ \mathrm{s}^{-1}$]. The total volume flux q_x per unit width of the aquifer in this case is constant before and after the location of the recharge well. The fluid flux entering the aquifer from the left upstream end as computed by the use of (3.12) is 0.0263 [$\mathrm{m}^2\ \mathrm{day}^{-1}$] and that leaving the aquifer at downstream end is 0.2855 [$\mathrm{m}^2\ \mathrm{day}^{-1}$]. There is a jump in the total volume flux in the aquifer at $x = x_0$ equal to $F_I h(x_0) = 0.0864 \times 3$ [$\mathrm{m}^2\ \mathrm{day}^{-1}$]. Again, note that the bottom surface of the aquifer as shown in the Figure 3.3 need not be planar. It is the thickness in confined aquifers that determines the dynamic pressure and not the top and the bottom boundary levels, provided that the slopes are not too high.

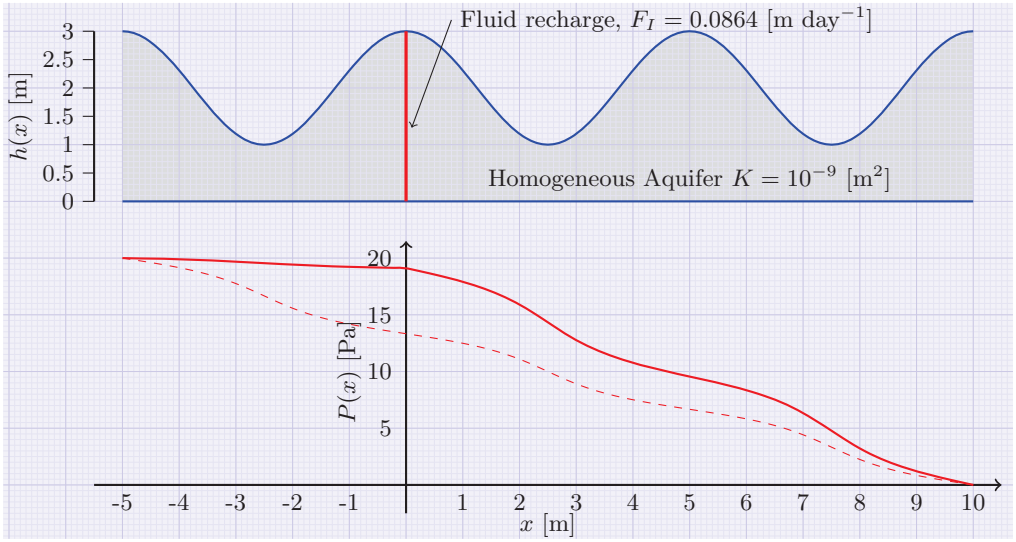

Figure 3.3: Homogeneous aquifer with thickness profile $h(x) = 2+\cos(\pi x/2.5)$ (top) with a recharge well at $x = x_0$ and dynamic pressure distribution in the aquifer (bottom). The dynamic pressure in absence of the recharge well is shown by the dashed curve.

3.2.2 Illustration: a two-dimensional single-layered (homogeneous) aquifer with a recharge well

Consider the homogeneous aquifer shown in the Figure 3.1 with a recharge well of strength F_I [(m^3 s^{-1}) m^{-1} = m^2 s^{-1}] at $(x_0, y_0) = (40, 50)$. The PDE (3.21) for the dynamic pressure in this case becomes

$$\frac{\partial}{\partial x}\left(-h\frac{\partial \bar{P}}{\partial x}\right) + \frac{\partial}{\partial y}\left(-h\frac{\partial \bar{P}}{\partial y}\right) = \frac{\mu h F_I}{K}\delta(x - x_0)\delta(y - y_0). \tag{3.24}$$

A numerical solution for the dynamic pressure is plotted as red contours (isobars) in Figure 3.4. It can be seen in the Figure that mean dynamic pressure $\bar{P}$ at the point of steady fluid injection $(x_0, y_0) = (40, 50)$ is higher than the neighbourhood area. Also, the smaller spacing in the isobars on the right hand side of point of fluid recharge, represent a higher dynamic pressure gradient and hence fluid speed is higher on the downstream side of the injection or recharge well as compared to the upstream side.

For this illustration, the physical properties of the aquifer and the fluid are taken as shown in Table 3.1. The boundary conditions for the mean dynamic pressure $\bar{P}(x, y)$ are the same as in Section 3.1.1.

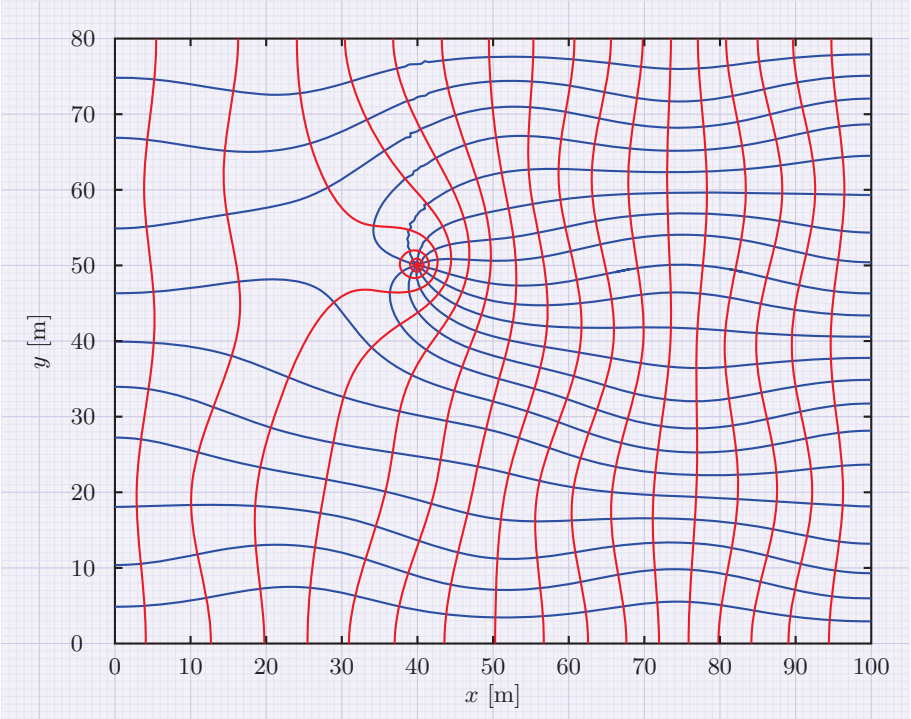

Figure 3.4: Streamlines (blue) and isobars (red) are orthogonal to each other wherever they intersect. Some streamlines originate from the recharge well.

Parameters	Values	units
permeability K	10^{-7}	$[\mathrm{m}^2]$
dynamic viscosity μ	1.002×10^{-3}	$[\mathrm{kg\ m^{-1}\ s^{-1}}]$
fluid injection rate F_I	86.4	$[(\mathrm{m^3\ day^{-1}})\ \mathrm{m^{-1}} = \mathrm{m^2\ day^{-1}}]$

Table 3.1: Parameters used in the simulation shown in Figure 3.4.

The streamlines can be computed indirectly from the dynamic pressure solution. Total volume flux per unit width of the aquifer in the x-direction can be computed by (3.12) and then the stream function can be computed by the integration of q_x from (say) $y = 0$ line to $y = 80$. The stream function has a discontinuity around the source equal to $F_I \times h(x_0, y_0) = 86.4 \times 1\ [\mathrm{m^3\ day^{-1}}]$. In this case, this discontinuity is in y-direction after the source. The numerical errors while removing this discontinuity have caused small wiggles along that line (see Figure 3.4). The streamlines are plotted as blue in Figure 3.4 after removing the discontinuity. Some of the streamlines are emerging from the recharge well showing that the fluid is being added from the recharge well into the

aquifer. The background flowing fluid seems to be pushed apart by the injected fluid.

3.2.3 Illustration: both recharge and pumping wells in two-dimensional aquifer

Consider the same homogeneous aquifer of Figure 3.1 with a recharge well of injection rate F_I [(m^3 s^{-1}) m^{-1} = m^2 s^{-1}] at (x_1, y_1) and a pumping well of withdrawal rate F_W [(m^3 s^{-1}) m^{-1} = m^2 s^{-1}] at (x_2, y_2). The governing equation for mean dynamic pressure $\bar{P}(x, y)$, in this case, becomes

$$\frac{\partial}{\partial x}\left(-h\frac{\partial \bar{P}}{\partial x}\right) + \frac{\partial}{\partial y}\left(-h\frac{\partial \bar{P}}{\partial y}\right) = \frac{\mu h}{K}\left[F_I\delta(x-x_1)\delta(y-y_1) - F_W\delta(x-x_2)\delta(y-y_2)\right]. \tag{3.25}$$

A numerical solution for the mean dynamic pressure in this aquifer when $(x_1, y_1) = (40, 50)$ and $(x_2, y_2) = (80, 30)$, is shown in Figure 3.5 as red contours (isobars). The boundary conditions on $\bar{P}(x, y)$ are the same as in Section 3.1.1, the withdrawal rate F_W is 83.4 [(m^3 day^{-1}) m^{-1} = m^2 day^{-1}], and rest of the parameters are as shown in Table 3.1. There is a high dynamic pressure at (x_1, y_1) induced by the injection of water and a low dynamic pressure at (x_2, y_2) because of withdrawal of water. The isobars have disturbed from the ones observed in the aquifer with no source or sink, shown in Figure 3.2. One can observe that the spacing in isobars in the region lying between the recharge and pumping wells is smaller than that in other regions. This is the region of steeper mean dynamic pressure and, therefore, higher groundwater velocity. Moreover, the spacing between the adjacent isobars on the left hand side of the recharge well at (x_1, y_1) and on the right hand side of the pumping well at (x_2, y_2) is larger than that in the rest of the aquifer. These are, therefore, regions of smaller fluid velocities.

Again, stream function $\psi(x, y)$ is computed numerically by integrating q_x from $y = 0$ to $y = 80$ (or q_y from $x = 0$ to $x = 100$). This time the stream function has two discontinuities; one around the recharge well equal to $F_I \times h(x_1, y_1) = 86.4$ [m^3 day^{-1}] and the other around the pumping well equal to $-F_W \times h(x_2, y_2) = -86.4$ [m^3 day^{-1}]. The streamlines have been plotted in blue in Figure 3.5 after removing those discontinuities. Some of the streamlines originate from the recharge well and some terminate at the pumping well depicting fluid injection and withdrawal from the recharge and the pumping wells, respectively.

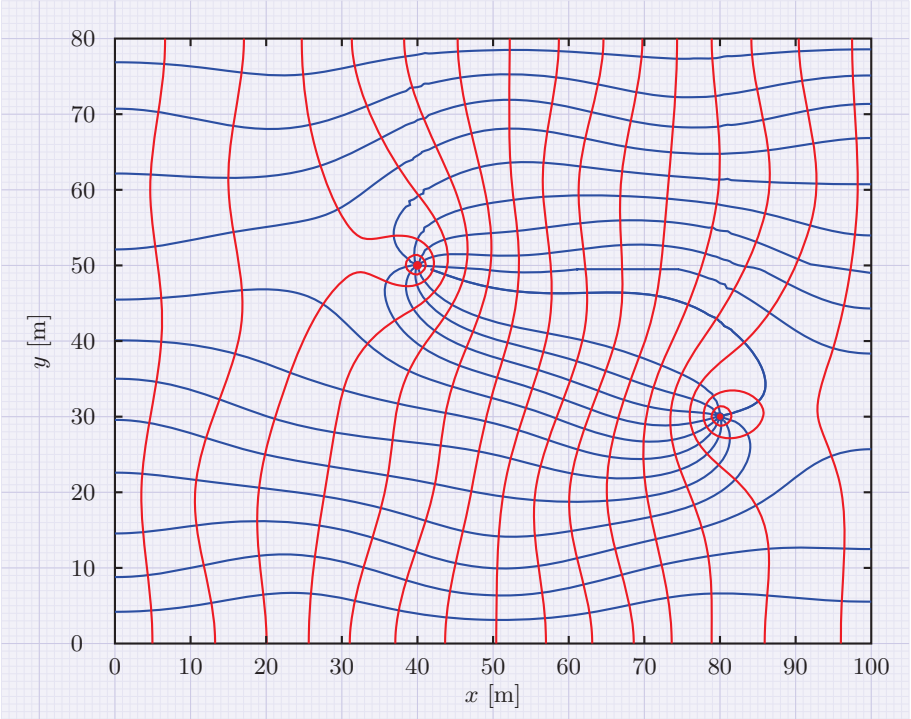

Figure 3.5: Streamlines (blue) and isobars (red) are orthogonal to each other wherever they intersect. Some streamlines originate from the discharge well and some terminate on the pumping well.

3.3 Flow in a layered aquifer with a point source

A non-homogeneous aquifer can be discretized vertically in sedimentary layers with different physical properties, i.e., porosities and permeabilities that do not vary vertically within a layer. Now, a fluid source can be assumed to be distributed vertically over the thickness of the sub-layer in which that source lies. Divergence of the total fluid flux through the thickness of the nth sub-layer in which fluid is being recharged with rate f_I, from (3.5), for this case results in

$$\nabla \cdot (q_{x_n}, q_{y_n}) = r_{n-1} - r_n + f_I h_n \tag{3.26}$$

The dynamic pressure that causes background flow is the same all through the thickness of the aquifer within a reasonable tolerance. In the case of a source in one particular layer, the dynamic pressure in that layer should increase to cause vertical flow to adjacent layers in addition to horizontal flow. Recalling the definition of directed

flux r_i from the ith layer to the $i+1$th layer normal to the layer interface, it is possible to replace it with the vertical flux across the layer interface, if the slope of the layer interface is small. Thus, in this case, horizontal total fluid fluxes through the thickness of the ith sub-layer in the left hand side of (3.26) can be written by Darcy's law in terms of dynamic pressure in the sub-layer. Suppose a nominal dynamic pressure P_0 at the layer interface between sub-layers i and $i+1$. Then, the Darcy velocity, r_i from the ith sub-layer to the $i+1$th sub-layer is approximated by

$$r_i = -\frac{K_i}{\mu}\frac{P_0 - P_i}{h_i/2}. \tag{3.27}$$

Similarly,

$$r_i = -\frac{K_{i+1}}{\mu}\frac{P_{i+1} - P_0}{h_{i+1}/2}, \tag{3.28}$$

now, comparing both (3.27) and (3.28), the value of P_0 can be found. Inserting P_0 in (3.27), the vertical flux r_i can be written as

$$r_i = \frac{2K_iK_{i+1}\left(P_i - P_{i+1}\right)}{\mu\left(h_{i+1}K_i + h_iK_{i+1}\right)}, \tag{3.29}$$

where, $r_0 = r_N = 0$. Now, (3.26) can be rewritten as

$$\begin{aligned}\frac{\partial}{\partial x}\left(-\frac{h_nK_n}{\mu}\frac{\partial P_n}{\partial x}\right) + \frac{\partial}{\partial y}\left(-\frac{h_nK_n}{\mu}\frac{\partial P_n}{\partial y}\right) &= \frac{2K_{n-1}K_n\left(P_{n-1} - P_n\right)}{\mu\left(h_nK_{n-1} + h_{n-1}K_n\right)} \\ &\quad -\frac{2K_nK_{n+1}\left(P_n - P_{n+1}\right)}{\mu\left(h_{n+1}K_n + h_nK_{n+1}\right)} \\ &\quad +f_Ih_n. \end{aligned} \tag{3.30}$$

In the case of constant permeabilies in each sub-layer, (3.30) reduces to

$$\begin{aligned}\frac{\partial}{\partial x}\left(-h_n\frac{\partial P_n}{\partial x}\right) + \frac{\partial}{\partial y}\left(-h_n\frac{\partial P_n}{\partial y}\right) &= \frac{2K_{n-1}\left(P_{n-1} - P_n\right)}{h_nK_{n-1} + h_{n-1}K_n} - \frac{2K_{n+1}\left(P_n - P_{n+1}\right)}{h_{n+1}K_n + h_nK_{n+1}} \\ &\quad +\frac{\mu}{K_n}f_Ih_n. \end{aligned} \tag{3.31}$$

Such an equation can be written for each of the sub-layers, but of course without the last fluid recharge term. The resultant set of N coupled equations, when fluid is being recharged only in the nth sub-layer, in a confined aquifer comprised of N sub-layers,

are

$$\begin{aligned}
\frac{\partial}{\partial x}\left(-h_1\frac{\partial P_1}{\partial x}\right)+\frac{\partial}{\partial y}\left(-h_1\frac{\partial P_1}{\partial y}\right) &= -\frac{2K_2\,(P_1-P_2)}{h_2K_1+h_1K_2} \\
\frac{\partial}{\partial x}\left(-h_i\frac{\partial P_i}{\partial x}\right)+\frac{\partial}{\partial y}\left(-h_i\frac{\partial P_i}{\partial y}\right) &= \frac{2K_{i-1}\,(P_{i-1}-P_i)}{h_iK_{i-1}+h_{i-1}K_i} \\
&\quad -\frac{2K_{i+1}\,(P_i-P_{i+1})}{h_{i+1}K_i+h_iK_{i+1}} \quad \text{for } \; 1<i<n \\
\frac{\partial}{\partial x}\left(-h_n\frac{\partial P_n}{\partial x}\right)+\frac{\partial}{\partial y}\left(-h_n\frac{\partial P_n}{\partial y}\right) &= \frac{2K_{n-1}\,(P_{n-1}-P_n)}{h_nK_{n-1}+h_{n-1}K_n} \\
&\quad -\frac{2K_{n+1}\,(P_n-P_{n+1})}{h_{n+1}K_n+h_nK_{n+1}}+\frac{\mu}{K_n}f_Ih_n \\
\frac{\partial}{\partial x}\left(-h_i\frac{\partial P_i}{\partial x}\right)+\frac{\partial}{\partial y}\left(-h_i\frac{\partial P_i}{\partial y}\right) &= \frac{2K_{i-1}\,(P_{i-1}-P_i)}{h_iK_{i-1}+h_{i-1}K_i} \\
&\quad -\frac{2K_{i+1}\,(P_i-P_{i+1})}{h_{i+1}K_i+h_iK_{i+1}} \quad \text{for } \; n<i<N \\
\frac{\partial}{\partial x}\left(-h_N\frac{\partial P_N}{\partial x}\right)+\frac{\partial}{\partial y}\left(-h_N\frac{\partial P_N}{\partial y}\right) &= \frac{2K_{N-1}\,(P_{N-1}-P_N)}{h_NK_{N-1}+h_{N-1}K_N}. \qquad (3.32)
\end{aligned}$$

A couple of two-dimensional examples are considered here to illustrate the implementation of the method.

3.3.1 Illustration: point fluid source in one sub-layer

Fluid flow problem for a multi-layered two-dimensional aquifer with a steady point source in one of its layers is solved as an example here. The confined aquifer is composed of three sedimentary sub-layers with different permeabilities (values labelled in Figure 3.6) that don't vary horizontally. The thicknesses of the layers are allowed to vary in one horizontal direction (x-direction). The impermeable bottom surface of the aquifer z_0 is taken as horizontal. The other two upward layer interfaces are defined as $z_1(x) = .5 + .2\sin(\pi x/3)$ [m], $z_2(x) = 1 + .25\sin(\pi x/4)$ [m] and the impermeable top boundary $z_3(x) = 1.5 + .3\sin(\pi x/5)$ [m]. The fluid flow problem for this aquifer is solved with two different layer compositions for comparison; with three "naturally occurring" sub-layers and with fifteen sub-layers where each natural layer is divided into five further sub-layers of equal thicknesses at each horizontal point. The purpose of dividing layers into further sub-layers is to achieve a better approximation of the true solution. The steady fluid injection rate at (x_0, z_0) is $F_I = 0.4/h_n(x_0)$ [$(\mathrm{m}^3\ \mathrm{hr}^{-1})$ $\mathrm{m}^{-2} = \mathrm{m\ hr}^{-1}$] in the nth sub-layer, where $h_n = z_n - z_{n-1}$ [m] is the thickness of the

nth sub-layer in which the fluid source lies. Thus, the fluid point source function $f_I(x)$ for the sub-layer containing the source is $F_I\delta(x - x_0)$.

Numerical solutions for the mean dynamic pressures $\bar{P}_i$ in the sub-layers of the aquifer are plotted in Figure 3.6 for both the cases in red contours. The boundary conditions on mean dynamic pressures are $\bar{P}_i(0) = 10$ and $\bar{P}_i(10) = 0$ [Pa] for $1 \leq i \leq 3$. The isobars in both the cases are quite similar as shown in the Figure 3.6 bottom two graphs. It can be concluded that dividing the aquifer up into fifteen sub-layers has no real advantage over dividing into the three layers because the solutions are similar enough. The top graph in the Figure shows the rate of fluid flowing in to the aquifer is equal to the rate of fluid flowing out of the aquifer in both the cases.

3.3.2 Distributed fluid source at the surface

In the next example, as shown in Figure 3.7, a confined aquifer composed of three natural sub-layers is considered with a transverse running stream in contact with the top sub-layer, where fluid can enter and leave the aquifer via this contact. The permeability values for all three sub-layers are labelled in the Figure. The bottom impermeable boundary $z_0(x)$ of the aquifer is defined by $z_0(x) = .3 + .2\sin(\pi x/5)$ [m]. The top partially impermeable boundary $z_3(x)$ is defined by $z_3(x) = 2.1 + .2\cos(2.32 + \pi x/2)$ [m] which is impermeable except for $4 \leq x \leq 5$ to allow water to enter or leave the aquifer from or into the stream. The two interlayer interfaces are $z_1(x) = 1 + .2\sin(\pi x/4)$ [m] and $z_2(x) = 1.5 + .2\sin(\pi x/3)$ [m]. The vertical fluid flux across the top boundary into the stream from the sub-layer three can be computed by the use of Darcy's law which is $-2K_3(P_{st} - P_3(x))/(\mu h_3(x))$, where P_{st} is the dynamic pressure in the stream given by $P_{st} = p_{\text{atm}} - p_0 + \rho g z_{st}$. Here, p_{atm} is the atmospheric pressure at the surface of the stream water, p_0 is the absolute pressure at the datum level and z_{st} is the height of the stream water surface above the datum level. Thus the set of coupled ODE's for

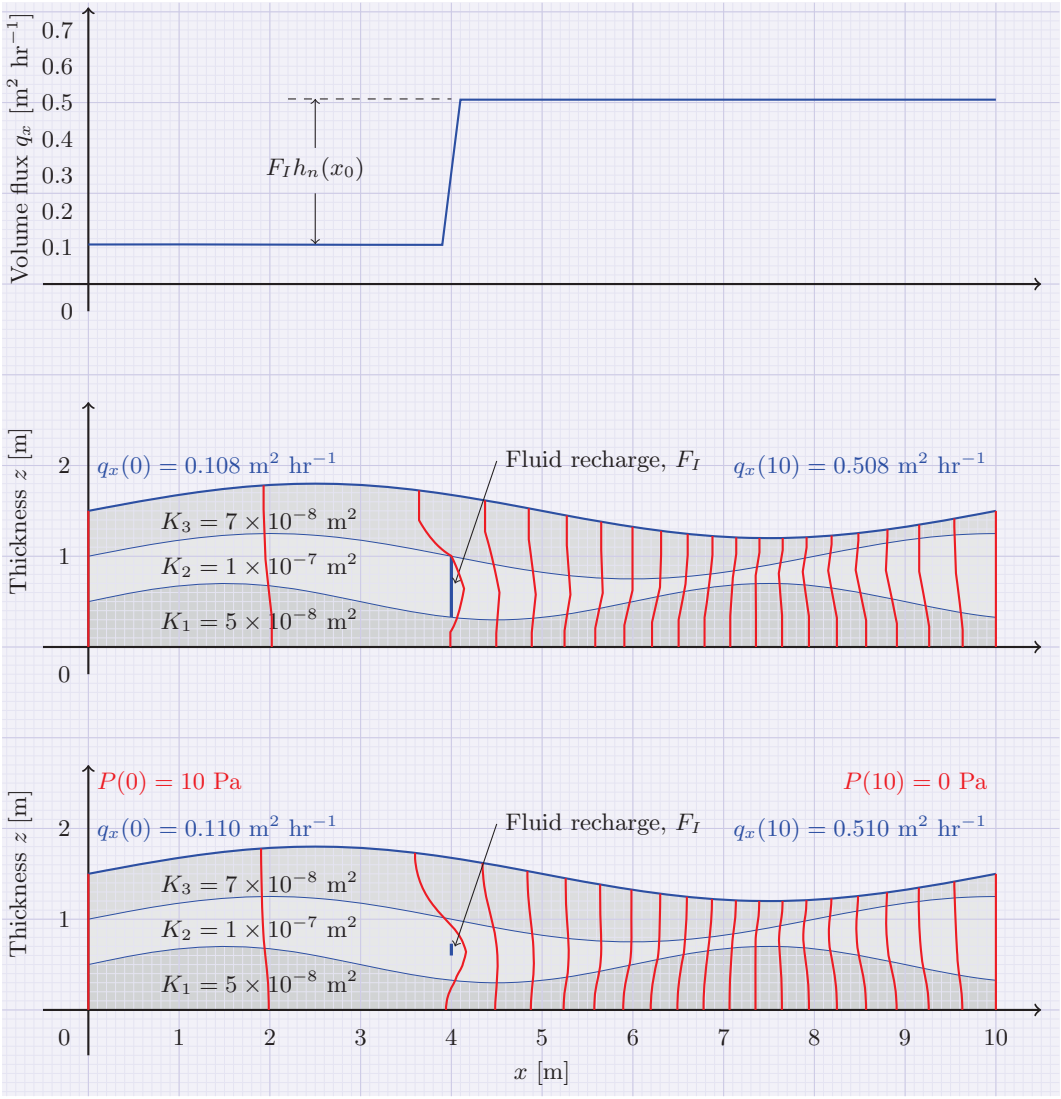

Figure 3.6: (Bottom) Isobars in a layered aquifer with a recharge well at (4,0.7) in which each layer is divided into five further sub-layers. (Middle) Isobars in a layered aquifer with a recharge well at (4,0.7) without dividing layers into further sub-layers. (Top) Total volumetric flux through the aquifer. The isobars in the two bottom graphs are quite similar.

the dynamic pressures in the three sub-layers of the aquifer takes the form

$$\begin{aligned}
\frac{d}{dx}\left(-h_1\frac{dP_1}{dx}\right) &= -\frac{2K_2\,(P_1-P_2)}{h_2K_1+h_1K_2} \\
\frac{d}{dx}\left(-h_2\frac{dP_2}{dx}\right) &= \frac{2K_1\,(P_1-P_2)}{h_2K_1+h_1K_2} - \frac{2K_3\,(P_2-P_3)}{h_3K_2+h_2K_3} \\
\frac{d}{dx}\left(-h_3\frac{dP_3}{dx}\right) &= \begin{cases} \dfrac{2K_2\,(P_2-P_3)}{h_3K_2+h_2K_3} - \dfrac{2(P_3-P_{st})}{h_3} & \text{for} \quad 4 \le x \le 5 \\ \dfrac{2K_2\,(P_2-P_3)}{h_3K_2+h_2K_3} & \text{otherwise.} \end{cases}
\end{aligned} \tag{3.33}$$

The isobars have been plotted in the Figure 3.7 to show the solution. The boundary conditions for the mean dynamic pressures in the three sub-layers are taken as $\bar{P}_i(0) = 10$ and $\bar{P}_i(10) = 0$ [pa] for $i \leq 1 \leq 3$ and the dynamic pressure at the water surface in the stream is $P_{st} = 6$ [Pa]. The dynamic viscosity of the groundwater for this illustration is taken as 1.002×10^{-3} [kg m^{-1} s^{-1}]. The top plot in the Figure 3.7 is the total volume flux per unit width of the aquifer. It is easy to see that the total volume flux through the aquifer decreases in some initial part of the region $4 \leq x \leq 5$ for these boundary conditions and stream water level and then it increases. This means that water enters the stream from the aquifer for some initial zone of their contact and then it penetrates into the aquifer from the stream. The net fluid flux, in this example, into the aquifer is equal to the difference $q_x(x > 5) - q_x(x < 4)$.

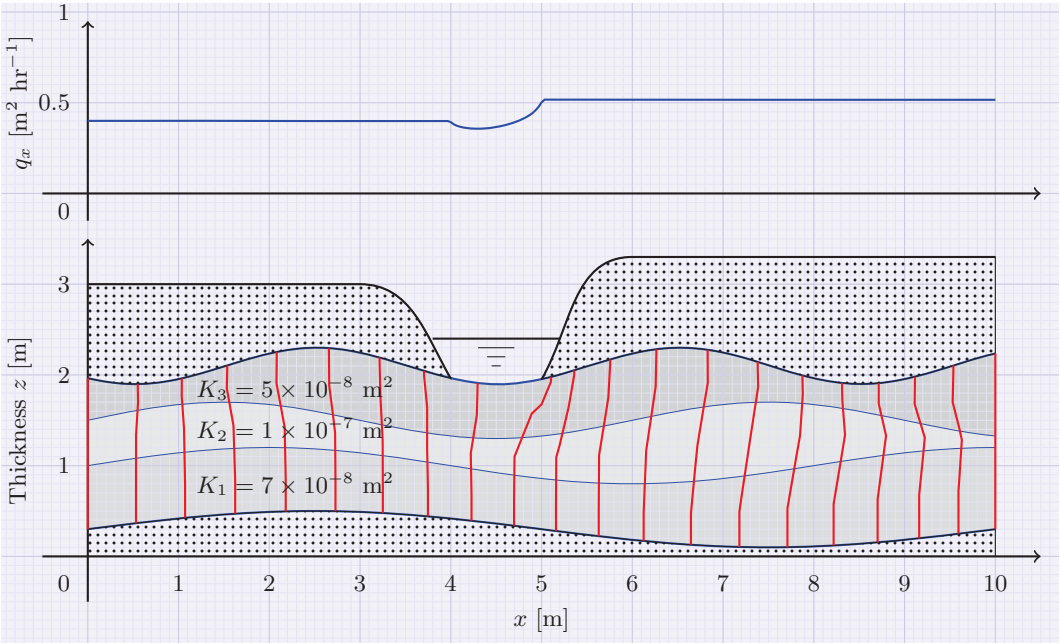

Figure 3.7: (Bottom) Isobars in a layered aquifer with a transverse running stream at the top from $x = 4$ to $x = 5$. (Top) The total volume flux q_x in the aquifer.

4

Fluid Flow Model for a Phreatic Aquifer

Aquifers that are not confined at the top by an impervious boundary are called phreatic aquifers or unconfined aquifers. This chapter deals with mathematical modelling of steady water flows in three types of phreatic aquifers;

1. in the absence of wells
2. in the presence of a recharge or pumping well across the aquifer thickness, and
3. in the presence of a recharge or pumping well that is present only in one sub-layer.

These three cases are discussed in detail here.

4.1 Fluid flow in absence of wells

The upper surface of phreatic aquifers is free and is generally time dependent. This surface, say $z_t(x, y, t)$ is called the phreatic surface. The absolute pressure $p(x, y)$ at the phreatic surface is constant and is close to the atmospheric pressure. Thus the dynamic pressure $P(x, y) = p_{atm} - p_0 + \rho g z_t(x, y)$ [Pa] on the phreatic surface depends on elevation of the surface at each point from a fixed datum level. This elevation from the fixed datum is also the hydraulic head of the phreatic surface. Consider a cross-section of the aquifer in the xz-plane and consider a curve s on the phreatic surface

in this plane. Then by Darcy's law, the specific discharge u_s $[(\mathrm{m}^3\ \mathrm{s}^{-1})\ \mathrm{m}^{-2} = \mathrm{m}\ \mathrm{s}^{-1}]$ along the phreatic surface curve is

$$u_s = -\frac{K\rho g}{\mu}\frac{dz_t}{ds}. \tag{4.1}$$

The slope of the phreatic surface is usually of the order 0.001 to 0.01 [13]. By the Dupuit assumption, due to this small slope, dz_t/ds can be replaced by dz_t/dx. That is, flow is considered essentially horizontal and the two-dimensional horizontal specific discharge may be approximated as

$$\bar{\mathbf{u}}(x,y,t) = (\bar{u},\bar{v}) = -\frac{K\rho g}{\mu}\left(\frac{\partial z_t}{\partial x},\frac{\partial z_t}{\partial y}\right). \tag{4.2}$$

Then total volume flux $\mathbf{q}(x,y,t) = (q_x(x,y,t), q_y(x,y,t))$ per unit width through the whole phreatic aquifer is

$$\begin{aligned}\mathbf{q} &= \left(\int_{z_b(x,y)}^{z_t(x,y,t)} u dz, \int_{z_b(x,y)}^{z_t(x,y,t)} v dz\right)\\ &= -\frac{K\rho g\,(z_t - z_b)}{\mu}\left(\frac{\partial z_t}{\partial x},\frac{\partial z_t}{\partial y}\right).\end{aligned} \tag{4.3}$$

Also, the vertically averaged horizontal two-dimensional fluid velocity $(\bar{u},\bar{v})$ at point (x,y) at time t is given as

$$(\bar{u},\bar{v}) = -\frac{K\rho g}{\mu}\left(\frac{\partial z_t}{\partial x},\frac{\partial z_t}{\partial y}\right).$$

If the bottom surface of the aquifer is impervious and if there is no fluid source or sink in the phreatic aquifer, then

$$\nabla\cdot\mathbf{q} = \frac{\partial q_x}{\partial x} + \frac{\partial q_y}{\partial y} = 0. \tag{4.4}$$

Thus the phreatic surface $z_t(x,y)$ satisfies

$$\frac{\partial}{\partial x}\left[-K\,(z_t - z_b)\,\frac{\partial z_t}{\partial x}\right] + \frac{\partial}{\partial y}\left[-K\,(z_t - z_b)\,\frac{\partial z_t}{\partial y}\right] = 0, \tag{4.5}$$

and for a homogeneous single-layered phreatic aquifer, the non-linear PDE (4.5) takes the form

$$\frac{\partial}{\partial x}\left[-\,(z_t - z_b)\,\frac{\partial z_t}{\partial x}\right] + \frac{\partial}{\partial y}\left[-\,(z_t - z_b)\,\frac{\partial z_t}{\partial y}\right] = 0. \tag{4.6}$$

In general, if the phreatic aquifer is composed of N different almost horizontal sub-layers with varying thicknesses, then the phreatic surface $z_t(x, y, t)$ satisfies

$$\begin{aligned}\frac{\partial}{\partial x}\left\{-\frac{\partial z_t}{\partial x}\left[\sum_{i=1}^{n-1} K_i h_i + K_n\left(z_t - \sum_{i=1}^{n-1} h_i\right)\right]\right\} \\ +\frac{\partial}{\partial y}\left\{-\frac{\partial z_t}{\partial y}\left[\sum_{i=1}^{n-1} K_i h_i + K_n\left(z_t - \sum_{i=1}^{n-1} h_i\right)\right]\right\} \\ = 0, \end{aligned} \tag{4.7}$$

where $n \leq N$ is the number of the layer in which the phreatic surface lies and h_i for $1 \leq i \leq n$ is the thickness of the ith layer. The interlayer flux from the ith sub-layer to the $i+1$th sub-layer can be written as

$$\nabla \cdot \mathbf{q}_i = r_{i-1} - r_i, \tag{4.8}$$

where r_0 and r_n are zero if z_t lies in the nth sub-layer. The horizontal volume flux vector $\mathbf{q}_i$ for the ith sub-layer is given by

$$\mathbf{q}_i = -\frac{K\rho g h_i}{\mu}\left(\frac{\partial z_t}{\partial x}, \frac{\partial z_t}{\partial y}\right). \tag{4.9}$$

4.1.1 Analytic solution for a special case of a non-homogeneous aquifer

Consider a one-dimensional problem of a non-homogeneous aquifer where sub-layer interfaces are parallel to the x-axis and the fluid flow is steady, i.e., there are no sources or sinks. Total volumetric flux q_x [$(\mathrm{m}^3\ \mathrm{s}^{-1})\ \mathrm{m}^{-1} = \mathrm{m}^2\ \mathrm{s}^{-1}$] must be constant in this case, where the total volumetric flux q_x in the phreatic aquifer is the sum of the volumetric fluxes in each sub-layer. Suppose that the aquifer is composed of N sub-layers, and suppose that the phreatic surface at x is $z_t(x)$. If $z_t(x)$ is located in the nth sub-layer ($n \leq N$), then the total volumetric flux q_x through the aquifer is

$$q_x = -\frac{\rho g}{\mu}\left(\sum_{i=1}^{n-1} K_i(z_i - z_{i-1}) + K_n(z_t - z_{n-1})\right)\frac{dz_t}{dx}, \tag{4.10}$$

where z_i is the elevation of the interface between the ith and the $i+1$th sub-layer. Now suppose $z_t(x)$ is descending, i.e. fluid speed is increasing with x, then $z_t(x)$ will meet z_{n-1} at some x, say x_1. Then the constant q_x, when $z_t(x)$ is in the $n-1$th sub-layer, satisfies

$$q_x = -\frac{\rho g}{\mu}\left(\sum_{i=1}^{n-2} K_i(z_i - z_{i-1}) + K_{n-1}(z_t - z_{n-2})\right)\frac{dz_t}{dx}. \tag{4.11}$$

If $z_t(x)$ meets z_{n-2} at x_2, then (4.11) is valid for $x_1 \le x \le x_2$. Similarly as a general case when $z_t(x)$ lies in the $n-k+1$th sub-layer, one may write

$$q_x = -\frac{\rho g}{\mu}\left(\sum_{i=1}^{n-k} K_i(z_i - z_{i-1}) + K_{n-k+1}(z_t - z_{n-k})\right)\frac{dz_t}{dx} \quad \text{for} \quad x_{k-1} \le x \le x_k. \tag{4.12}$$

The analytic solution of (4.12), when $z_t(x_0) = h_0$, can be written as

$$\frac{q_x \mu (x - x_0)}{\rho g} = \begin{cases} (h_0 - z_t)\sum_{i=1}^{n-1} K_i(z_i - z_{i-1}) \\ \quad + K_n\left[\frac{h_0^2}{2} - z_{n-1}(h_0 - z_t) - \frac{z_t^2}{2}\right] & \text{for} \quad x_0 \le x \le x_1 \\ (h_0 - z_t)\sum_{i=1}^{n-2} K_i(z_i - z_{i-1}) \\ \quad + K_{n-1}\left[(h_0 - z_{n-1})(z_{n-1} - z_{n-2})\right. \\ \quad \left. + \frac{z_{n-1}^2}{2} - z_{n-2}(z_{n-1} - z_t) - \frac{z_t^2}{2}\right] \\ \quad + K_n \frac{(h_0 - z_{n-1})^2}{2} & \text{for} \quad x_1 \le x \le x_2 \\ (h_0 - z_t)\sum_{i=1}^{n-k} K_i(z_i - z_{i-1}) \\ \quad + K_{n-k+1}\left[(h_0 - z_{n-k+1})(z_{n-k+1} - z_{n-k})\right. \\ \quad \left. + \frac{z_{n-k+1}^2}{2} - z_{n-k}(z_{n-k+1} - z_t) - \frac{z_t^2}{2}\right] \\ \quad + \sum_{i=n-k+2}^{n-1} K_i\left((h_0 - z_i)(z_i - z_{i-1}) + \frac{(z_i - z_{i-1})^2}{2}\right) \\ \quad + K_n \frac{(h_0 - z_{n-1})^2}{2} & \text{for} \quad x_{k-1} \le x \le x_k, \end{cases} \tag{4.13}$$

where

$$x_1 = x_0 + \frac{\rho g}{q_x \mu}\left[(h_0 - z_{n-1})\sum_{i=1}^{n-1} K_i(z_i - z_{i-1}) + K_n \frac{(h_0 - z_{n-1})^2}{2}\right], \tag{4.14}$$

and

$$\begin{aligned} x_k = & x_0 + \frac{\rho g}{q_x \mu}\left[(h_0 - z_{n-k})\sum_{i=1}^{n-k} K_i(z_i - z_{i-1})\right. \\ & + \sum_{i=n-k+1}^{n-1} K_i\left((h_0 - z_i)(z_i - z_{i-1}) + \frac{(z_i - z_{i-1})^2}{2}\right) \\ & \left. + K_n \frac{(h_0 - z_{n-1})^2}{2}\right] \quad \text{for} \quad 2 \le k \le n. \end{aligned} \tag{4.15}$$

Now for $x_{k-1} \le x \le x_k$ and for $1 \le k \le n$, the volume flux through the ith sub-layer is

$$q_{xi} = \frac{(z_i - z_{i-1})K_i}{\sum_{i=1}^{n-k}(z_i - z_{i-1})K_i + (z_t - z_{n-k})K_{n-k+1}} q_x \quad \text{for} \quad 1 \le i \le n-k, \tag{4.16}$$

and

$$q_{xn-k+1} = \frac{(z_t - z_{n-k})K_{n-k+1}}{\sum_{i=1}^{n-k}(z_i - z_{i-1})K_i + (z_t - z_{n-k})K_{n-k+1}} q_x. \tag{4.17}$$

Then for $x_{k-1} \leq x \leq x_k$ and for $1 \leq k \leq n$, the interlayer flux r_i from the ith sub-layer to the $i+1$th sub-layer, normal to the sub-layer interface is

$$r_i(x) - r_{i-1}(x) = -\frac{dq_{xi}}{dx} \quad \text{for} \quad 1 \leq i \leq n-k, \tag{4.18}$$

where $r_0(x) = r_{n-k+1}(x) = 0$. Then

$$r_i(x) - r_{i-1}(x) = \frac{K_i K_{n-k+1}(z_i - z_{i-1})}{\left(\sum_{j=1}^{n-k} K_j(z_j - z_{j-1}) + K_{n-k+1}(z_t - z_{n-k})\right)^2} q_x \quad \text{for} \quad 1 \leq i < n-k. \tag{4.19}$$

The analytic solution for the phreatic surface in an aquifer composed of three planar sub-layers of different permeabilities is plotted in Figure 4.1. The boundary conditions for the phreatic surface as shown in the Figure are $h(0) = 3$ [m] and $h(10) = 0.5$ [m]. The permeabilities of three sub-layers are labelled in the Figure.

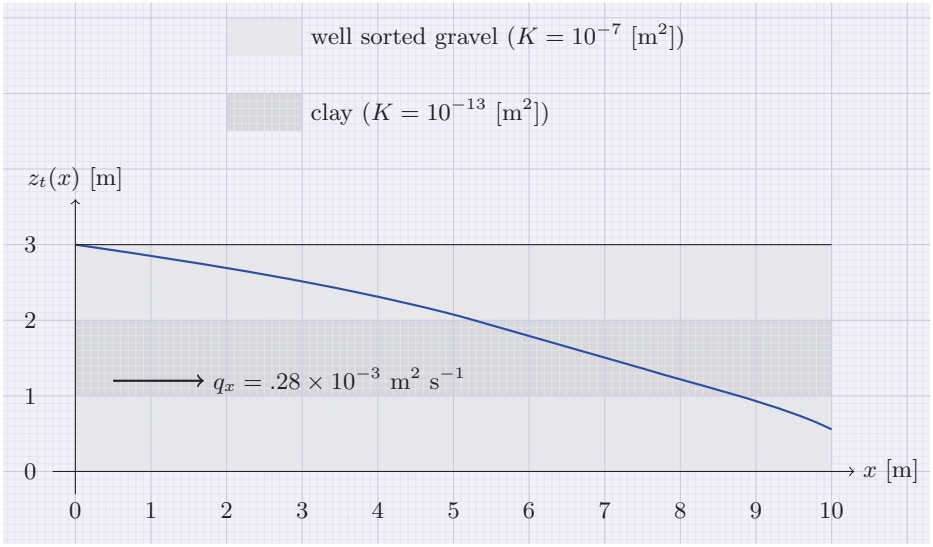

Figure 4.1: Analytic solution for the phreatic surface in an unconfined aquifer composed of three planar homogeneous (individually) sub-layers. The permeabilities of sub-layers are labelled.

The phreatic surface predicted for the aquifer shown in Figure 4.1 seems to drop almost linearly as it passes through the sub-layers composed of clay (almost impermeable with permeability $K = 10^{-13}$ [m^2]). The reason for this linear drop of phreatic surface

is due to the fact that the dynamic pressure $P(x)$ is proportional to the phreatic surface $z_t(x)$, and the gradient of the dynamic pressure should be constant for a confined homogeneous constant thickness aquifer. Here, when the phreatic surface $z_t(x)$ passes through the almost impermeable clay layer, the whole aquifer below this layer behaves almost like a confined aquifer, therefore the dynamic pressure gradient is constant in this region and hence the gradient of the phreatic surface $z_t(x)$.

4.1.2 A one-dimensional phreatic aquifer with K as a function of x

Consider a one-dimensional aquifer with the phreatic level at upstream point x_u equal to h_u and with the horizontal base $z_b = 0$. The total volume flux q_x per unit width of this aquifer remains constant. As it is discussed earlier that the gradient of the phreatic surface z_t in groundwater aquifers is very small except in the vicinity of fluid sources or sinks, the flow can be assumed essentially horizontal and $P = P(x)$. The differential equation for the Darcy velocity u_x can be written as

$$u_x = -\frac{K}{\mu}\frac{dP}{dx}. \tag{4.20}$$

The Darcy velocity $u_x(x)$ can, therefore, be approximated by

$$u_x = -\frac{K\rho g}{\mu}\frac{dz_t}{dx}, \qquad \text{(By Dupuit assumption)} \tag{4.21}$$

and an integration of the Darcy velocity u_x over the fluid height gives the total volume flux q_x as

$$q_x = -\frac{K\rho g}{\mu} z_t \frac{dz_t}{dx}. \tag{4.22}$$

For the given initial condition and for the varying permeability $K(x)$, the phreatic surface has solution

$$z_t(x) = \sqrt{h_u^2 - \frac{2\mu q_x}{\rho g}\int_{x_u}^{x}\frac{d\xi}{K(\xi)}}. \tag{4.23}$$

As an illustration, two one-dimensional horizontal bottomed phreatic aquifers are considered. In the first aquifer (Figure 4.2 (top)), permeability K decreases linearly as $K(x) = -10^{-8}x + 1.1 \times 10^{-7}$ [m^2]. It is obvious that the phreatic surface $z_t(x)$ here has small gradient to start with and, as the fluid reaches the less permeable porous material, the phreatic surface gradient (and hence dynamic pressure gradient) increases to push the fluid through the less permeable material.

In the next example, the permeability increases linearly as $K(x) = 10^{-8}x + 10^{-8}$ [m^2] and the phreatic surface is plotted in Figure 4.2 (bottom).

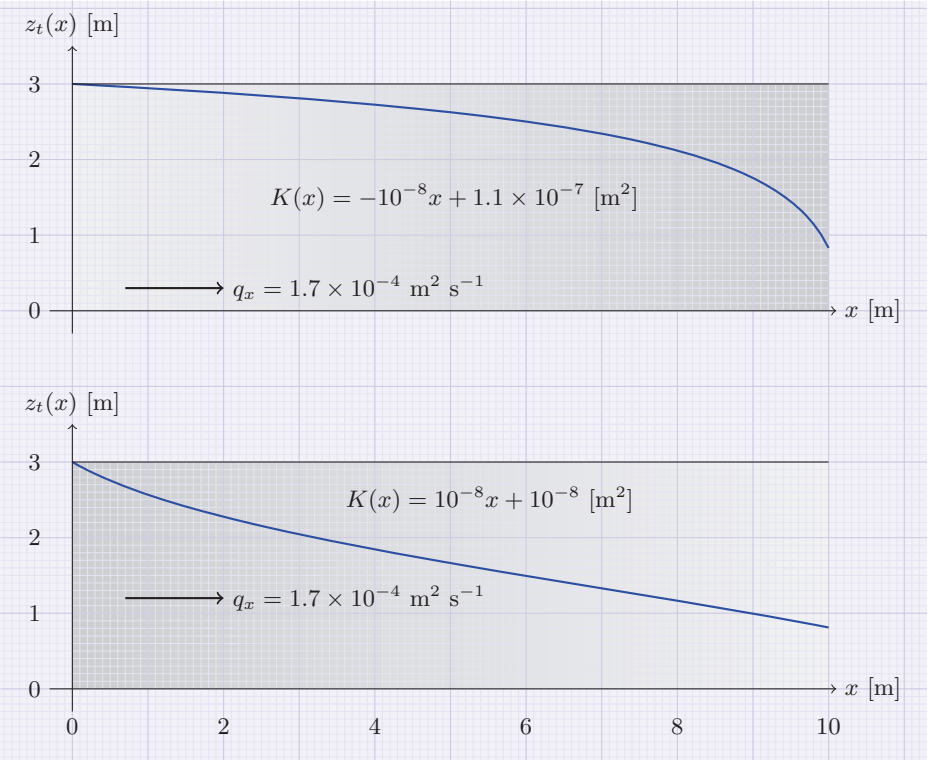

Figure 4.2: Phreatic surface analytic solutions when K varies in one horizontal direction, x and the bottom surface is $z_b = 0$. (Top) The permeability decreases linearly and phreatic surface drops more sharply in lesser permeable zone. (Bottom) The permeability increases linearly and phreatic surface can be seen dropping slowly in higher permeable porous material.

4.1.3 A lens in a phreatic aquifer

Consider a one-dimensional homogeneous phreatic (unconfined at the top) aquifer with permeability K and horizontal base that has a lens of different permeability K_l in the water table as shown in Figure 4.3. The total volumetric flux per unit width q_x must be constant in this case when there is no source or sink for the fluid.

Suppose that the aquifer upstream and downstream boundaries are x_u and x_d, respectively and the lens top and bottom interfaces are $l_t(x)$ and $l_b(x)$ for $x_1 < x < x_2$.

The phreatic surface $z_t(x)$ satisfies [4]

$$\frac{q_x \mu}{\rho g} = \begin{cases} -K z_t \frac{dz_t}{dx} & \text{for } x_u \leq x < x_1 \\ -\left[K l_b + K_l(l_t - l_b) + K(z_t - l_t)\right] \frac{dz_t}{dx} & \text{for } x_1 \leq x \leq x_2 \\ -K z_t \frac{dz_t}{dx} & \text{for } x_2 <\leq x_d \end{cases} \tag{4.24}$$

The resultant predicted phreatic surface when $z_t(x_u) = h_u = 3.5$ [m] is plotted in Figure 4.3. The dashed line in Figure 4.3 shows the phreatic surface for a totally homogeneous aquifer with the same $z_t(x_u)$ and all the same other parameters (except that there is no lens of lesser permeability). One can see the difference in the phreatic surfaces when there is a lens of different permeability and when the aquifer is totally homogeneous.

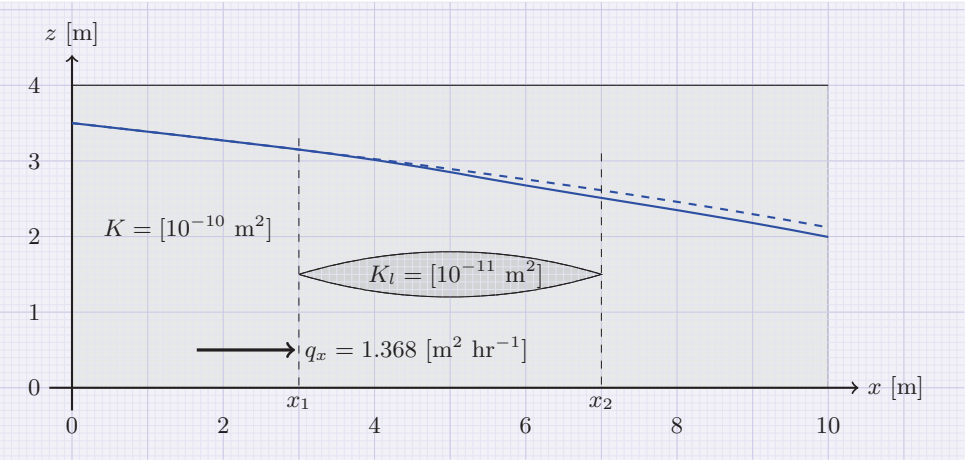

Figure 4.3: The predicted phreatic surface when the aquifer has permeability K and the lens has lower permeability K_l. The dashed curve is the predicted phreatic surface when the aquifer does not have a lens and has permeability K.

The right hand side of (4.24) is constant. Thus, in case of $K_l < K$, the coefficient of dz_t/dx decreases in the vicinity of this sub-layer as compared to the regions where it is not present. Hence, $z_t(x)$ has higher slope (or dynamic pressure) in the vicinity of a less permeable sub-layer. In other words, a higher dynamic pressure gradient is needed in the zone of a lesser permeable lens to maintain the same constant total volume flux q_x. The dynamic pressure gradient in phreatic aquifers is proportional to the phreatic surface gradient.

4.2 Phreatic aquifer with pumping or recharge well across the aquifer thickness

Suppose $f_I(x,y)$ and $f_W(x,y)$ [$(\mathrm{m}^3\ \mathrm{s}^{-1})\ \mathrm{m}^{-3} = \mathrm{s}^{-1}$] are vertically averaged fluid recharge and pumping, respectively through wells that are right through the whole thickness of the aquifer (wells that do not cause significant vertical flows). If the permeability of the aquifer is uniform, then conservation of mass (3.20) for a phreatic aquifer gives

$$\frac{\partial}{\partial x}\left[-\left(z_t - z_b\right)\frac{\partial z_t}{\partial x}\right] + \frac{\partial}{\partial y}\left[-\left(z_t - z_b\right)\frac{\partial z_t}{\partial y}\right] = \frac{\mu}{Kg\rho}\left(f_I - f_W\right). \tag{4.25}$$

4.2.1 Analytic solution for a special case

Suppose a one-dimensional homogeneous aquifer, with planar horizontal bottom surface and with a recharge well at x_0 in it that is recharging the aquifer with water at a constant rate of F_I [$(\mathrm{m}^3\ \mathrm{s}^{-1})\ \mathrm{m}^{-1} = \mathrm{m}^2\ \mathrm{s}^{-1}$], is averaged vertically over the aquifer thickness. Then, the governing equation for the phreatic surface $z_t(x)$ satisfies

$$\frac{d}{dx}\left[-z_t\frac{dz_t}{dx}\right] = \frac{\mu F_I}{Kg\rho}\delta\left(x - x_0\right). \tag{4.26}$$

The analytic solution of (4.26) can be written as

$$z_t(x) = \begin{cases} \sqrt{\left(\frac{h_d^2 - h_u^2}{x_d - x_u} + \frac{2\mu F_I}{Kg\rho}\frac{x_d - x_0}{x_d - x_u}\right)x + \frac{h_u^2 x_d - h_d^2 x_u}{x_d - x_u} - \frac{2\mu F_I x_u}{Kg\rho}\frac{x_d - x_0}{x_d - x_u}} & \text{for } \ x \le x_0 \\ \sqrt{\left(\frac{h_d^2 - h_u^2}{x_d - x_u} - \frac{2\mu F_I}{Kg\rho}\frac{x_0 - x_u}{x_d - x_u}\right)x + \frac{h_u^2 x_d - h_d^2 x_u}{x_d - x_u} + \frac{2\mu F_I x_d}{Kg\rho}\frac{x_0 - x_u}{x_d - x_u}} & \text{for } \ x > x_0 \end{cases} \tag{4.27}$$

This solution is plotted in Figure 4.4. The total fluid flux out of the downstream end of the aquifer is equal to the sum of the background fluid flux from upstream and the recharge flux at $x = x_0$.

The solution for a constant pumping or withdrawal rate F_W [$(\mathrm{m}^3\ \mathrm{s}^{-1})\ \mathrm{m}^{-1} = \mathrm{m}^2\ \mathrm{s}^{-1}$] can be written simply by replacing F_I in the solution with $-F_W$.

4.2.2 Analytic solution for a special case of pumping well

Suppose a one-dimensional homogeneous aquifer with planar horizontal bottom surface and with a pumping well at x_0 in it that is pumping water from the aquifer with a rate

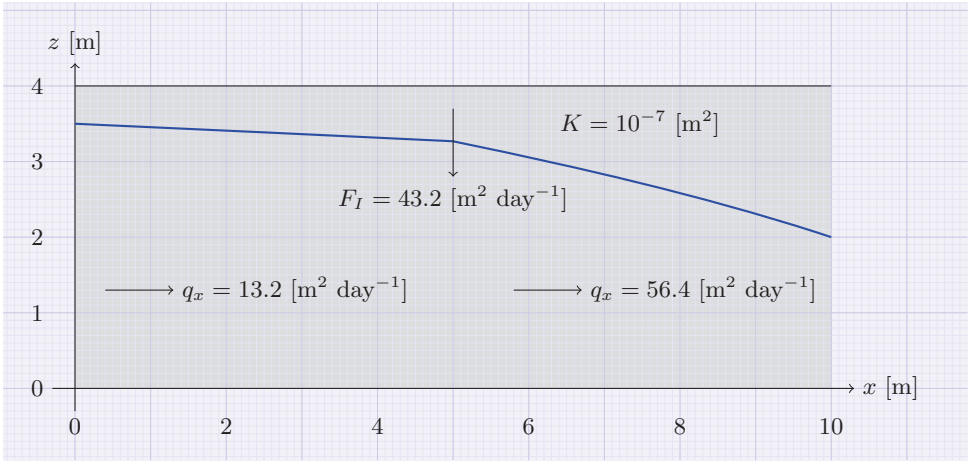

Figure 4.4: The analytic solution of the phreatic surface when fluid is being recharged at $x_0 = 5$ [m] with a steady rate $F_I = 43.2$ [(m^3 day^{-1}) m^{-1} = m^2 day^{-1}].

F_W [(m^3 s^{-1}) m^{-2} = m s^{-1}] at x_0. In this case, pumping is done at a rate proportional to the water level in the pumping well. This can be achieved by maintaining a constant pressure for suction by the pump and allowing only water to be sucked in. The governing equation for the phreatic surface, $z_t(x)$ now satisfies

$$\frac{d}{dx}\left[-z_t\frac{dz_t}{dx}\right] = -\frac{\mu F_W}{Kg\rho}z_t\delta\left(x-x_0\right). \tag{4.28}$$

The analytic solution of (4.28) can be written as

$$z_t(x) = \begin{cases} \sqrt{\left(\frac{h_d^2-h_u^2}{x_d-x_u} - \frac{2\mu F_W h_0}{Kg\rho}\frac{x_d-x_0}{x_d-x_u}\right)x + \frac{h_u^2 x_d - h_d^2 x_u}{x_d-x_u} + \frac{2\mu F_W h_0 x_u}{Kg\rho}\frac{x_d-x_0}{x_d-x_u}} & \text{for } x \le x_0 \\ \sqrt{\left(\frac{h_d^2-h_u^2}{x_d-x_u} + \frac{2\mu F_W h_0}{Kg\rho}\frac{x_0-x_u}{x_d-x_u}\right)x + \frac{h_u^2 x_d - h_d^2 x_u}{x_d-x_u} - \frac{2\mu F_W h_0 x_d}{Kg\rho}\frac{x_0-x_u}{x_d-x_u}} & \text{for } x > x_0, \end{cases} \tag{4.29}$$

where

$$\begin{aligned} h_0 &= -\frac{\mu F_W\left(x_d-x_0\right)\left(x_0-x_u\right)}{Kg\rho\left(x_d-x_u\right)} \\ &\quad + \sqrt{\left(\frac{\mu F_W\left(x_d-x_0\right)\left(x_0-x_u\right)}{Kg\rho\left(x_d-x_u\right)}\right)^2 + \frac{h_u^2\left(x_d-x_0\right)+h_d^2\left(x_0-x_u\right)}{x_d-x_u}}. \end{aligned} \tag{4.30}$$

The analytic solution is plotted in Figure 4.5. The fluid flux out of the pumping well is equal to the total inward fluxes from both sides of the well.

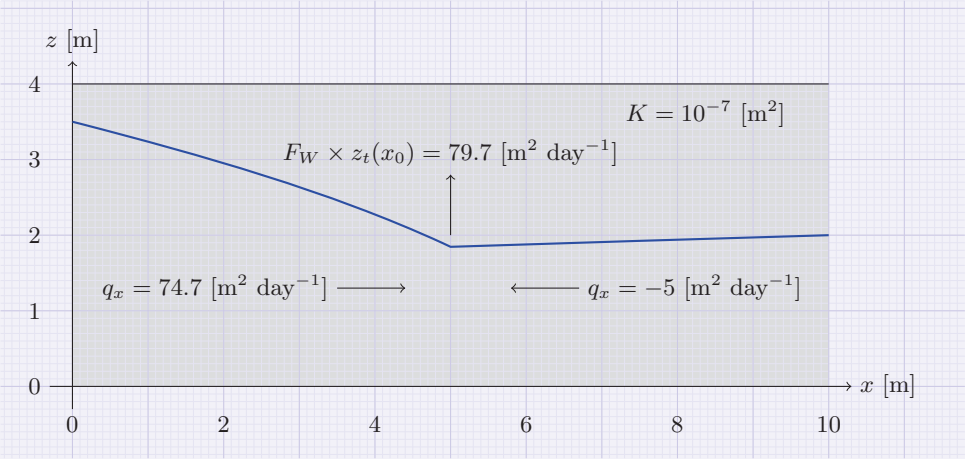

Figure 4.5: The analytic solution of the phreatic surface when fluid is being pumped out from $x_0 = 5$ with a steady rate $F_W = 79.7$ [(m^3 day^{-1}) m^{-2} = m day^{-1}].

4.3 Multi-layered phreatic aquifer with pumping or recharge in one of the sub-layers

In general, the phreatic aquifers may have a recharge or a pumping well in one of its sub-layers. Suppose, the aquifer is composed of N sedimentary sub-layers, and there is a fluid recharge well with a steady recharge volume flux F_I [m^3 s^{-1}] at the point (x_0, y_0) of the nth sub-layer averaged over the sub-layer thickness. It is more convenient to use hydraulic head values in this case instead of dynamic pressures. Hydraulic head $H(x, y, z)$ is the level of water maintained in a well that is exposed only to the point (x, y, z) of the aquifer. The mean hydraulic head $\bar{H}_i$ at the point (x, y) of the ith sub-layer is defined as $\bar{H}_i = \int_{z_{i-1}}^{z_i} H(x, y, z)dz/h_i$. The fluid flux from the $n-1$th sub-layer to the nth sub-layer can be computed by use of the Darcy's law as

$$r_{n-1} = \frac{2K_{n-1}K_n\rho g\left(\bar{H}_{n-1} - \bar{H}_n\right)}{\mu\left(K_{n-1}h_n + K_n h_{n-1}\right)}. \tag{4.31}$$

Thus, divergence of the total volume flux of isothermal, incompressible fluid in the nth sub-layer of the aquifer can be written as

$$\begin{aligned}&\frac{\partial}{\partial x}\left(\frac{-h_n K_n\rho g}{\mu}\frac{\partial \bar{H}_n}{\partial x}\right) + \frac{\partial}{\partial y}\left(\frac{-h_n K_n\rho g}{\mu}\frac{\partial \bar{H}_n}{\partial y}\right)\\ =&\frac{2K_{n-1}K_n\rho g\left(\bar{H}_{n-1} - \bar{H}_n\right)}{\mu\left(K_{n-1}h_n + K_n h_{n-1}\right)} - \frac{2K_n K_{n+1}\rho g\left(\bar{H}_n - \bar{H}_{n+1}\right)}{\mu\left(K_n h_{n+1} + K_{n+1}h_n\right)} + F_I\delta(x - x_0)\delta(y - y_0).\end{aligned} \tag{4.32}$$

Note that this fluid mass conservation equation is valid only if the phreatic surface $z_t(x,y)$ lies in the $n+2$th sub-layer or higher. If z_t lies in the $n+1$th sub-layer, h_{n+1} in the denominator of the second term on the right hand side of (4.32) is replaced with $z_t - z_n$, where z_n is the interface level between the $n+1$th sub-layer and nth sub-layer. Moreover, if z_t passes through the nth sub-layer, (4.32) is non-linear with $\bar{H}_n = z_t$, $h_n = z_t - z_{n-1}$ and $h_{n+1} = 0$. For a homogeneous nth sub-layer of the aquifer, i.e., when K_n is a constant, (4.32) simplifies to

$$\begin{aligned}
&\frac{\partial}{\partial x}\left(-h_n\frac{\partial \bar{H}_n}{\partial x}\right) + \frac{\partial}{\partial y}\left(-h_n\frac{\partial \bar{H}_n}{\partial y}\right) \\
=&\frac{2K_{n-1}\left(\bar{H}_{n-1}-\bar{H}_n\right)}{K_{n-1}h_n + K_n h_{n-1}} - \frac{2K_{n+1}\left(\bar{H}_n-\bar{H}_{n+1}\right)}{K_n h_{n+1} + K_{n+1}h_n} + \frac{\mu \bar{F}_I}{K_n \rho g}\delta(x-x_0)\delta(y-y_0). \qquad (4.33)
\end{aligned}$$

If the phreatic surface z_t goes through the Nth sub-layer (say), the mean hydraulic head in the Nth sub-layer $\bar{H}_N$ is equal to z_t and the coupled system for the fluid flow may be written as

$$\begin{aligned}
\frac{\partial}{\partial x}\left[-h_1\frac{\partial \bar{H}_1}{\partial x}\right] + \frac{\partial}{\partial y}\left[-h_1\frac{\partial \bar{H}_1}{\partial y}\right] &= -\frac{2K_2\left(\bar{H}_1-\bar{H}_2\right)}{K_1h_2+K_2h_1} \\
\frac{\partial}{\partial x}\left[-h_i\frac{\partial \bar{H}_i}{\partial x}\right] + \frac{\partial}{\partial y}\left[-h_i\frac{\partial \bar{H}_i}{\partial y}\right] &= \frac{2K_{i-1}\left(\bar{H}_{i-1}-\bar{H}_i\right)}{K_{i-1}h_i+K_ih_{i-1}} \\
&\quad -\frac{2K_{i+1}\left(\bar{H}_i-\bar{H}_{i+1}\right)}{K_ih_{i+1}+K_{i+1}h_i} \quad \text{for} \quad 1<i<n \\
\frac{\partial}{\partial x}\left[-h_n\frac{\partial \bar{H}_n}{\partial x}\right] + \frac{\partial}{\partial y}\left[-h_n\frac{\partial \bar{H}_n}{\partial y}\right] &= \frac{2K_{n-1}\left(\bar{H}_{n-1}-\bar{H}_n\right)}{K_{n-1}h_n+K_nh_{n-1}} \\
&\quad -\frac{2K_{n+1}\left(\bar{H}_n-\bar{H}_{n+1}\right)}{K_nh_{n+1}+K_{n+1}h_n} \\
&\quad +\frac{\mu F_I}{\rho g K_n}\delta(x-x_0)\delta(y-y_0) \\
\frac{\partial}{\partial x}\left[-h_i\frac{\partial \bar{H}_i}{\partial x}\right] + \frac{\partial}{\partial y}\left[-h_i\frac{\partial \bar{H}_i}{\partial y}\right] &= \frac{2K_i\left(\bar{H}_{i-1}-\bar{H}_i\right)}{K_{i-1}h_i+K_ih_{i-1}} \\
&\quad -\frac{2K_{i+1}\left(\bar{H}_i-\bar{H}_{i+1}\right)}{K_ih_{i+1}+K_{i+1}h_i} \quad \text{for} \quad n<i<N-1 \\
\frac{\partial}{\partial x}\left[-h_{N-1}\frac{\partial \bar{H}_{N-1}}{\partial x}\right] + \frac{\partial}{\partial y}\left[-h_{N-1}\frac{\partial \bar{H}_{N-1}}{\partial y}\right] &= \frac{2K_{N-2}\left(\bar{H}_{N-2}-\bar{H}_{N-1}\right)}{K_{N-2}h_{N-1}+K_{N-1}h_{N-2}} \\
&\quad -\frac{2K_N\left(\bar{H}_{N-1}-z_t\right)}{K_{N-1}\left(z_t-z_{N-1}\right)+K_Nh_{N-1}} \\
\frac{\partial}{\partial x}\left[-\left(z_t-z_{N-1}\right)\frac{\partial z_t}{\partial x}\right] + \frac{\partial}{\partial y}\left[-\left(z_t-z_{N-1}\right)\frac{\partial z_t}{\partial y}\right] &= \frac{2K_{N-1}\left(\bar{H}_{N-1}-z_t\right)}{K_{N-1}(z_t-z_{N-1})+K_Nh_{N-1}}. \qquad (4.34)
\end{aligned}$$

Note that the PDE for the Nth sub-layer from the bottom is non-linear in $z_t = \bar{H}_N$. This system remains valid only if $z_t(x, y)$ passes through the Nth sub-layer. For example, if z_t enters into the lower $N-1$th sub-layer, the total system reduces to $N-1$ coupled PDE's, where the PDE for the $N-1$th sub-layer becomes non-linear in $z_t = \bar{H}_{N-1}$. The Two PDE's for the $N-2$th and $N-1$th sub-layers may then be written as

$$\begin{aligned}
\frac{\partial}{\partial x}\left[-h_{N-2}\frac{\partial \bar{H}_{N-2}}{\partial x}\right] + \frac{\partial}{\partial y}\left[-h_{N-2}\frac{\partial \bar{H}_{N-2}}{\partial y}\right] &= \frac{2K_{N-3}\left(\bar{H}_{N-3} - \bar{H}_{N-2}\right)}{K_{N-3}h_{N-2} + K_{N-2}h_{N-3}} \\
&\quad - \frac{2K_{N-1}\left(\bar{H}_{N-2} - z_t\right)}{K_{N-2}\left(z_t - z_{N-2}\right) + K_{N-1}h_{N-2}} \\
\frac{\partial}{\partial x}\left[-\left(z_t - z_{N-2}\right)\frac{\partial z_t}{\partial x}\right] + \frac{\partial}{\partial y}\left[-\left(z_t - z_{N-2}\right)\frac{\partial z_t}{\partial y}\right] &= \frac{2K_{N-2}\left(\bar{H}_{N-2} - z_t\right)}{K_{N-2}(z_t - z_{N-2}) + K_{N-1}h_{N-2}},
\end{aligned} \tag{4.35}$$

and so on.

4.3.1 Point recharge well in a sub-layer

Consider a phreatic aquifer composed of six sedimentary sub-layers as shown in Figure 4.6. The interface levels z_i for $0 \le i \le 6$ are:

$$\begin{aligned}
z_0(x) &= \frac{2.1}{2+x}, \\
z_1(x) &= \frac{8.6}{7.1+x}, \\
z_2(x) &= \frac{20}{10+x}, \\
z_3(x) &= \frac{43.1}{18.75+x}, \\
z_4(x) &= \frac{120}{50+x}, \\
z_5(x) &= \frac{338}{125+x}, \quad \text{and} \\
z_6(x) &= \frac{-900}{-300+x}.
\end{aligned}$$

The permeability, K_i, for each of the sub-layer and other groundwater parameters are given in Table 4.1. Suppose that the mean hydraulic heads $\bar{H}_i$ and hence the phreatic surface z_t are given at both the boundaries as $\bar{H}_i(0) = 2.9$ and $\bar{H}_i(10) = 2.6$ [m] for $1 \le i \le 6$ and $\bar{H}_6 = z_t$ when z_t passes through the 6th sub-layer. If there is a fluid recharge well in the second sub-layer with a steady head level 2.9 [m] at $x_0 = 4$, then

the numerical solution for the mean hydraulic heads is computed by (4.34) and contours of constant mean hydraulic heads $\bar{H}_i$ are plotted in Figure 4.6. Note that the recharge well in sub-layer 3 is like a transverse plane at $x = 4$ (marked as a blue line in the 3rd sub-layer).

Parameters	**Values**	**Units**
fluid dynamic viscosity μ	1.002×10^{-3}	[kg m^{-1} s^{-1}]
gravitational acceleration g	9.8	[m s^{-2}]
fluid density ρ	1000	[kg m^{-3}]
permeabilities $(K_1, K_2, K_3, K_4, K_5, K_6)$	$(0.7, 1, 0.5, 0.1, 1, 0.3) \times 10^{-7}$	[m^2]

Table 4.1: Parameters used for the simulation shown in Figure 4.6.

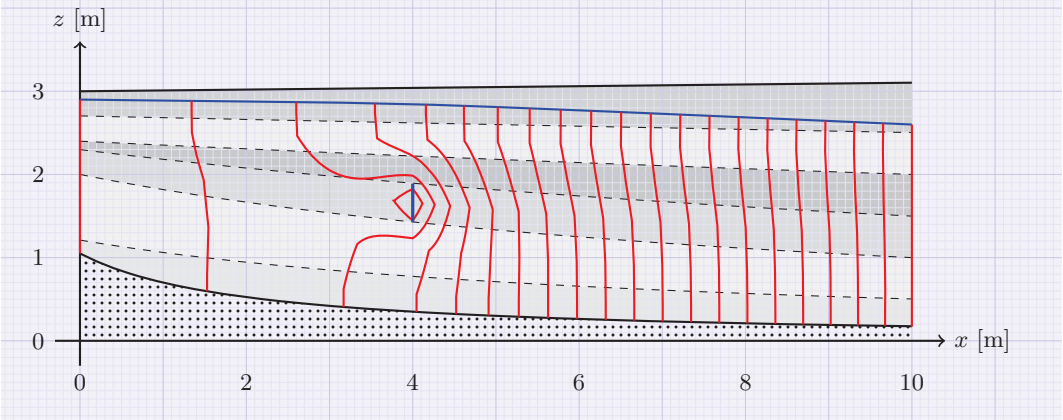

Figure 4.6: Isobars (contours of constant hydraulic head) in a layered aquifer composed of six sub-layers with a recharge well at $x = 4$ (marked as blue line) in the third sub-layer in which the water level is maintained at 2.9 [m]. The hydraulic heads at $x = 0$ are 2.9 [m] and at $x = 10$ are 2.6 [m]. All other parameters are mentioned in Table 4.1.

4.3.2 Transverse running stream in the top sub-layer

Consider a one-dimensional phreatic aquifer (thicknesses of whose sub-layers vary only in one horizontal direction) composed of four sedimentary sub-layers, with interface

levels z_i defined as

$$\begin{aligned} z_0(x) &= 0.3 + 0.15\sin\left(\frac{\pi x}{5}\right), \\ z_1(x) &= 1 + 0.25\sin\left(\frac{\pi x}{4}\right), \\ z_2(x) &= 1.5 + 0.05\sin\left(\frac{\pi x}{3}\right), \\ z_3(x) &= 2.1 + 0.13\cos\left(2.32 + \frac{\pi x}{2}\right), \quad \text{and} \\ z_4(x) &= 3 - \exp\left[-(x-4.5)^2\right]. \end{aligned}$$

Also, consider a transverse running stream of surface water at the surface of the aquifer, i.e., above top (4th) sub-layer, in the ditch. Suppose that the boundary conditions for the mean hydraulic heads $\bar{H}_i(x)$ are $\bar{H}_i(0) = 2.9$ and $\bar{H}_i(10) = 2.4$ [m] for $1 \le i \le 4$ and the water level in the stream z_{st} is 2.7 [m]. The system of ODE's for mean hydraulic heads in this aquifer can be written as

$$\begin{aligned} \frac{d}{dx}\left[-h_1\frac{d\bar{H}_1}{dx}\right] &= -\frac{2K_2\left(\bar{H}_1 - \bar{H}_2\right)}{K_1h_2 + K_2h_1} \\ \frac{d}{dx}\left[-h_2\frac{d\bar{H}_2}{dx}\right] &= \frac{2K_1\left(\bar{H}_1 - \bar{H}_2\right)}{K_1h_2 + K_2h_1} - \frac{2K_3\left(\bar{H}_2 - \bar{H}_3\right)}{K_2h_3 + K_3h_2} \\ \frac{d}{dx}\left[-h_3\frac{d\bar{H}_3}{dx}\right] &= \begin{cases} \dfrac{2K_2\left(\bar{H}_2 - \bar{H}_3\right)}{K_2h_3 + K_3h_2} - \dfrac{2K_4\left(\bar{H}_3 - z_t\right)}{K_3(z_t - z_3) + K_4h_3} & \text{when } \ z_t < z_4 \\ \dfrac{2K_2\left(\bar{H}_2 - \bar{H}_3\right)}{K_2h_3 + K_3h_2} - \dfrac{2K_4\left(\bar{H}_3 - z_{st}\right)}{K_3h_4 + K_4h_3} & \text{otherwise} \end{cases} \\ \frac{d}{dx}\left[-\left(z_t - z_3\right)\frac{dz_t}{dx}\right] &= \begin{cases} \dfrac{2K_3\left(\bar{H}_3 - z_t\right)}{K_3(z_t - z_3) + K_4h_3} & \text{when } \ z_t < z_4 \\ \dfrac{2K_3\left(\bar{H}_3 - z_t\right)}{K_3(z_t - z_3) + K_4h_3} - \dfrac{2\left(\bar{H}_4 - z_{st}\right)}{h_4} & \text{otherwise.} \end{cases} \end{aligned} \tag{4.36}$$

A numerical solution for the mean hydraulic heads $H_i(x)$ is found and plotted as isobars in bottom graph of Figure 4.7 with the values of parameters as mentioned in Table 4.2. The blue curve in the 4th sub-layer is phreatic surface $z_t = \bar{H}_4$. A red line in the ditch area shows the level of stream water above datum. The $z_t(x)$ or $\bar{H}_4$ in the zone of surface water stream is plotted as blue dashed curve. This is the hydraulic head in the middle of underlying 4th sub-layer. The hydraulic head being above ground level means that the water level in a well in the 4th sub-layer will maintain that height.

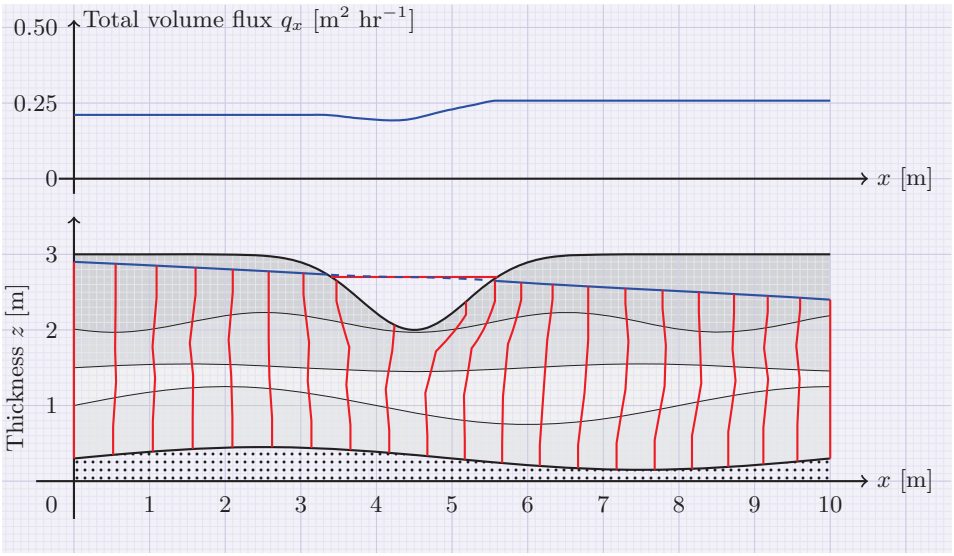

Figure 4.7: (Bottom) Isobars in a layered aquifer with a transverse running stream at the top. (Top) Total volume flux q_x [(m^3 hr^{-1}) m^{-1} = m^2 hr^{-1}] through the thickness of the aquifer. The parameters used in this simulation are given in Table 4.2.

Parameters	**Values**	**Units**
fluid dynamic viscosity μ	1.002×10^{-3}	[kg m^{-1} s^{-1}]
gravitaional acceleration g	9.8	[m s^{-2}]
fluid density ρ	1000	[kg m^{-3}]
permeabilities (K_1, K_2, K_3, K_4)	$(0.7, 1, 0.5, 0.1) \times 10^{-10}$	[m^2]

Table 4.2: Parameters used for the simulation shown in Figures 4.7 and 4.8.

The top graph in Figure 4.7 shows the total volume flux q_x [(m^3 hr^{-1}) m^{-1} = m^2 hr^{-1}] through the aquifer. One can observe that the q_x decreases in the aquifer for some initial zone of contact with the above lying stream. This is evident from the difference of water level in stream z_{st} (dashed blue) and the mean hydraulic head in the 4th sub-layer $\bar{H}_4$ (red) in the lower graph of Figure 4.7. Here, the mean hydraulic head in the 4th sub-layer is higher than the water table in the stream, causing flow up into the stream. After some distance, $\bar{H}_4$ drops and water begins to seep into the 4th sub-layer from the stream.

The phreatic surface $z_t(x)$ may also drop into the lower 3rd sub-layer, in which case

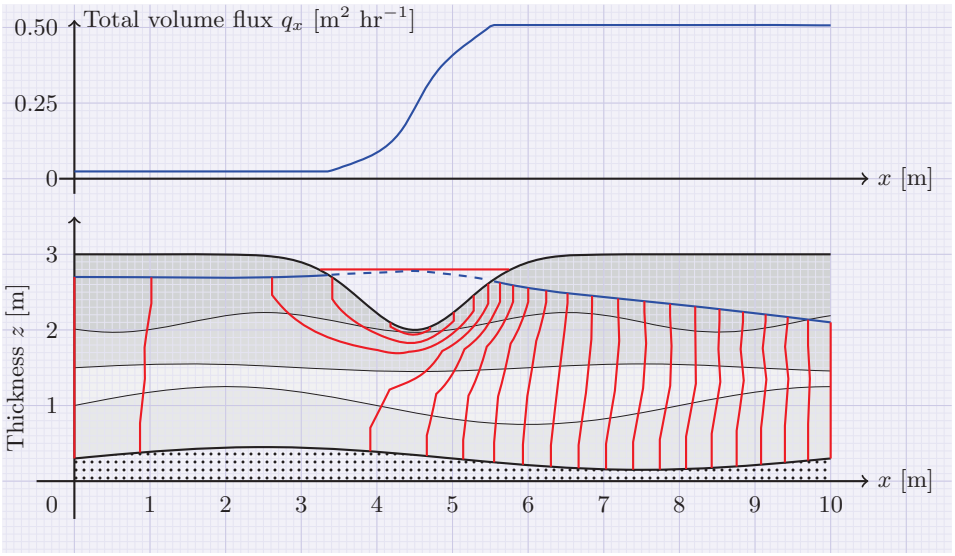

Figure 4.8: (Bottom) Isobars in a layered aquifer with a transverse running stream at the top. (Top) Total volume flux q_x [(m^3 hr^{-1}) m^{-1} = m^2 hr^{-1}] through the thickness of the aquifer. The parameters used in this simulation are given in Table 4.2.

$\bar{H}_3 = z_t$ and system (4.36) reduces to a system of 3 coupled ODE's as

$$\begin{aligned}
\frac{d}{dx}\left[-h_1\frac{d\bar{H}_1}{dx}\right] &= -\frac{2K_2\left(\bar{H}_1-\bar{H}_2\right)}{K_1h_2+K_2h_1}\\
\frac{d}{dx}\left[-h_2\frac{d\bar{H}_2}{dx}\right] &= \frac{2K_1\left(\bar{H}_1-\bar{H}_2\right)}{K_1h_2+K_2h_1}-\frac{2K_3\left(\bar{H}_2-z_t\right)}{K_2(z_t-z_2)+K_3h_2}\\
\frac{d}{dx}\left[-(z_t-z_2)\frac{dz_t}{dx}\right] &= \frac{2K_2(\bar{H}_2-z_t)}{K_2(z_t-z_2)+K_3h_2}.
\end{aligned} \tag{4.37}$$

The downstream boundary conditions on $\bar{H}_i$ can be taken as $\bar{H}_i(10) = 2.1$ to introduce this effect. A numerical solution can be found by solving (4.36) when z_t lies in the 4th sub-layer and by solving (4.37) when z_t lies in the 3rd sub-layer. Figure 4.8 shows this solution as isobars. One can observe bigger spacing between adjacent isobars upstream and smaller spacing downstream. This shows a lower pressure gradient upstream and higher downstream, i.e., a higher influx from the stream. The upper graph of total volume flux q_x shows this effect. There is a higher overall volume flux in this case compared to the case shown in Figure 4.7.

5

Pollutant Transport in Steady Fluid Flow

So far in this thesis, the movement of groundwater in the confined and the phreatic aquifers has been discussed while overlooking an important factor involved in the "quality" of groundwater. There are very rare chances of groundwater being polluted with bacteria as compared to the surface water but still some mineral and organic constituents are dissolved in groundwater in various concentrations. Some of those minerals are harmless and even good for health while others are harmful. In recent years, the growth of industry and population has added more soluble and insoluble constituents in groundwater. The municipal and industrial wastes, chemical fertilizers, herbicides and pesticides have infiltrated into the groundwater and have degraded the quality of water. In coastal areas, extensive pumping of freshwater may result in salty seawater intrusion into the fresh water aquifers.

The materials that pollute groundwater may be dissolved or be suspended in it. In the case of suspended materials, modelling becomes more challenging as water may get filtered as it passes through complex pores of the soil. Also, the physical properties of soil such as permeability and porosity may change with the passage of time. The problem of groundwater pollution should not be associated only with domestic or agricultural use, serious problems may arise when polluted groundwater emerges on the surface or enters a lake or river.

Fluid flow models for both the confined and the phreatic aquifers have been developed and solved for illustrative examples in Chapters 3 and 4, respectively. Once,

the fluid flow problem is solved, the velocity field in all the sub-layers of the aquifer is determined. Then, pollutant transport in both the confined and the phreatic aquifers could be modelled similarly.

5.1 Conceptual model

Let $c_i(x, y, t)$ be the average concentration [kg m^{-3}] of dissolved pollutant in water in the ith sub-layer of the aquifer that is composed of N sedimentary sub-layers. The pollutant advects with the water velocity and it disperses in all directions. Consider a control box in the ith sub-layer centred at the (x, y) horizontal point and which has small length Δx in the x-direction and a small width Δy in the y-direction as shown in Figure 5.1. The layer interfaces are not necessarily constant. The movement of the pollutant in and out of the control box is the result of the advective and dispersive fluxes from all six faces of the control box:

1. The advective flux of the pollutant into the control box from the x-direction through the wall of the control box at $x - \Delta x/2$ is $\Delta y \times q_{x_i} \bar{c}_i|_{(x-\Delta x/2,y)}$ [kg s^{-1}] and that from the y-direction through the wall at $y - \Delta y/2$ is $\Delta x \times q_{y_i} \bar{c}_i|_{(x,y-\Delta y/2)}$ [kg s^{-1}].

2. The advective flux out of the control box in the x-direction through the wall at $x + \Delta x/2$ is $\Delta y \times q_{x_i} \bar{c}_i|_{(x+\Delta x/2,y)}$ and that out of the control box in the y-direction through the wall at $y + \Delta y/2$ is $\Delta x \times q_{y_i} \bar{c}_i|_{(x,y+\Delta y/2)}$.

3. The total dispersive fluxes within the aquifer are the sum of the mechanical dispersive fluxes and molecular diffusive fluxes and if the x-axis is aligned with the main direction of groundwater flow then the off-diagonal entries of the symmetric tensor $\mathbf{D}$ shown in (2.10) are zero. In this case, the entries of the dispersion tensor for the ith sub-layer are

$$\begin{bmatrix} D_{x_i} & 0 & 0 \\ 0 & D_{y_i} & 0 \\ 0 & 0 & D_{z_i} \end{bmatrix} = \frac{1}{\phi_i h_i} \begin{bmatrix} \alpha_L |\mathbf{q}_i| & 0 & 0 \\ 0 & \alpha_T |\mathbf{q}_i| & 0 \\ 0 & 0 & \alpha_T |\mathbf{q}_i| \end{bmatrix}. \tag{5.1}$$

The two-dimensional dispersion tensor for vertically averaged flows when the x-axis is aligned with the main direction of flow is

$$\begin{bmatrix} D_{x_i} & 0 \\ 0 & D_{y_i} \end{bmatrix} = \frac{1}{\phi_i h_i} \begin{bmatrix} \alpha_L |\mathbf{q}_i| & 0 \\ 0 & \alpha_T |\mathbf{q}_i| \end{bmatrix}. \tag{5.2}$$

By Fick's law, the total dispersive flux into the control box through the wall at $x - \Delta x/2$ is $\Delta y \times \phi_i h_i(-D_{x_i}\partial\bar{c}_i/\partial x)|_{(x-\Delta x/2,y)}$ [kg s^{-1}] and that into the control box through the wall at $y - \Delta y/2$ is $\Delta x \times \phi_i h_i(-D_{y_i}\partial\bar{c}_i/\partial y)|_{(x,y-\Delta y/2)}$ [kg s^{-1}].

4. The total dispersive flux out of the control box through the wall at $x + \Delta x/2$ is $\Delta y \times \phi_i h_i(-D_{x_i}\partial\bar{c}_i/\partial x)|_{(x+\Delta x/2,y)}$ and that out of the control box through the wall at $y + \Delta y/2$ is $\Delta x \times \phi_i h_i(-D_{y_i}\partial\bar{c}_i/\partial y)|_{(x,y+\Delta y/2)}$.

5. The advective flux into the ith sub-layer from the lower $i-1$th sub-layer through the layer interface $z_{i-1}(x, y)$ is caused by the interlayer flux $r_{i-1}(x, y)$. The interlayer flux transfer $r_i(x, y)$ normal to the layer interface from the ith sub-layer to the $i+1$th sub-layer is given by (3.5) or (3.29) in a layered confined aquifer when vertically constant or different dynamic pressures are used, respectively. In a layered phreatic aquifer, $r_i(x, y)$ is given by (4.8) or (4.31) when vertically the same mean hydraulic head or different mean hydraulic heads are used for each sub-layer, respectively. The advective flux into the control box from the lower sub-layer is, therefore, $\Delta x\times\Delta y\times r_{i-1}\bar{c}_{i-1}\left(1+\operatorname{sgn}(r_{i-1})\right)/2$ [kg s^{-1}] and that out of the control box into the lower sub-layer is $\Delta x \times \Delta y \times r_{i-1}\bar{c}_i\left(1-\operatorname{sgn}(r_{i-1})\right)/2$ [kg s^{-1}], where $\bar{c}_{i-1}(x, y, t)$ is the concentration of the pollutant in the $i-1$th sub-layer. Similarly, the advective flux out of the control box into the upper $i+1$th sub-layer through the $z_i(x, y)$ layer interface is $\Delta x \times \Delta y \times \left(-r_i\bar{c}_i\left(1+\operatorname{sgn}(r_i)\right)/2\right)$ and that into the control box from the upper sub-layer is $\Delta x\times\Delta y\times\left(-r_i\bar{c}_{i+1}\left(1-\operatorname{sgn}(r_i)\right)/2\right)$, where $\bar{c}_{i+1}(x, y, t)$ is the concentration of the pollutant in the upper $i+1$th sub-layer.

6. The dispersive flux in and out of the control box from the upper layer interface $z_i(x, y)$ is proportional to the difference in concentrations $\bar{c}_{i+1} - \bar{c}_i$ in the neighbouring sub-layers and the constant of proportionality, say $\tau_i(x, y)$ [m s^{-1}] is called the *interlayer dispersive transfer coefficient* across the layer interface z_i. The τ_i can be approximated by using Fick's law and assuming a nominal pollution concentration, say $\gamma_i(x, y, t)$ at the layer interface $z_i(x, y)$. The dispersive fluxes above and below z_i must match, so

$$-\tau_i(\bar{c}_{i+1} - \bar{c}_i) \approx -\phi_{i+1}D_{z_{i+1}}(x, y)\left(\frac{\partial c}{\partial z}\right)_{z=z_i^+} \approx -\phi_i D_{z_i}(x, y)\left(\frac{\partial c}{\partial z}\right)_{z=z_i^-}. \quad (5.3)$$

The derivatives of the concentrations of the pollutant across z_i can be approximated by the finite difference formulae as:

$$-\tau_i(\bar{c}_{i+1} - \bar{c}_i) \approx -\phi_{i+1} D_{z_{i+1}}(x, y) \frac{\bar{c}_{i+1} - \gamma_i}{h_{i+1}/2}, \tag{5.4}$$

and

$$-\tau_i(\bar{c}_{i+1} - \bar{c}_i) \approx -\phi_i D_{z_i}(x, y) \frac{\gamma_i - \bar{c}_i}{h_i/2}, \tag{5.5}$$

equating the Right Hand Sides of (5.4) and (5.5), it is found that

$$\gamma_i \approx \frac{\phi_{i+1} D_{z_{i+1}} h_i \bar{c}_{i+1} + \phi_i D_{z_i} h_{i+1} \bar{c}_i}{\phi_{i+1} D_{z_{i+1}} h_i + \phi_i D_{z_i} h_{i+1}}. \tag{5.6}$$

Now putting (5.6) in (5.4) gives

$$\frac{1}{\tau_i} \approx \frac{h_i/2}{\phi_i D_{z_i}} + \frac{h_{i+1}/2}{\phi_{i+1} D_{z_{i+1}}}; \qquad 1 \leq i \leq N-1 \tag{5.7}$$

where $\tau_0 = \tau_N = 0$.

Thus the total pollutant dispersive flux into the control box from the bottom wall is $-\Delta x \times \Delta y \times \tau_{i-1}(\bar{c}_i - \bar{c}_{i-1})$ [kg s^{-1}] and that out of the control box through the top wall is $-\Delta x \times \Delta y \times \tau_i(\bar{c}_{i+1} - \bar{c}_i)$.

Suppose $f_{P_i}(x, y, t)$ [kg m^{-3} s^{-1}] is a source function of a distributed pollutant, averaged over the thickness of the ith sub-layer. The total change in mass of the pollutant in the control box in a small time Δt is $\phi_i h_i \Delta x \Delta y[\bar{c}_i(x, y, t + \Delta t) - \bar{c}_i(x, y, t)]$. Thus, a balance of the pollutant mass for the control box shown in Figure 5.1 can be written as

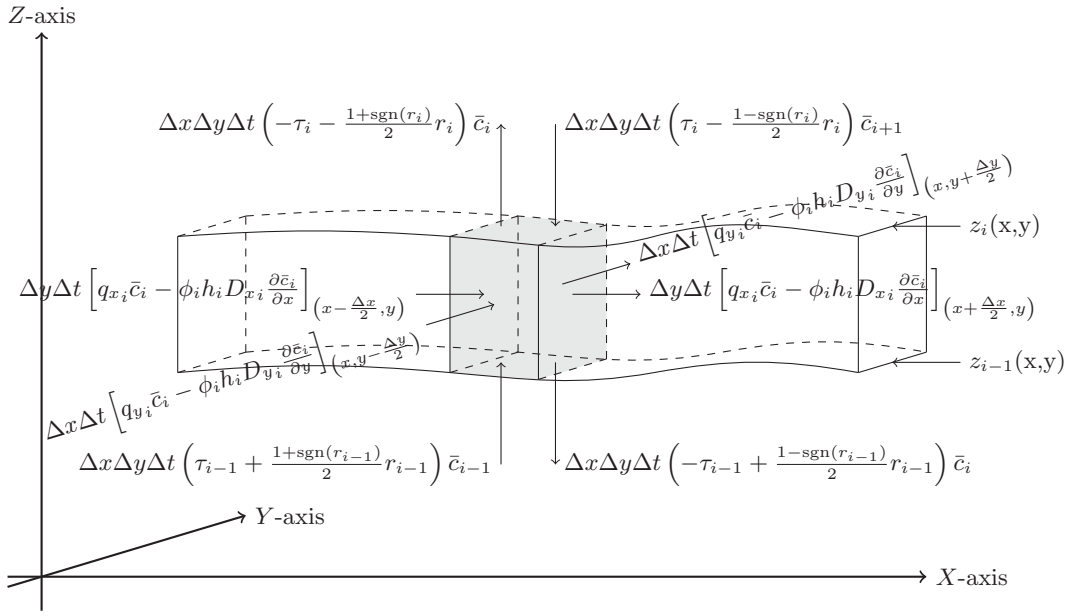

Figure 5.1: A schematic of the pollutant flow in a layered-aquifer.

$$
\begin{aligned}
&\phi_i h_i \Delta x \Delta y \left[\bar{c}_i(x,y,t+\Delta t)-\bar{c}_i(x,y,t)\right] \\
&= \Bigg[\Delta y q_{x_i}(x-\frac{\Delta x}{2},y)-\Delta y q_{x_i}(x+\frac{\Delta x}{2},y)+\Delta x q_{y_i}(x,y-\frac{\Delta y}{2})-\Delta x q_{y_i}(x,y+\frac{\Delta y}{2}) \\
&\quad +\Delta y\phi_i h_i\left(-D_{x_i}\frac{\partial \bar{c}_i}{\partial x}\right)_{(x-\frac{\Delta x}{2},y)}-\Delta y\phi_i h_i\left(-D_{x_i}\frac{\partial \bar{c}_i}{\partial x}\right)_{(x+\frac{\Delta x}{2},y)} \\
&\quad +\Delta x\phi_i h_i\left(-D_{y_i}\frac{\partial \bar{c}_i}{\partial y}\right)_{(x,y-\frac{\Delta y}{2})}-\Delta x\phi_i h_i\left(-D_{y_i}\frac{\partial \bar{c}_i}{\partial y}\right)_{(x,y+\frac{\Delta y}{2})} \\
&\quad +\Delta x\Delta y\left(\frac{1+\mathrm{sgn}(r_{i-1})}{2}r_{i-1}\bar{c}_{i-1}+\frac{1-\mathrm{sgn}(r_{i-1})}{2}r_{i-1}\bar{c}_i\right) \\
&\quad +\Delta x\Delta y\left(-\frac{1+\mathrm{sgn}(r_i)}{2}r_i\bar{c}_i-\frac{1-\mathrm{sgn}(r_i)}{2}r_i\bar{c}_{i+1}\right) \\
&\quad +\Delta x\Delta y\big(-\tau_{i-1}\left(\bar{c}_i-\bar{c}_{i-1}\right)+\tau_i\left(\bar{c}_{i+1}-\bar{c}_i\right)\big)+\Delta x\Delta y\phi_i h_i f_{P_i}(x,y,t)\Bigg]\Delta t. \qquad (5.8)
\end{aligned}
$$

Divide both sides of (5.8) by $\Delta x\Delta y\Delta t$ and allow $\Delta x, \Delta y, \Delta t \to 0$ to get [25]

$$\begin{aligned}\phi_i h_i \frac{\partial \bar{c}_i}{\partial t} &= \frac{\partial}{\partial x}\left(-q_{x_i}\bar{c}_i + \phi_i h_i D_{x_i}\frac{\partial \bar{c}_i}{\partial x}\right) + \frac{\partial}{\partial y}\left(-q_{y_i}\bar{c}_i + \phi_i h_i D_{y_i}\frac{\partial \bar{c}_i}{\partial y}\right) \\ &+ \left(\tau_{i-1} + \frac{1+\text{sgn}(r_{i-1})}{2}r_{i-1}\right)\bar{c}_{i-1} + \left(-\tau_{i-1} + \frac{1-\text{sgn}(r_{i-1})}{2}r_{i-1}\right)\bar{c}_i \\ &+ \left(-\tau_i - \frac{1+\text{sgn}(r_i)}{2}r_i\right)\bar{c}_i + \left(\tau_i - \frac{1-\text{sgn}(r_i)}{2}r_i\right)\bar{c}_{i+1} \\ &+ \phi_i h_i f_{P_i}(x,y,t). \end{aligned} \tag{5.9}$$

These are N linear, coupled partial differential equations and can generally be solved numerically with suitable boundary conditions.

5.2 Illustrations: confined aquifers

Fluid flow and pollutant transport in homogeneous and layered aquifer systems when top and bottom surfaces of the aquifer are impermeable are illustrated as examples:

5.2.1 Homogeneous aquifers

If thickness of the homogeneous aquifer varies in one horizontal direction (say x), then total volume flux q_x per unit aquifer width along x is constant. The advection-dispersion equation to predict averaged pollutant concentration $\bar{c}(x,t)$ over layer thickness is [25]

$$\phi h(x)\frac{\partial \bar{c}}{\partial t} = -q_x\frac{\partial \bar{c}}{\partial x} - \phi\frac{\partial}{\partial x}\left[h(x)D_x(x)\left(-\frac{\partial \bar{c}}{\partial x}\right)\right] + \phi h(x) f_P(x,t), \tag{5.10}$$

with initial and boundary conditions:

$$\begin{aligned} c(x,0^-) &= 0, \qquad -\infty < x < +\infty, \\ c(x,t) \to 0 \quad \text{as} \quad x \to -\infty, &\qquad c(x,t) \text{ is bounded as } x \to +\infty. \end{aligned} \tag{5.11}$$

Here $f_P(x,t)$ [kg m^{-3} s^{-1}] is a vertically averaged pollutant source function; the source may be distributed over some area or it may be a point source acting as a slice of input pollution. If there is an instantaneous plane source Q_P [kg m^{-2}] acting on $x = x_0$ and at time $t = t_0$, then $f_P(x,t) = Q_P\delta(x-x_0)\delta(t-t_0)$. For a continuous plane source acting on $x = x_0$ with a rate q_P [kg m^{-2} s^{-1}], $f_P(x,t) = q_P\delta(x-x_0)$.

This model equation is solved for certain special cases:

Example 5.2.1 *Thickness h of the homogeneous aquifer is constant, horizontal dispersion coefficient D_x [m^2 s^{-1}] is constant, and pollutant is injected continuously at $x = x_0$ with mass flow rate q_P [kg m^{-2} s^{-1}], so that $f_P(x,t) = q_P\delta(x - x_0)$.*

The steady-state solution of (5.10) subject to boundary conditions (5.11) can be found as [29]

$$\bar{c}(x) = \begin{cases} \frac{q_P}{\bar{U}} \exp\left(\frac{\bar{U}}{D_x}(x - x_0)\right) & \text{for } x \le x_0 \\ \frac{q_P}{\bar{U}} & \text{for } x \ge x_0 \end{cases} \tag{5.12}$$

where $\bar{U} = \bar{u}/\phi$ is the interstitial velocity of the fluid and is constant in this case. For an aquifer shown in Figure 5.2 (top), the solution is plotted in Figure 5.2 (middle). The fluid is flowing from left to right with a speed $\bar{u} = 0.1$ [m hr^{-1}] and the porosity of the aquifer is $\phi = 0.1$ [-]. The pollutant concentration steadies at a constant level downstream from the injection point. Upstream from the release point, it steadies at a level defined by the downstream advection by the fluid flow and the upstream dispersion. Thus, the higher the advection-dispersion ratio, the shorter the upstream tail of concentration profile, and vice versa.

Example 5.2.2 *Thickness profile h of the aquifer is constant, D_x a constant and the mass Q_P [kg m^{-2}] is injected instantaneously at $x = x_0$ at a time $t = 0$ [s].*

The analytic solution can be written as a Green's function [29]

$$\bar{c}(x,t) = \frac{Q_P}{\sqrt{4\pi D_x t}} \exp\left(-\frac{\left(x - \left(x_0 + \bar{U}t\right)\right)^2}{4D_x t}\right), \tag{5.13}$$

and is represented graphically in Figure 5.2 (bottom) in red solid and red dashed at two different times $t_1 = 0.5$ and $t_2 = 1.5$ [hr], respectively after release at $x = x_0$. It is clear that the distribution of the pollutant is symmetric around the point $x_0 + \bar{U}t$ and it is dispersed around this point by an amount which depends on the coefficient of dispersion D_x.

Example 5.2.3 *Aquifer thickness $h(x)$ varies in one horizontal x-direction, dispersion coefficient D_x is uniform and pollutant is injected with a constant mass flow rate q_P per unit area per unit time.*

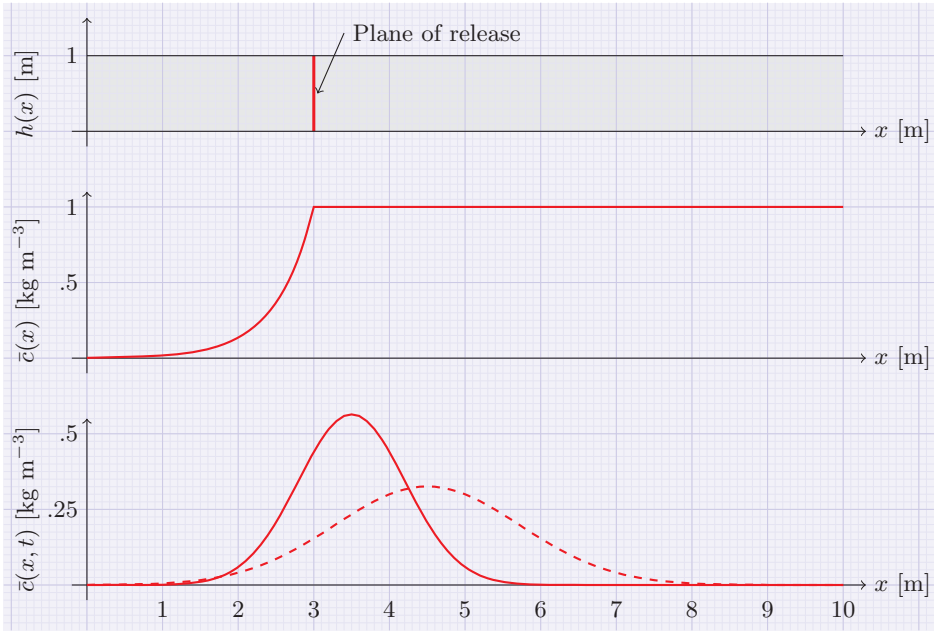

Figure 5.2: (Top) Homogeneous aquifer with uniform thickness. Plane of pollutant release is indicated as a red line. (Middle) Steady-state concentration solution in the aquifer when pollutant is injected at the indicated position with a rate $q_P = 1$ [kg m^2 hr^{-1}]. (Bottom) Concentration solutions at times $t_1 = 0.5$ [hr] (solid) and $t_1 = 1.5$ [hr] (dashed) after the pollutant of mass $Q_m = 1$ [kg m^{-2}] is injected instantaneously at the indicated position. Parameter values are: $\bar{U} = 1$ [m hr^{-1}], $\phi = 0.1$ [-] and $D_x = 0.5$ [m^2 hr^{-1}].

The steady-state analytic solution for continuous injection can be written as

$$\bar{c}(x) = \begin{cases} \frac{q_P \phi h(x_0)}{q_x} \exp\left(-\frac{q_x}{\phi D_x} \int_x^{x_0} \frac{1}{h(\xi)} d\xi \right) & \text{for } x < x_0 \\ \frac{q_P \phi h(x_0)}{q_x} & \text{for } x \geq x_0 \end{cases} \tag{5.14}$$

Thus, variations in thickness have no effect on the concentration level downstream of the release point. For a simple varying thickness profile $h(x) = 1 + 0.3\cos(\pi x + \pi/2)$ (Figure 5.3 top), the analytical solution is represented graphically in blue curve in Figure 5.3 (middle). The concentration level of the pollutant depends on thickness variations upstream of the release point.

Example 5.2.4 *Thickness varies in one horizontal direction, dispersion coefficient is uniform and pollutant of mass Q_m [kg m^{-2}] is injected instantaneously at time $t = 0$ as a plane source at position $x = x_0$.*

In general, for a non-uniform aquifer thickness, it is either not easy to find an analytic solution of (5.10) or not possible. For those cases numerical techniques are developed to compute pollutant concentration. The pollutant concentration computed by numerical methods in the same aquifer with thickness $h(x) = 1 + 0.3\cos(\pi x + \pi/2)$ (Figure 5.3 top) is plotted against x in the bottom plot of the same Figure at two times $t_1 = 0.5$ and $t_2 = 1.5$ [hr] in blue solid and blue dashed curves, respectively. Note the disturbance in the symmetry of the solution curves due to variations in thickness.

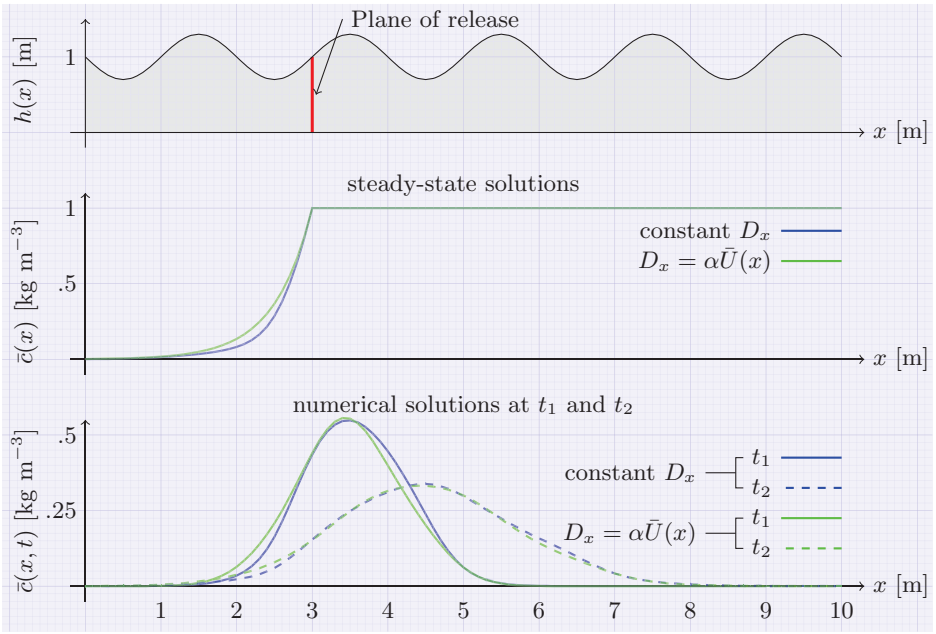

Figure 5.3: (Top) A homogeneous aquifer with varying thickness $h(x) = 1 + 0.3\cos(\pi x + \pi/2)$, the plane of pollutant release is marked as a red line. (Middle) Analytic steady-state solutions after continuous release of pollutant at the indicated position of the aquifer for a constant D_x (blue) and for $D_x = \alpha\bar{U}_x$ (green). (Bottom) Numerical solution snapshots at times $t_1 = 0.5$ [hr] (solid) and $t_2 = 1.5$ [hr] (dashed) after instantaneous release at the indicated position of the aquifer for a constant D_x (blue) and for $D_x = \alpha\bar{U}_x$ (green). Here $\alpha = 0.5$ [m], all other parameters are the same as in Figure 5.2.

Example 5.2.5 *Horizontal dispersion coefficient is proportional to the interstitial velocity of the fluid $\bar{U}(x)$, i.e., $D_x(x) = \alpha\bar{U}(x)$, where α [m] is dispersion length (dispersivity) that depends on the matrix structure (see for example, [11], [13] and [12]). Thickness varies in one horizontal direction and pollutant is injected continuously with mass flow rate q_P [kg m^{-2} s^{-1}].*

The steady-state analytic solution for the pollutant concentration in the same aquifer of Figure 5.3 (top) can easily be found as

$$\bar{c}(x) = \begin{cases} \frac{\phi q_P h(x_0)}{q_x} \exp\left(-\frac{1}{\alpha}(x_0 - x)\right) & \text{for } x < x_0 \\ \frac{\phi q_P h(x_0)}{q_x} & \text{for } x \geq x_0 \end{cases} \tag{5.15}$$

This solution is plotted in Figure 5.3 (middle) in green. In this case, the concentration level of the pollutant does not depend on thickness variations both upstream and downstream of the release point.

Example 5.2.6 *Pollutant is injected instantaneously as a plane source, thickness is non-uniform and* $D_x(x) = \alpha \bar{U}(x)$.

Numerical computation gives the concentration profile shown in Figure 5.3 (bottom) green plots at two times $t_1 = 0.5$ and $t_2 = 1.5$ [hr] in solid and dashed curves, respectively. The symmetry of concentration levels is disturbed again but not as much as for the case of constant dispersion coefficient D_x. This is because, as fluid passes through the narrower regions of the aquifer, it speeds up and, therefore, pollutant dispersion also increases.

Pollutant transport equation in a two-dimensional, confined, and single-layered aquifer can be written as [25]

$$\phi h \frac{\partial \bar{c}}{\partial t} = -q_x \frac{\partial \bar{c}}{\partial x} - q_y \frac{\partial \bar{c}}{\partial y} - \frac{\partial}{\partial x}\left[h\phi D_x \left(-\frac{\partial \bar{c}}{\partial x}\right)\right] - \frac{\partial}{\partial y}\left[h\phi D_y \left(-\frac{\partial \bar{c}}{\partial y}\right)\right] + h\phi f_P(x, y, t), \tag{5.16}$$

where $f_P(x, y, t)$ is vertically averaged pollutant distributed or a line source function. If $f_P(x, y, t)$ is an instantaneous line source function acting on $(x, y) = (x_0, y_0)$ at a time $t = t_0$ with a quantity Q_P [kg m^{-1}], then $f_P(x, y, t) = Q_P \delta(x - x_0)\delta(y - y_0)\delta(t - t_0)$. Similarly, if $f_P(x, y, t)$ is acting continuously on (x_0, y_0) at a time t_0 as a line source with an injection rate q_P [kg m^{-1} s^{-1}], then $f_P(x, y, t) = q_P \delta(x - x_0)\delta(y - y_0)$.

This equation can be solved numerically with suitable boundary conditions, i.e.,

$$\begin{aligned} &\bar{c}(x, y, 0^-) = 0, && -\infty \leq x \leq \infty, \quad 0 \leq y \leq W \\ &\bar{c}(-\infty, y, t) = 0, && \bar{c}(+\infty, y, t) \text{ is bounded,} \\ &\frac{\partial \bar{c}(x, 0, t)}{\partial y} = 0, && \frac{\partial \bar{c}(x, W, t)}{\partial y} = 0, \end{aligned} \tag{5.17}$$

where W is the width of the aquifer.

Example 5.2.7 *Pollutant is injected instantaneously at* $(x_0, y_0) = (10, 30)$ *as a line source at time* $t = 0$ *in quantity* Q_P *[kg* m^{-1}*] in a rectangular aquifer with thickness profile* $h(x, y) = 1 + 0.5\cos(\pi x/25)\cos(\pi y/20)$*;* $0 \le x \le 100, 0 \le y \le 80$.

Taking the dispersion coefficient to be proportional to the mean interstitial fluid velocity $\left|\bar{\mathbf{U}}\right| = |\bar{\mathbf{u}}/\phi|$ and aligning the x-axis with the main direction of groundwater flow, the longitudinal dispersion coefficient D_x and the transverse dispersion coefficient D_y as shown in (5.2), can be written as

$$D_x(x, y) = \alpha_L \frac{|\mathbf{q}(x, y)|}{\phi(x, y)h(x, y)}, \qquad D_y(x, y) = \alpha_T \frac{|\mathbf{q}(x, y)|}{\phi(x, y)h(x, y)}. \tag{5.18}$$

The vertically averaged pollutant concentration contours as predicted by the model at times $t_1 = 1$ [day] and $t_2 = 4$ [day] after release are shown in Figure 5.4. The pollutant concentration measured at the fixed point (80,30) of the aquifer plotted against time (usually known as the breakthrough curve) is also shown in the Figure 5.4.

It is obvious from the breakthrough curve that the pollutant concentration at (80,30) is practically zero until 2.5 [days] after the release of pollutant at (10,30). Then concentration starts increasing and reaches to its maximum i.e., almost 30 [g m^{-3}] at 4 [days] after the release. It again decreases and becomes almost zero again after 7 [days] of the release.

Figure 5.5 shows the total amount of the pollutant present in the aquifer and the total amount of the pollutant that flowed out from the downstream end $(100, y)$ of the aquifer. The sum of both the quantities always remains equal to the mass of pollutant released in the aquifer at (10,30).

Example 5.2.8 *The injection is continuous, with a rate* q_P *[kg* m^{-1} s^{-1}*], i.e.,* $f_P(x, y, t) = q_P\delta(x - x_0)\delta(y - y_0)$.

A numerical solution for steady-state pollutant concentration is shown in Figure 5.6. The pollutant steadily released advects along with the fluid flow and it disperses in longitudinal and transverse directions with the rates that depend on the fluid speed and longitudinal and transverse dispersivities $\alpha_L = 3$ and $\alpha_T = 0.7$ [m], respectively. The pollutant disperses upstream of the pollutant release point and its concentration balances at a level defined by the advection to dispersion ratio. The plume of the pollutant concentration would spread more in the transverse direction if α_T was higher.

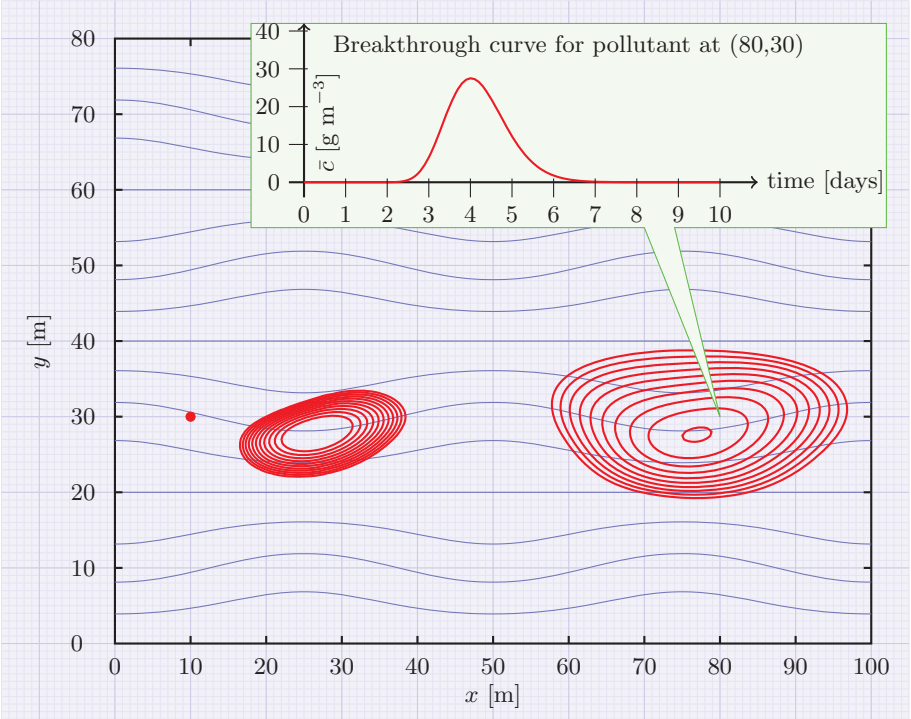

Figure 5.4: Pollutant concentration at times t_1 and t_2 after release at $(10, 30)$ as a line source (marked as •). The parameter values are: $\alpha_L = 3$, $\alpha_T = 0.7$ [m], $\phi = 0.1$ [-], $Q_P = 1$ [kg m^{-1}], $K/\mu = 1.155 \times 10^{-9}$ [m^3 s kg^{-1}]. The contours are plotted at $10^{-3(0.2)-1}$ [kg m^{-3}] from the outer contour to the inner ones. In this thesis, $a(b)c$ means a sequence $a, a + b, a + 2b, \cdots, c$.

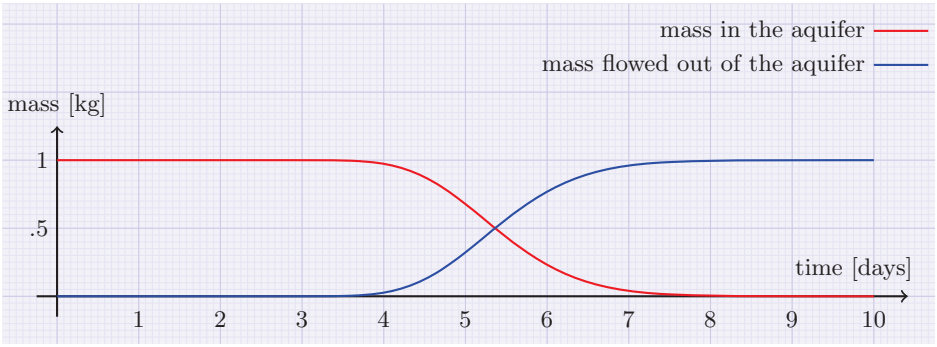

Figure 5.5: The total mass of the pollutant that has flowed out of the downstream boundary and the total mass in the aquifer, both plotted against time.

A breakthrough curve at the point (80,30) shows concentration of the pollutant against time. The concentration at (80,30) starts building up after almost 2.5 [days] and reaches

to a peak value of almost 50 [g m^{-3}] after almost 6 [days]. It stays constant at this peak value as long as the pollutant is being released with the same rate.

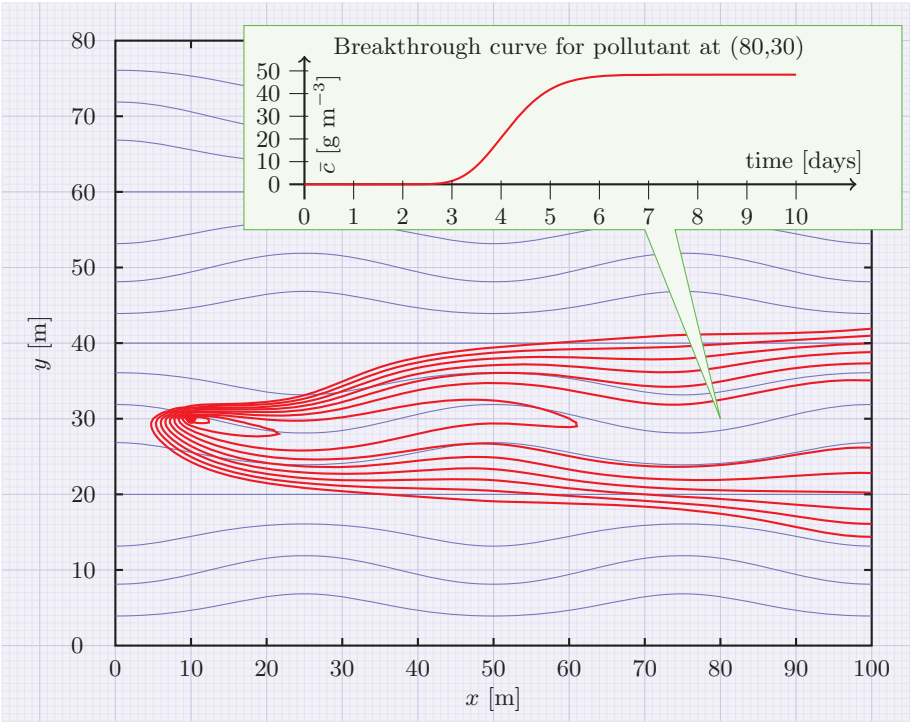

Figure 5.6: Steady-state pollution concentration when pollutant is released continuously at a constant rate $q_P = 1$ [kg m^{-1} day^{-1}] (all parameters are same as in Figure 5.4). The pollutant injection point is marked as •. The contours are plotted at $10^{-3(0.3)0}$ [kg m^{-3}] from the outer contour to the inner ones. Note: $a(b)c$ means $a, a+b, a+2b, \cdots, c$.

Figure 5.7 shows the rate with which the pollutant is being flowed out of the downstream boundary plotted against time. One can see that the pollutant starts flowing out of the boundary after almost 4 [days]. The rate of pollutant mass flowing out increases and finally becomes stable at a rate with which the pollutant is being released in the aquifer at (10,30).

Note that the pollutant mass released in all the above mentioned transport problems does not contain much water to effect the fluid flow in the aquifers. In the following example, injected fluid is contaminated with a pollutant and it does affect the fluid flow.

Example 5.2.9 *The two-dimensional homogeneous aquifer is being recharged with a contaminated fluid at* (x_1, y_1) *with a steady rate* F_I *[*$(m^3\ s^{-1})\ m^{-1} = m^2\ s^{-1}$*] and*

Figure 5.7: The rate of pollutant mass that is flowing out of the downstream boundary of the aquifer plotted against time.

fluid is being pumped out from (x_2, y_2) *with a rate* F_W *[*$(m^3\ s^{-1})\ m^{-1} = m^2\ s^{-1}$*]. The concentration of the pollutant in the injected fluid is* C_P*.*

Consider again the two-dimensional homogeneous aquifer shown in Figure 3.1 with a fluid injection well of strength $F_I = 86.4$ [m^2 day^{-1}] at $(x_1, y_1) = (40, 50)$ and a fluid withdrawal well of strength $F_W = 86.4$ [m^2 day^{-1}] at $(x_2, y_2) = (80, 30)$ and whose fluid flow problem is solved and plotted (isobars and streamlines) in Figure 3.5. Suppose that the injected fluid is polluted with a hazardous chemical whose concentration in the fluid is $C_P = 1$ [kg m^{-3}].

A numerical solution of steady-state pollutant concentration is plotted in Figure 5.8. Streamlines are also plotted in blue to see the fluid flow paths. The dispersivities are the same as in the simulation whose results are plotted in Figure 5.6. Note that the pollutant seems to have spread more in the transverse direction compared to that in Figure 5.8, whereas dispersivities are the same in both the simulations. This is because the polluted fluid that is being injected at (40,50) makes its way by spreading apart the clean groundwater that is flowing from the upstream. Hence, a plateau of concentration profile is observed downstream of the injection well. The pumping well at (80,30) is withdrawing water at a constant rate of F_W. A breakthrough curve is shown at the pumping well which shows concentration of the pollutant in the pumped water plotted against time. The peak concentration at the pumping well is smaller than that in the middle of plateau because some of the clean water is also being pumped out here (see the streamlines coming from low concentration zone and ending at the pumping well).

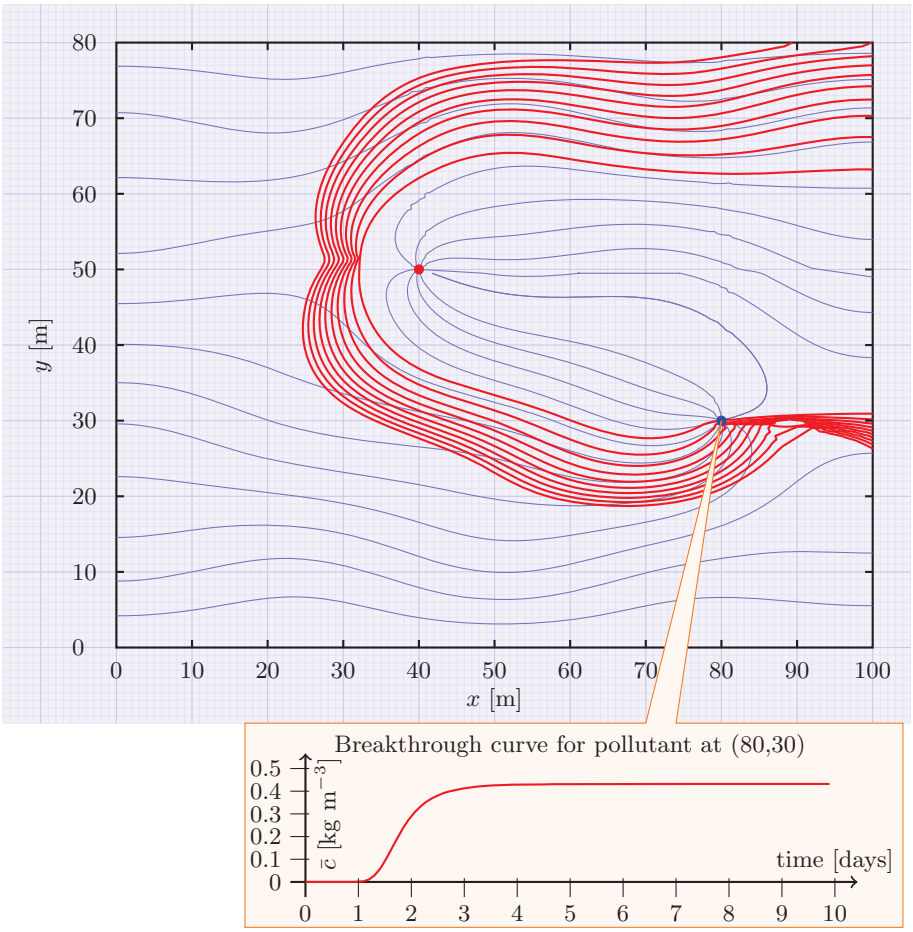

Figure 5.8: Steady-state pollution concentration when water in the recharge well (marked as •) is contaminated with concentration 1 [kg m^{-3}] (all parameters are same as in Figure 5.6). The pumping well is marked as •.The contours are plotted at $10^{-3(0.3)0}$ [kg m^{-3}] from the outer contour to the inner ones.

5.2.2 One-dimensional multi-layered aquifers

The mass-balance equation for a multi-layered one-dimensional aquifer composed of N sedimentary layers can be written as

$$\begin{aligned}\phi_i h_i \frac{\partial \bar{c}_i}{\partial t} &= \frac{\partial}{\partial x}\left[-q_{x_i}\bar{c}_i + \phi_i h_i D_{x_i}\frac{\partial \bar{c}_i}{\partial x}\right] + \left[\tau_{i-1} + \frac{1+\text{sgn}(r_{i-1})}{2}r_{i-1}\right]\bar{c}_{i-1} \\ &+ \left[-\tau_{i-1} + \frac{1-\text{sgn}(r_{i-1})}{2}r_{i-1}\right]\bar{c}_i + \left[-\tau_i - \frac{1+\text{sgn}(r_i)}{2}r_i\right]\bar{c}_i \\ &+ \left[\tau_i - \frac{1-\text{sgn}(r_i)}{2}r_i\right]\bar{c}_{i+1} + \phi_i h_i f_{Pi}(x,t) \quad \text{for} \quad 1 \le i \le N. \end{aligned} \tag{5.19}$$

Here total volumetric flux q_x through the whole aquifer is constant. As an illustration, a one-dimensional multi-layered model is tested on a homogeneous aquifer of constant thickness against the tracer transport model equation for horizontal fluid flow with impervious top and bottom boundaries. The tracer transport equation for horizontal fluid flow in such aquifer is written as

$$\phi h \frac{\partial \bar{c}}{\partial t} = -q_x \frac{\partial \bar{c}}{\partial x} + \phi h D_x \frac{\partial^2 \bar{c}}{\partial x^2} + \phi h D_z \frac{\partial^2 \bar{c}}{\partial z^2} + \phi h f(x,z,t). \tag{5.20}$$

Here D_x and D_z are horizontal and vertical dispersion coefficients respectively, and $f(x,z,t)$ is a distributed or a line pollutant source function. The source function, $f(x,z,t) = Q_m\delta(x-x_0)\delta(z-z_0)\delta(t)$ is a line source of Q_P [kg m^{-1}] released at $(x,z) = (x_0,z_0)$ at time $t=0$. If coordinates are transformed as $X = x - \bar{U}_x t$, $Z = z$, and $s = t$ and then $\bar{c}(x,y,t)$ is replaced with $\hat{\bar{c}}(X,Z,s)$ in the new coordinates (X,Z,s), then (5.20) takes the form

$$-\bar{U}_x\frac{\partial \hat{\bar{c}}}{\partial X} + \frac{\partial \hat{\bar{c}}}{\partial s} = -\bar{U}_x\frac{\partial \hat{\bar{c}}}{\partial X} + D_x\frac{\partial^2 \hat{\bar{c}}}{\partial X^2} + D_z\frac{\partial^2 \hat{\bar{c}}}{\partial Z^2} + Q_P\delta(X-x_0)\delta(Z-z_0)\delta(s),$$

or

$$\frac{\partial \hat{\bar{c}}}{\partial s} = D_x\frac{\partial^2 \hat{\bar{c}}}{\partial X^2} + D_z\frac{\partial^2 \hat{\bar{c}}}{\partial Z^2} + Q_P\delta(X-x_0)\delta(Z-z_0)\delta(s). \tag{5.21}$$

Its solution can be written as [29]

$$\hat{\bar{c}}(X,Z,s) = \frac{Q_P}{4\pi s\sqrt{D_x D_z}}\exp\left(-\frac{(X-x_0)^2}{4D_x s} - \frac{(Z-z_0)^2}{4D_z s}\right). \tag{5.22}$$

Writing concentration back in the original coordinates

$$\bar{c}(x,z,t) = \frac{Q_P}{4\pi t\sqrt{D_x D_z}}\exp\left(-\frac{((x-x_0)-\bar{U}_x t)^2}{4D_x t} - \frac{(z-z_0)^2}{4D_z t}\right). \tag{5.23}$$

Note that this solution is for infinite boundaries. When the top boundary z_t and the bottom boundary z_b of the aquifer are finite, then the boundary conditions for the pollutant concentration on these boundaries are

$$\frac{\partial \bar{c}}{\partial z}(x,z_b,t) = \frac{\partial \bar{c}}{\partial z}(x,z_t,t) = 0.$$

To overcome this difficulty on the upper boundary z_t, one may assume to have infinite many identical aquifers above this aquifer with the pollutant release points located at such vertical positions, so that the interfaces between these horizontally uniform aquifers act like mirrors. This condition will help to make sure that the boundary condition $\partial\bar{c}/\partial z(x, z_t, t) = 0$ is satisfied. Similarly, an infinite number of identical aquifers on the lower side may also be assumed with the pollutant injection points located at levels to satisfy the other boundary condition.

In this case, constrained to boundary conditions stated above $\bar{c}(x, z, t)$ can be written as

$$\begin{aligned}
\bar{c}(x,z,t) &= \frac{Q_P}{4\pi t\sqrt{D_x D_z}} e^{-\frac{((x-x_0)-\bar{U}_x t)^2}{4D_x t}} \Bigg[e^{-\frac{(z-z_0)^2}{4D_z t}} + e^{-\frac{(z-2h+z_0)^2}{4D_z t}} + e^{-\frac{(z-2h-z_0)^2}{4D_z t}} \\
&\quad + e^{-\frac{(z-4h+z_0)^2}{4D_z t}} + e^{-\frac{(z-4h-z_0)^2}{4D_z t}} + \cdots \\
&\quad + e^{-\frac{(z+z_0)^2}{4D_z t}} + e^{-\frac{(z+2h-z_0)^2}{4D_z t}} + e^{-\frac{(z+2h+z_0)^2}{4D_z t}} + e^{-\frac{(z+4h-z_0)^2}{4D_z t}} \\
&\quad + e^{-\frac{(z+4h+z_0)^2}{4D_z t}} + \cdots \Bigg] \\
&= \frac{Q_P}{4\pi t\sqrt{D_x D_z}} e^{-\frac{((x-x_0)-\bar{U}_x t)^2}{4D_x t}} \sum_{n=-\infty}^{\infty} \left(e^{-\frac{(z+2nh+z_0)^2}{4D_z t}} + e^{-\frac{(z+2nh-z_0)^2}{4D_z t}} \right)
\end{aligned}$$

Here both the series converge (trivially) as $h > 0$. Consider the first series $\sum_{n=-\infty}^{\infty} e^{-\frac{(z+2nh+z_0)^2}{4D_z t}}$,

$$\begin{aligned}
\sum_{n=-\infty}^{\infty} e^{-\frac{(z+2nh+z_0)^2}{4D_z t}} &= \sum_{n=-\infty}^{\infty} e^{-\left(\frac{z+2nh+z_0}{2\sqrt{D_z t}}\right)^2} \\
&= e^{-\frac{(z+z_0)^2}{4D_z t}} \sum_{n=-\infty}^{\infty} e^{-\frac{n^2h^2}{D_z t} - \frac{nh(z+z_0)}{D_z t}} \\
&= e^{-\frac{(z+z_0)^2}{4D_z t}} \sum_{n=-\infty}^{\infty} q^{n^2} e^{2in\nu_1}.
\end{aligned}$$

Here $q = \exp\left(-h^2/(D_z t)\right)$ and $\nu_1 = ih(z + z_0)/(2D_z t)$, then $|q| < 1$, since $h^2/(D_V t) > 0$. This series can thus be written as a Jacobi Theta function of the third type (in terms of the nome $q = e^{i\pi\tau}$) [10] as

$$\sum_{n=-\infty}^{\infty} e^{-\frac{(z+2nh+z_0)^2}{4D_z t}} = e^{-\frac{(z+z_0)^2}{4D_z t}} \theta_3(\nu_1, q), \tag{5.24}$$

where ν_1 is a complex variable and $q = \exp(i\pi\tau) \in \mathbb{C}$ (real in this case) is a parameter with $\tau = ih^2/(\pi D_z t)$ having a positive imaginary part (upper half plane). For a fixed τ

(i.e., for a fixed t) this becomes a Fourier series of a periodic entire function in variable ν_1 with a period π. Similarly, taking $\nu_2 = ih(z - z_0)/(2D_z t)$, the second series can be written as

$$\sum_{n=-\infty}^{\infty} e^{-\frac{(z+2nh-z_0)^2}{4D_z t}} = e^{-\frac{(z-z_0)^2}{4D_z t}} \theta_3(\nu_2, q). \tag{5.25}$$

Thus, the pollutant concentration can be written as

$$\bar{c}(x,z,t) = \frac{Q_P}{4\pi t\sqrt{D_x D_z}} e^{-\frac{((x-x_0)-\bar{U}_x t)^2}{4D_x t}} \left(e^{-\frac{(z+z_0)^2}{4D_z t}} \theta_3(\nu_1, q) + e^{-\frac{(z-z_0)^2}{4D_z t}} \theta_3(\nu_2, q) \right). \tag{5.26}$$

The first Theta function $\theta_3(\nu_1, q)$ is symmetrical around $\nu_1 = 0$, i.e., $z = -z_0$ and the second Theta function $\theta_3(\nu_2, q)$ is symmetrical around $z = z_0$. The snapshot of the resultant solution (5.26) is plotted for two different times t_1 and t_2 in Figure 5.9.

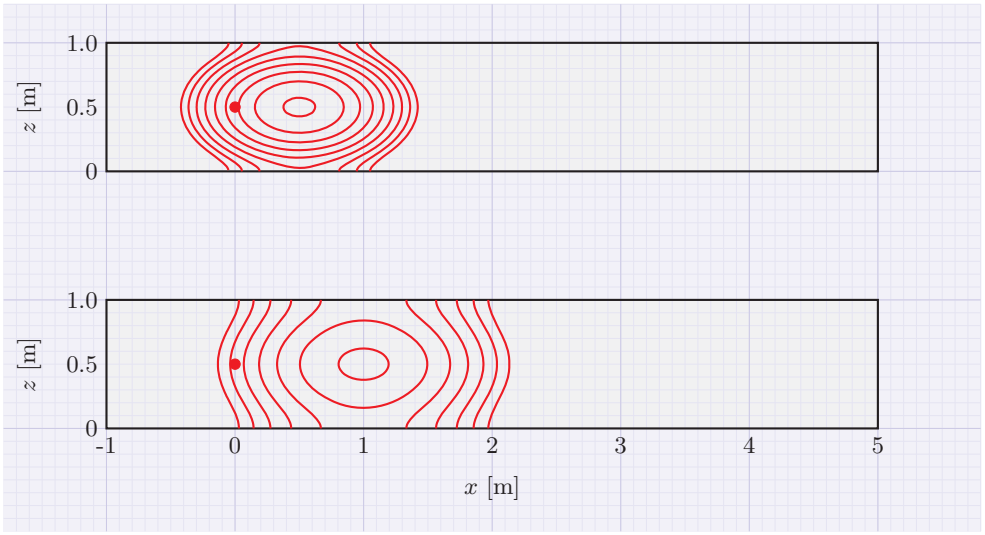

Figure 5.9: Analytic solution of the pollutant concentration in a homogeneous aquifer at times $t_1 = 0.5$ and $t_2 = 1.0$ [hr] after release when $Q_m = 1/11$ [kg m^{-1}] is released at $(0, 0.5)$ as a line source (marked as •). The parameter values are: $D_H = 0.15$ [m^2 hr^{-1}], $D_z = 0.05$ [m^2 hr^{-1}], $\bar{u} = 0.1$ [m hr^{-1}], $\phi = 0.1$ [-]. The contours are plotted at $10^{-2(0.15)-0.8}$ [kg m^{-3}] from the outer contour to the inner ones.

The same homogeneous aquifer is discretized in 11 layers and the layered model (5.19) is applied to compare the results with those of (5.26) when the same amount of the pollutant is injected as a plane source in layer 6 as shown in Figure 5.10. The concentration profile in this case is quite similar to that in Figure 5.9.

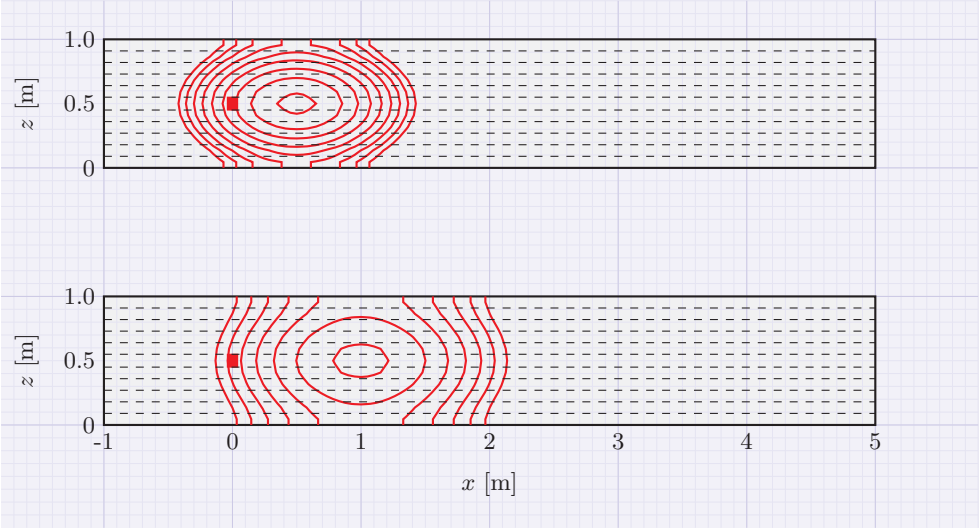

Figure 5.10: Numerical solution of the pollutant concentration in a homogeneous aquifer at times $t_1 = 0.5$ and $t_2 = 1.0$ [hr] after release when aquifer is discretized in 11 layers and $Q_P = 1$ [kg m^{-2}] pollutant is assumed to be released as a vertical plane source at $x = 0$ (marked as a vertical thick red bar) in the 6th layer of the aquifer. The parameter values are the same as in Figure 5.9 and the contours are also plotted at the same levels.

5.2.3 Signalled sources

If a pollutant source is active for a certain interval of time $t_1 \leq t \leq t_2$ and it is distributed over a region $x_1 \leq x \leq x_2$, then $f_{Pi}(x,t) = q_P$ [kg m^{-3} s^{-1}] for $t_1 \leq t \leq t_2$ and $x_1 \leq x \leq x_2$. As an example, this kind of problem is solved when a source is active on the surface of a homogeneous aquifer at $-5/3 \leq x \leq 5/3$ [m] during $0 \leq t \leq 1.2$ [hr]. The homogeneous aquifer may be discretized vertically in different layers and model (5.19) may be applied by assuming the source to be available only in the top sub-layer. Ten layers have been assumed here and the concentration contours are plotted in Figure 5.11 at times $t = 1.2$ and $t = 2.0$ [hr]. The bold line at the top $-5/3 \leq x \leq 5/3$ [m] shows the region where the source is active during $0 \leq t \leq 1.2$ [hr].

5.2.4 Layered aquifer with a point pollutant source with negligible fluid recharge

When a pollutant is injected in a confined aquifer, it advects with the fluid flow and disperses in all directions, the rate of which depends on the porous structure and the fluid speed. As an illustration, pollutant transport in a homogeneous aquifer is

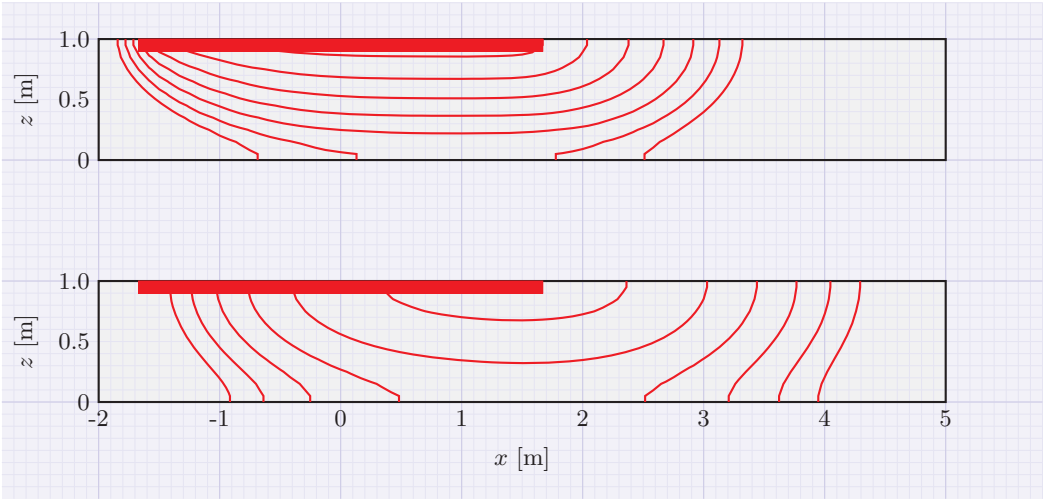

Figure 5.11: Concentration contours as predicted by the model at times $t = 1.2$ and $t = 2.0$ [hr]. The region of pollutant release is marked as a horizontal thick red bar at the top. The parameter values are: $q_x = 0.1$ [m^2 hr^{-1}], $q_P = 1$ [kg m^{-3} hr^{-1}], $D_x = 0.15$ [m^2 hr^{-1}], $D_z = 0.05$ [m^2 hr^{-1}], $\phi = 0.1$ [-]. The contours are plotted at $10^{-1(0.25)0.5}$ [kg m^{-3}] from the outer contour to the inner ones.

compared to that in a non-homogeneous aquifer consisting of three different layers where both the horizontal and the vertical dispersion coefficients are assumed constant. The homogeneous and the non-homogeneous aquifers are shown at the top and the bottom of Figure 5.12, respectively. The aquifers are discretized vertically in further layers in order to get better results for plotting purposes. Here, the homogeneous aquifer is discretized into 20 layers with all having the same thicknesses proportional to the total thickness of the aquifer. The three different layers of the bottom non-homogeneous aquifer are discretized further into 7, 6 and 7 sub-layers from bottom to top, respectively. Within each layer, the sub-layer thicknesses are chosen to be equal. A pollutant Q_{P_1} [kg m^{-2}] is injected in a sub-layer of the homogeneous aquifer containing the point $(x_0, z_0) = (2, 1.5)$ as a plane source as shown by a red rectangle in Figure 5.12. If $h_{j_1}(x_0)$ is the thickness of the jth layer containing the injection point in the homogeneous aquifer and $h_{k_1}(x_0)$ is the thickness of the kth layer in the non-homogeneous aquifer, then $Q_{P_2} = Q_{P_1} h_{j_1}/h_{k_2}$ [kg m^{-2}] pollutant is assumed to be injected in the non-homogeneous aquifer, so that the total mass of the pollutant remains the same in both the aquifers. Assuming the parameters shown in Table 5.1, the model is applied to both the aquifers and the predicted contours are plotted at two

different times $t_1 = 3$ [hr] and $t_2 = 7$ [hr].

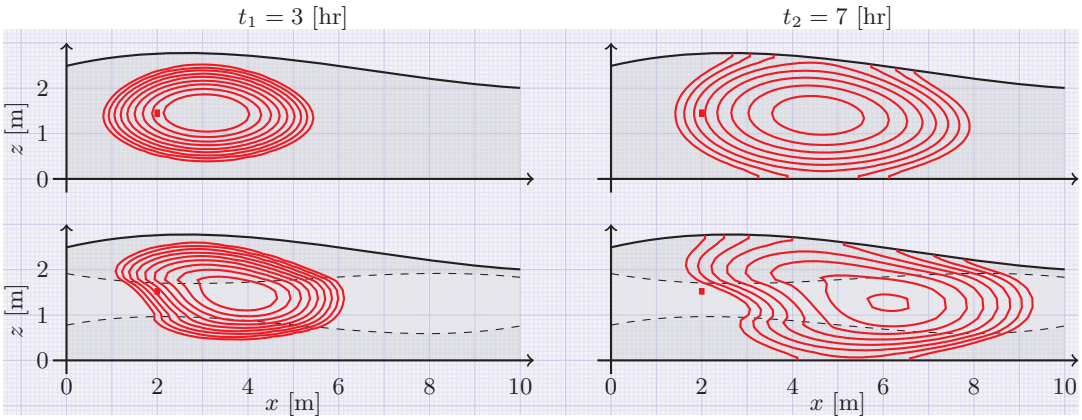

Figure 5.12: Pollutant concentration contours at times t_1 and t_2 after it is injected instantaneously as a planar strip source indicated as a red rectangle in the layer containing (2,1.5). The aquifer at the top is a homogeneous aquifer and the bottom one is non-homogeneous with the middle layer being more permeable. The contours are plotted at the same levels from the outer contours to the inner ones on an equally spaced logarithmic scale $10^{-2(.2)-0.4}$ [kg m^{-3}]. The values of the parameters used are mentioned in Table 5.1.

The pollutant in the higher permeability middle layer of the non-homogeneous aquifer seems to move faster due to higher fluid speed as compared to the outer layers. The pollutant concentration contours in the homogeneous aquifer are disturbed from being symmetric due to only varying thickness of the aquifer whereas in the non-homogeneous aquifer, difference in permeabilities of the layers also plays a role in interlayer fluid flux (and hence pollutant flux) and different fluid speeds in different layers. Note that the total volume flux q_x is assumed the same for both the aquifers in this example, although the dynamic pressure gradient in the two aquifers differs due to the difference in permeabilities (look at (3.18) for explanation).

5.2.5 A lens in a confined aquifer

A one-dimensional varying thickness confined aquifer with a sub-layer of finite length is considered here for illustration. It is assumed that the permeability of the sub-layer K_l is smaller than the permeability K of the rest of the homogeneous aquifer. For the purpose of implementation of numerical procedure, the sub-layer can be assumed to exist all over the extent of the aquifer with a negligible constant thickness $\delta > 0$ where

Parameters	Values	Units
The injected mass Q_{P_1} in the homogeneous aquifer	1	[kg m^{-2}]
Porosity ϕ of both the aquifers	0.1	[-]
Permeability of the homogeneous aquifer K	6.55×10^{-8}	[m^2]
Permeabilities (K_1, K_2, K_3) of the layers of the non-homogeneous aquifer (from bottom to top)	$(.4, 1, .4) \times 10^{-7}$	[m^2]
Coefficient of horizontal dispersion D_x	0.10	[m^2 hr^{-1}]
Coefficient of vertical dispersion D_z	0.02	[m^2 hr^{-1}]
Total volume flux through the whole aquifer q_x (both aquifers)	0.1	[m^2 hr^{-1}]

Table 5.1: Parameters used in Figure 5.12

it does not exist. This is a reasonable assumption, as $\nabla \cdot \mathbf{q}_i = 0$ in (3.5) as thickness becomes constant, i.e., $h_i = \delta$ and it suggests that $r_i(x, y) = r_{i-1}(x, y)$, i.e., almost all of the fluid entering from any of the neighbouring layers goes into the neighbouring layer on the other side. That is, this narrow sub-layer acts *almost* as an interface. Moreover, if $\phi_{i-1}, \phi_i, \phi_{i+1}$ and $D_{z_{i-1}}, D_{z_i}, D_{z_{i+1}}$ are the porosities and coefficients of dispersion in z-direction in the $i-1$th, ith and the $i+1$th sub-layers, respectively then the effective porosity below the centre of the ith sub-layer to the centre of the $i-1$th sub-layer is $(\delta\phi_i + h_{i-1}\phi_{i-1})/(\delta + h_{i-1})$ and the effective coefficient of vertical dispersion is $(\delta D_{z_i} + h_{i-1}D_{z_{i-1}})/(\delta + h_{i-1})$. Similarly, the effective porosity and the effective coefficient of vertical dispersion from the middle of ith sub-layer to the middle of $i+1$th sub-layer are $(h_{i+1}\phi_{i+1} + \delta\phi_i)/(h_{i+1} + \delta)$ and $(h_{i+1}D_{z_{i+1}} + \delta D_{z_i})/(h_{i+1} + \delta)$, respectively. Then, by matching dispersive fluxes above and below the middle of the ith sub-layer, the resultant interlayer transfer coefficient $\tau_R(x, y)$ can be approximated by using Fick's law above and below the middle of the ith sub-layer as

$$\begin{aligned} -\tau_R(\bar{c}_{i+1} - \bar{c}_{i-1}) &\approx -\frac{h_{i+1}\phi_{i+1} + \delta\phi_i}{h_{i+1} + \delta} \times \frac{h_{i+1}D_{z_{i+1}} + \delta D_{z_i}}{h_{i+1} + \delta} \times \frac{\bar{c}_{i+1} - \bar{c}_i}{(h_{i+1} + \delta)/2} \\ &\approx -\frac{\delta\phi_i + h_{i-1}\phi_{i-1}}{\delta + h_{i-1}} \times \frac{\delta D_{z_i} + h_{i-1}D_{z_{i-1}}}{\delta + h_{i-1}} \times \frac{\bar{c}_i - \bar{c}_{i-1}}{(\delta + h_{i-1})/2} \end{aligned} \tag{5.27}$$

which, on solving for $\bar{c}_i$ gives

$$\bar{c}_i \approx \frac{\frac{h_{i+1}\phi_{i+1}+\delta\phi_i}{h_{i+1}+\delta}\frac{h_{i+1}D_{z_{i+1}}+\delta D_{z_i}}{h_{i+1}+\delta}(\delta+h_{i-1})\bar{c}_{i+1} + \frac{\delta\phi_i+h_{i-1}\phi_{i-1}}{\delta+h_{i-1}}\frac{\delta D_{z_i}+h_{i-1}D_{z_{i-1}}}{\delta+h_{i-1}}(h_{i+1}+\delta)\bar{c}_{i-1}}{\frac{h_{i+1}\phi_{i+1}+\delta\phi_i}{h_{i+1}+\delta}\frac{h_{i+1}D_{z_{i+1}}+\delta D_{z_i}}{h_{i+1}+\delta}(\delta+h_{i-1}) + \frac{\delta\phi_i+h_{i-1}\phi_{i-1}}{\delta+h_{i-1}}\frac{\delta D_{z_i}+h_{i-1}D_{z_{i-1}}}{\delta+h_{i-1}}(h_{i+1}+\delta)}. \tag{5.28}$$

When $\delta \to 0$, this reduces to

$$\bar{c}_i \approx \frac{\phi_{i+1}D_{z_{i+1}}h_{i-1}\bar{c}_{i+1} + \phi_{i-1}D_{z_{i-1}}h_{i+1}\bar{c}_{i-1}}{\phi_{i+1}D_{z_{i+1}}h_{i-1} + \phi_{i-1}D_{z_{i-1}}h_{i+1}}. \tag{5.29}$$

Thus, the resultant interlayer transfer coefficient becomes

$$\frac{1}{\tau_R} \approx \frac{(\delta+h_{i-1})/2}{\frac{\delta\phi_i+h_{i-1}\phi_{i-1}}{\delta+h_{i-1}}\frac{\delta D_{z_i}+h_{i-1}D_{z_{i-1}}}{\delta+h_{i-1}}} + \frac{(h_{i+1}+\delta)/2}{\frac{h_{i+1}\phi_{i+1}+\delta\phi_i}{h_{i+1}+\delta}\frac{h_{i+1}D_{z_{i+1}}+\delta D_{z_i}}{h_{i-1}+\delta}}, \tag{5.30}$$

allowing $\delta \to 0$, (5.30) approaches to

$$\frac{1}{\tau_R} \approx \frac{h_{i-1}/2}{\phi_{i-1}D_{z_{i-1}}} + \frac{h_{i+1}/2}{\phi_{i+1}D_{z_{i+1}}}. \tag{5.31}$$

This interlayer transfer coefficient is same as if there was no thin ith sub-layer in between. Now, if the sub-layer of finite length (lens) is as shown in the bottom two plots of Figure 5.13, it can be assumed to be present and have infinitesimal thickness all along the length of the aquifer where it does not exist.

The whole aquifer, then, can be discretized vertically in further sub-layers for implementation of the simplified layered model. The bottom two plots in Figure 5.13 show contour plots of tracer concentration after two different times of instantaneous tracer release mass 1 [kg] at the indicated position. The sub-layer has a lower permeability here and seems to behave as more resistant to the fluid and tracer flow (bottom left in Figure 5.13). Moreover, it traps tracer within it as tracer flows through it and keeps leaking while most of it has passed through the neighbouring higher permeability regions (bottom right in Figure 5.13).

The same amount of tracer transport is simulated in a totally homogeneous aquifer of the same thickness profile except it does not have a finite sub-layer of different permeability. This aquifer is also vertically discretized into further sub-layers and the resultant contour plots are shown in the top two plots of Figure 5.13. The asymmetry caused by the less permeable sub-layer is obvious. The contours in all four plots are plotted on a logarithmic scale in increasing order from the outer contours to the inner ones.

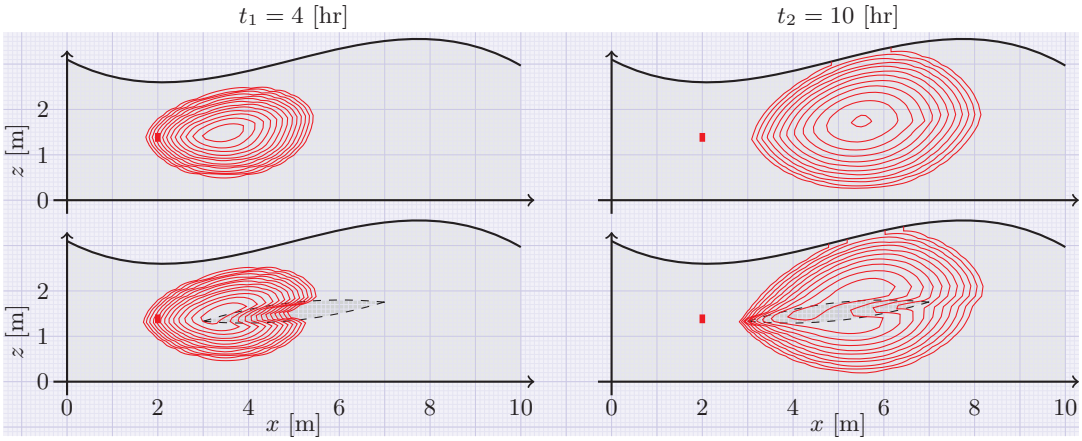

Figure 5.13: Pollutant concentration contours at times t_1 and t_2 after it is injected instantaneously as a planar strip source indicated as a red rectangle in the layer containing (2,1.4). The aquifer at the top is a homogeneous aquifer and the bottom one has a less permeable lens in it. The contours are plotted at the same levels from the outer contours to the inner ones on an equally spaced logarithmic scale of $10^{-3(.25)0}$ [kg m^{-3}].

All the parameters used in these simulations are listed in Table 5.2. Note that the total volume flux q_x is the same in both the aquifers, which means that the mean dynamic pressure at the boundaries of two aquifers is different to maintain same volume flux.

Parameters	**Values**
total volume flux q_x	0.1 [m^2 hr^{-1}]
permeability of aquifer K	10^{-7} [m^2]
permeability of lens K_l	10^{-8} [m^2]
coefficient of horizontal dispersion D_x	0.03 [m^2 hr^{-1}]
coefficient of vertical dispersion D_z	0.005 [m^2 hr^{-1}]
aquifer porosity ϕ	0.1 [-]

Table 5.2: The parameter values used for the confined aquifers shown in Figure 5.13.

5.2.6 Point source of contaminated fluid in one sub-layer

Consider again the aquifer shown in Figure 3.6 and whose fluid flow problem is solved in Section 3.3.1. Also, suppose that the fluid properties and geometrical characteristics of the aquifer are the same and the aquifer is still modelled in two different ways; (1) the three sedimentary layers are used as vertical discretization, and (2) the three layers are subdivided into five further sub-layers to get more refined results. Suppose that the injected fluid is contaminated with a pollutant and has a concentration C_P [kg m^{-3}]. Since the volumetric rate of contaminated fluid entering the aquifer in both the models is the same, the rate of pollutant mass entering the aquifer is also the same.

Numerical solutions for the steady pollutant concentrations in both the cases are plotted in Figure 5.14. The top graph is the concentration profile in the aquifer when natural layering is used for vertical discretization while the bottom graph is with a more refined vertical discretization, i.e., each sedimentary layer is divided into five further sub-layers. Although, the concentration profile in the bottom graph seems more refined, the upper graph is still good enough for practical purposes. The further vertical discretization is possible and the decision for that depends that how much detail of the aquifer is known and how accurate the results are required to be.

5.2.7 A stream of contaminated water at the surface

Consider the aquifer with a transverse running stream of water at the surface and whose fluid flow problem is solved in Section 3.3.2. Now assume that the fluid flowing in the stream is contaminated with a "well mixed" pollutant and has a concentration C_P. Suppose that the fluid and the geometric characteristics of the aquifer are the same as those used in the simulation in Figure 3.7. A numerical solution of the steady-state pollutant concentration is contoured in Figure 5.15 with the transport properties as mentioned in Table 5.3. As mentioned in Section 3.3.2, for some initial zone where the stream is in contact with the top sub-layer, groundwater flows up in the stream with these boundary conditions. Therefore, the pollutant concentration contours do not start immediately from the first point of contact.

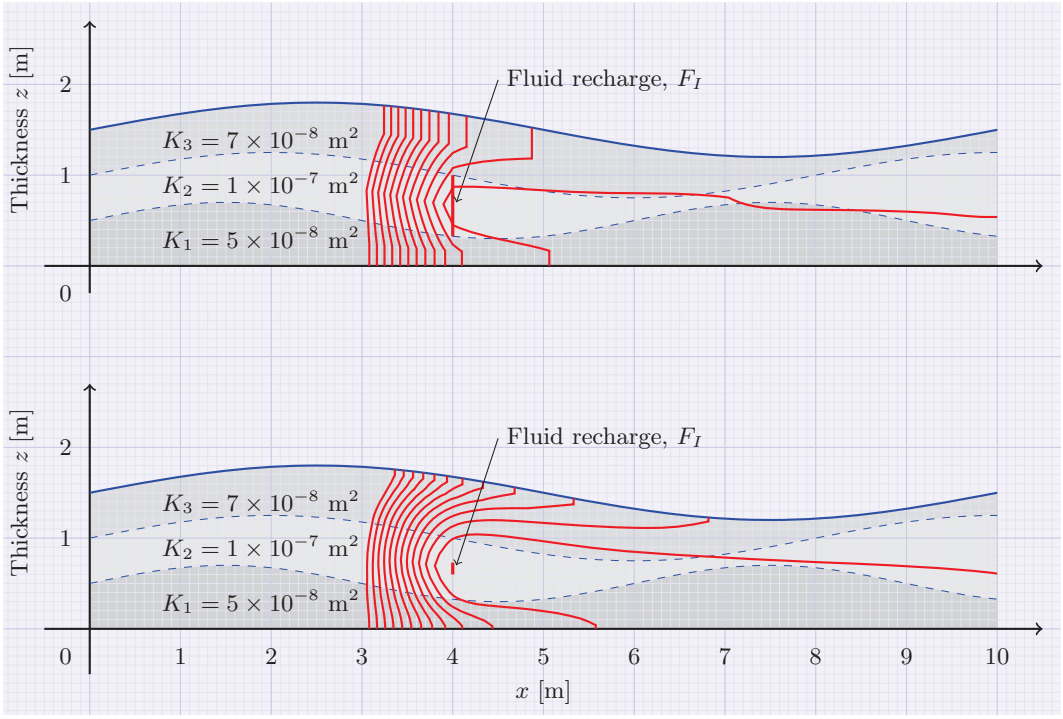

Figure 5.14: Pollutant concentration in a layered aquifer with a recharge well at (4,0.7) of injection rate $0.4/h_n(4)$ [(m^3 hr^{-1}) m^{-2} = m hr^{-1}] where the injected water is polluted with a contaminant of concentration $C_P = 1$ [kg m^{-3}]. (Top) Concentration contours when natural layering is used for vertical discretization. (Bottom) Pollutant concentration contours when each sedimentary layer is divided into five further sub-layers. The concentration contours are plotted at levels $10^{-1.2(0.1)-0.1}$ [kg m^{-3}].

5.3 Illustrations: phreatic aquifers

The pollutant transport equations (5.9) for the confined aquifers remain valid for phreatic aquifers and once the phreatic surface is found, the application of the model is similar. The interlayer transfer coefficient τ_i between layer i and $i+1$ and the interlayer flux normal to the layer interface r_i from layer i to $i+1$ are again given by (5.7) and (4.8), respectively. The total volume flux $\mathbf{q}(x, y)$ through the whole aquifer is given by (4.3) and the specific flux per unit width of layer i is given by (4.9).

5.3.1 Effect of varying bottom surface in a homogeneous aquifer

Now consider a homogeneous phreatic aquifer. The boundary conditions for the phreatic surface are assumed to be $z_t(0) = 3$ and $z_t(10) = 1.5$ [m], i.e. the fluid is flowing from

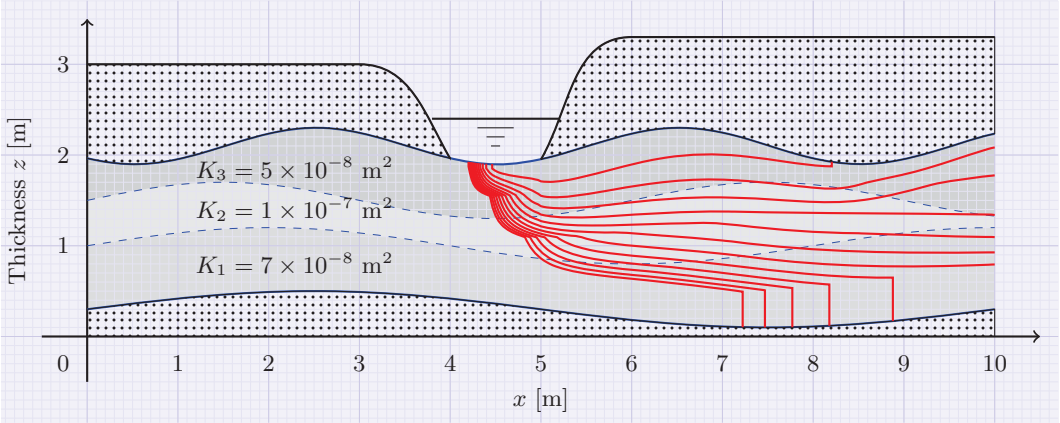

Figure 5.15: Concentration contours in a layered aquifer with a transverse running stream at the top from $x = 4$ to $x = 5$. The values of the parameters used in this simulation are given in Table 5.3. The concentration contours are plotted at levels $10^{-1.2(0.1)-0.1}$ [kg m^{-3}].

left to right. Imagining that there is no source or sink in the phreatic aquifer, the phreatic surface $z_t(x)$ is found by using a one-dimensional version of (4.5) while taking $z_b(x) = 0$. The resultant phreatic surface is shown in Figure 5.16. Once, the phreatic surface is computed, the pollutant transport can be treated exactly in the same way as for the confined aquifers. The homogeneous aquifer here is discretized vertically into 21 sub-layers of equal thicknesses proportional to the total thickness of the aquifer. A pollutant Q_{P1} [kg m^{-2}] is assumed to be injected instantaneously in the jth sub-layer containing the point $(2, 1.4)$ as a planar strip source. Model equations (5.9) are applied to predict pollutant concentration at times t_1, t_2 and t_3 while using the parameter values listed in Table 5.4. The resultant pollutant concentration contours are plotted in Figure 5.16.

It is evident from the concentration contours that the fluid speed increases as it reaches the thinner region of the phreatic aquifer. The longer nose at front of the concentration profile shows that the fluid is moving faster there.

Now if the base of the homogeneous aquifer is not planar, the phreatic surface z_t depends on the shape of the base. As an illustration, an impervious hump is assumed in the base of the homogeneous aquifer as shown in Figure 5.17.

Maintaining all other parameters the same, a pollutant $Q_{P2} = Q_{P1} h_{j_1}/h_{k_2}$ [kg m^{-2}] is injected in the kth layer of the aquifer containing the same release point $(2, 1.4)$ to

Parameters	Values
pollutant concentration in injected water C_P	1 [kg m^{-3}]
coefficient of horizontal dispersion (D_{x1}, D_{x2}, D_{x3})	(0.037,0.040,0.035) [m^2 hr^{-1}]
coefficient of vertical dispersion (D_{z1}, D_{z2}, D_{z3})	(0.022,0.025,0.020) [m^2 hr^{-1}]
aquifer porosity ϕ	0.1 [-]

Table 5.3: The parameter values used for the confined aquifers shown in Figure 5.15.

Parameters	Values
the injected mass Q_{P1}	1 [kg m^{-2}]
porosity ϕ	0.1 [-]
coefficient of horizontal dispersion D_x	0.10 [m^2 hr^{-1}]
coefficient of vertical dispersion D_z	0.02 [m^2 hr^{-1}]
total volume flux through the whole aquifer q_x	0.1 [m^2 hr^{-1}]

Table 5.4: Parameters used in Figures 5.16 and 5.17

maintain the same released mass for comparison. Here, h_{j1} and h_{k2} are thicknesses of the jth sub-layer of the aquifer with the planar base and the kth sub-layer of the aquifer with the humped base. The pollutant concentration contours at all three times again are plotted with the same colour for the same level. Now, we see that the phreatic surface adjusts itself depending on the shape and size of the hump. Also when fluid enters into the narrow region over the hump, it speeds up and therefore, the pollutant also moves faster.

5.3.2 A lens in a phreatic aquifer

Consider the phreatic aquifer with a lens of lower permeability in it discussed in Section 4.1.3 and whose fluid flow problem is already solved and shown in Figure 4.3. Suppose that the aquifer is vertically discretized in $N = 19$ sub-layers and a pollutant of mass $Q_P = 1$ [kg m^{-2}] is injected instantaneously in the sub-layer containing the point

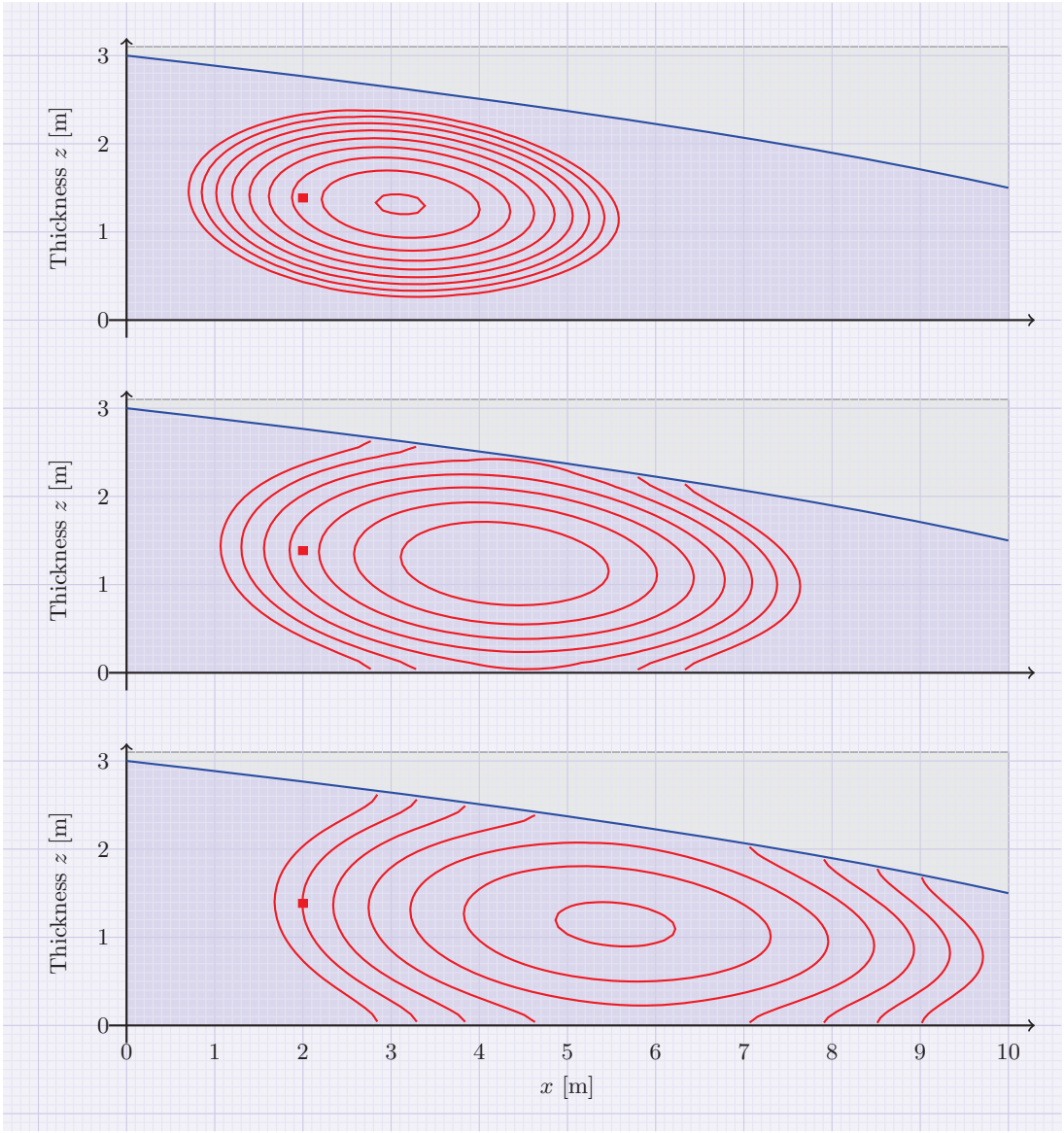

Figure 5.16: Pollutant concentration contours at times $t_1 = 3$ [hr] (Top), $t_2 = 6$ [hr] (Middle) and $t_3 = 9$ [hr] (Bottom), when it is injected instantaneously as a planar strip source (red rectangle) in a layer containing the point (2,1.4) in a homogeneous phreatic aquifer with a planar base. The contours are plotted at the same levels from the outer contours to the inner ones on an equally spaced logarithmic scale $10^{-2.25(0.25)-0.25}$ [kg m^{-3}].

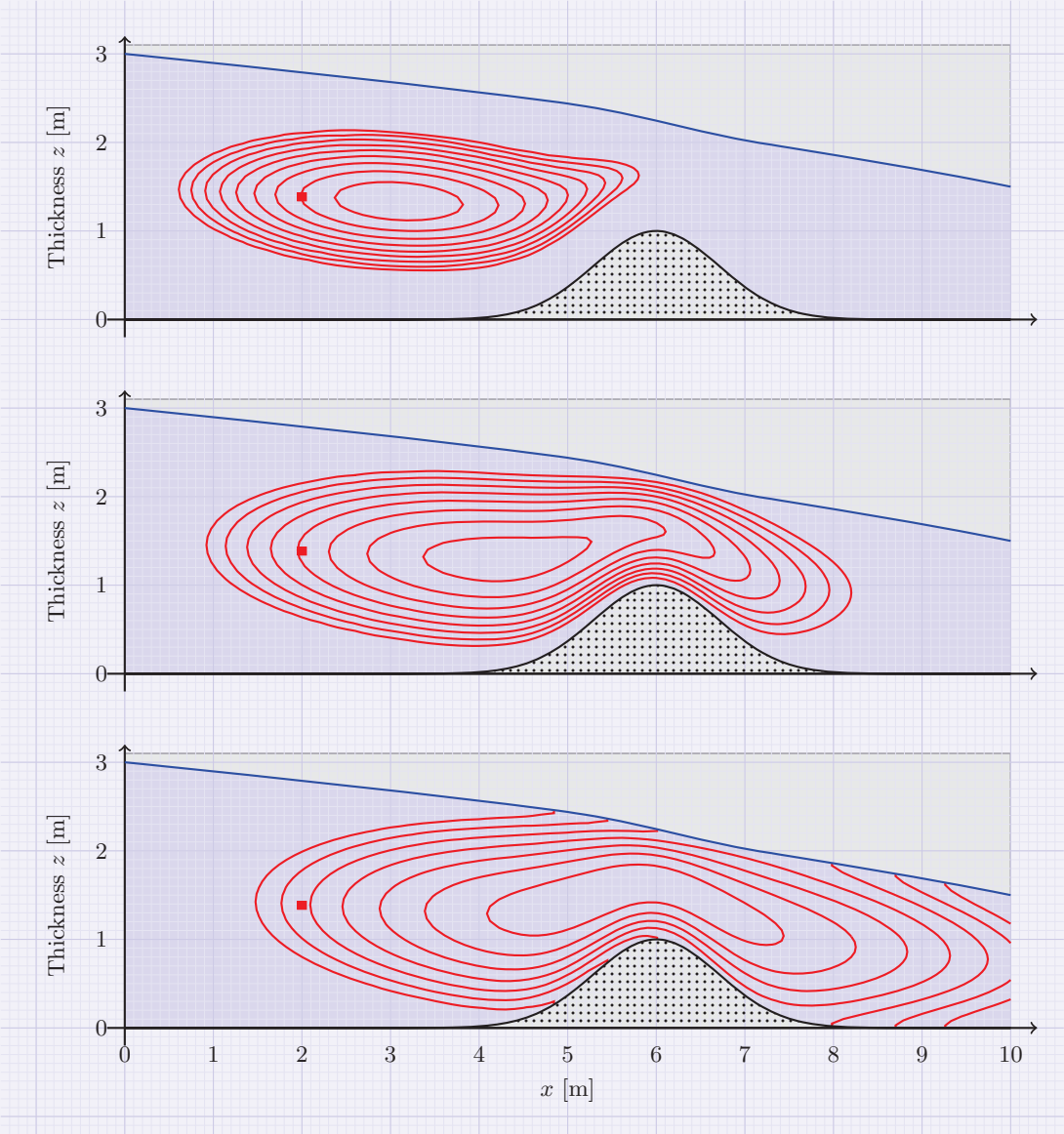

Figure 5.17: Pollutant concentration contours at times $t_1 = 3$ [hr] (Top), $t_2 = 6$ [hr] (Middle) and $t_3 = 9$ [hr] (Bottom), when it is injected instantaneously as a planar strip source (red rectangle) in a layer containing the point (2,1.4) in a homogeneous phreatic aquifer with a base containing an impervious hump. The contours are plotted at the same levels from the outer contours to the inner ones on an equally spaced logarithmic scale $10^{-2.25(0.25)-0.25}$ [kg m^{-3}].

$(x, z) = (2, 1.4)$. The transport model is applied on this aquifer with the parameter values mentioned in Table 5.5 and the resultant concentration of the pollutant is plotted in Figure 5.18 as contours after times $t_1 = 0.5$ and $t_2 = 1.0$ [hr]. The top plot in Figure 5.18 is pollutant concentration snapshot after $t_1 = 0.5$ [hr]. One may observe that as pollutant advects with the fluid and disperses, it enters into the less permeable lens and as fluid speed is a lot lower in the lens compared to that in the other parts of the aquifer, it seems to have jammed in there.

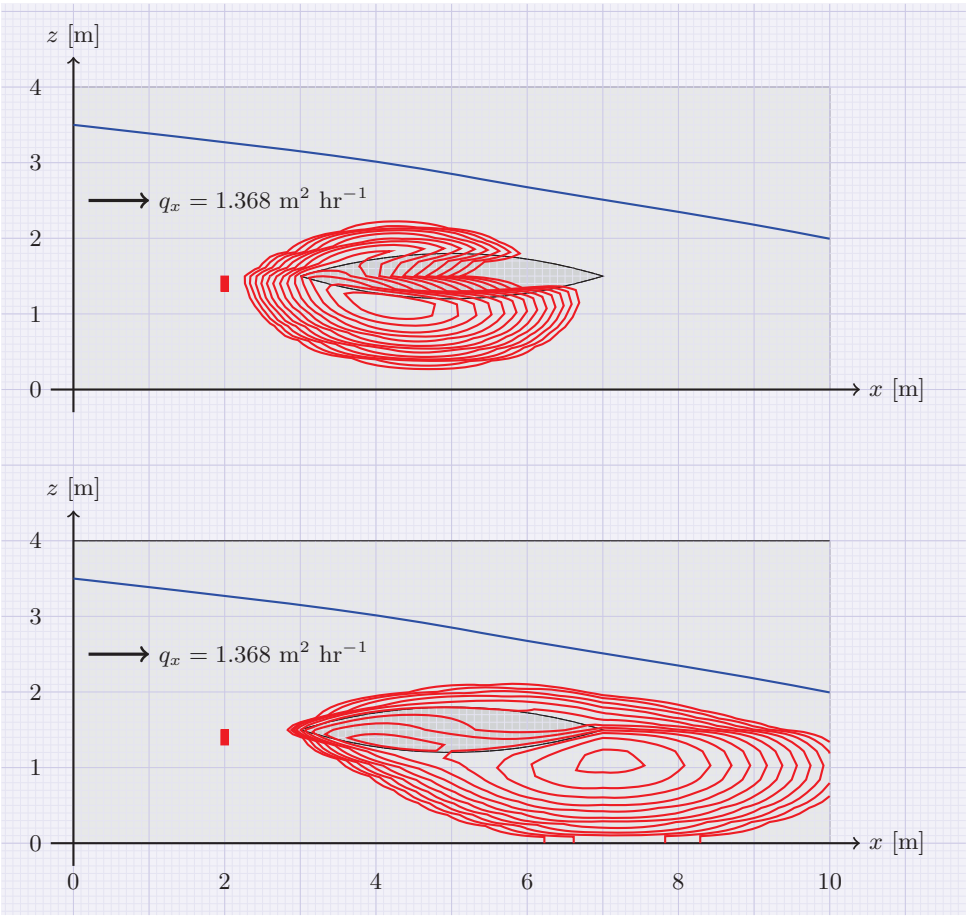

Figure 5.18: (Top) The pollutant concentration contours at time $t_1 = 0.5$ [hr] after release as a planar source in the sub-layer containing $(2, 1.4)$ marked as red rectangle. (Bottom) The pollutant concentration at time $t_2 = 1.0$ [hr]. The transport parameters are mentioned in Table 5.5. The contours in both the graphs are plotted on an equally spaced logarithmic scale $10^{-3(0.25)0}$ [kg m^{-3}] from the outer contours to the inner ones.

In the bottom plot of Figure 5.18, pollutant concentration after time $t_2 = 1.0$ [hr]

is plotted. The pollutant in the lens of lower permeability is moving slowly while that in the rest of the aquifer has gone past the lens and pollutant is slowly bleeding in the neighbouring areas of the lens. The release point of the pollutant is marked as red rectangles in both the plots.

Parameters	**Values**
the injected mass Q_P	1 [kg m^{-2}]
porosity ϕ	0.1 [-]
coefficient of horizontal dispersion D_x	0.25 [m^2 hr^{-1}]
coefficient of vertical dispersion D_z	0.02 [m^2 hr^{-1}]
total volume flux through the whole aquifer q_x	1.368 [m^2 hr^{-1}]
density of groundwater ρ	1000 [kg m^{-3}]
gravitational acceleration g	9.8 [m s^{-2}]
dynamic viscosity of groundwater μ	1.002 $\times 10^{-3}$ [kg m^{-1} s^{-1}]

Table 5.5: Parameters used in the simulation whose results are shown in Figure 5.18.

5.3.3 A point source of contaminated fluid in one sub-layer

Consider again the aquifer shown in the Figure 4.6 and whose fluid flow problem has already been solved in 4.3.1. Now suppose that the injected fluid in the 3rd sub-layer is contaminated with the pollutant where concentration of the pollutant in the injected water is $C_P = 1$ [kg m^{-3}]. The pollutant transport model (5.19) can be solved for this aquifer and the resultant steady-state concentration profile of the pollutant is plotted in Figure 5.19. The contaminated fluid is assumed to be injected as a planar source in the 3rd sub-layer, marked as a red thick line in the Figure.

The parameter values used for transport modelling are those mentioned in Table 5.6. The geometric characteristics of the aquifer and the fluid properties are shown in Table 4.1. The pollutant concentration in the 4th sub-layer (from the bottom), which has comparatively low permeability, is higher at the steady-state.

5.3.4 Contaminated stream at the top

Consider the phreatic aquifer that has the transverse running stream over the top sub-layer shown in Figure 4.7 and discussed in Section 4.3.2. Now suppose that the

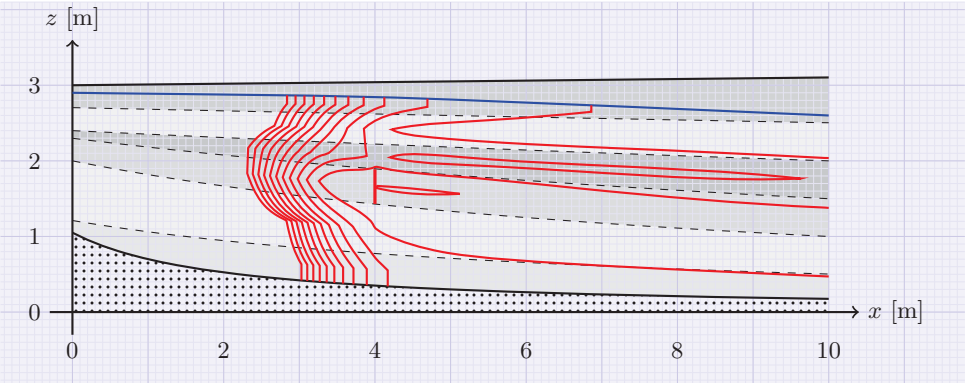

Figure 5.19: The pollutant concentration contours in the phreatic aquifer composed of six sub-layers. The contours are plotted on an equally spaced logarithmic scale $10^{-1.8(0.15)-0.15}$ from the outer contour to the inner ones. The injection well of contaminated fluid is indicated as a red line in the 3rd sub-layer at $x = 4$ [m].

Parameters	**Values**
the pollutant concentration in the injected fluid C_P	1 [kg m^{-3}]
porosity ϕ	0.1 [-]
coefficients of horizontal dispersion $(D_{x1}, D_{x2}, D_{x3}, D_{x4}, D_{x5}, D_{x6})$	$(3.7, 4.0, 3.5, 3.0, 4.1, 3.0) \times 10^{-2}$ [m^2 hr^{-1}]
coefficient of vertical dispersion $(D_{z1}, D_{z2}, D_{z3}, D_{z4}, D_{z5}, D_{z6})$	$(13.2, 15.0, 12.0, 6.0, 16.2, 9.0) \times 10^{-3}$ [m^2 hr^{-1}]

Table 5.6: The transport parameters used in the simulation whose results are shown in Figure 5.19.

stream water is contaminated with a pollutant which has a concentration $C_P = 1$ [kg m^{-3}] in the water. The transport model is solved by using the transport parameters as mentioned in Table 5.7. The flow parameters are the same as those mentioned in Table 4.2. The resultant pollutant concentration contours are plotted in Figure 5.20. As previously mentioned in Section 4.3.2, the fluid flows back into the stream for some initial zone of contact of the stream and the top (4th) sub-layer. Therefore, the pollutant does not start building up in the aquifer right from the start of the "zone of contact", instead it advects downward with the fluid at $x > x_t$, where x_t is the point after which water table in the stream z_{st} is higher than the hydraulic head in the 4th sub-layer $\bar{H}_4$. Some of the downward advecting pollutant disperses back into the

stream and to the upstream of the aquifer.

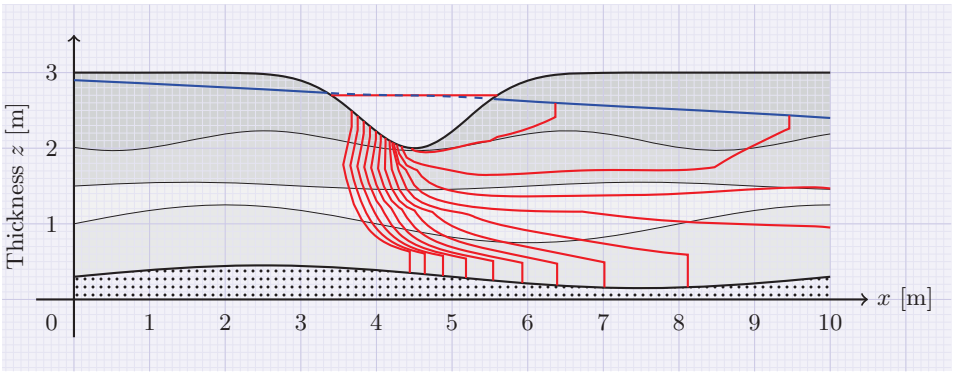

Figure 5.20: The pollutant concentration contours in a layered phreatic aquifer with a transverse running stream at the top. The contour levels are $10^{-2.5(0.2)-0.1}$ [kg m^{-3}].

Parameters	Values
the pollutant concentration in the stream C_P	1 [kg m^{-3}]
porosity ϕ	0.1 [-]
longitudinal dispersivities $(\alpha_{L1}, \alpha_{L2}, \alpha_{L3}, \alpha_{L4})$	$(.230, .250, .225, .200)$ [m]
coefficient of vertical dispersion $(D_{z1}, D_{z2}, D_{z3}, D_{z4})$	$(.046, .050, .045, .040)$ [m^2 hr^{-1}]

Table 5.7: The transport parameters used in the simulation whose results are shown in Figure 5.20 and Figure 5.21.

For the illustration of a transport problem when the phreatic surface z_t crosses a sub-layer interface, consider again the same aquifer with fluid flow boundary conditions as shown in Figure 4.8. The z_t from the 4th sub-layer crosses the lower layer interface and enters into the 3rd sub-layer. The top sub-layer, when phreatic surface drops below it, can be assumed to be continuous with a very small thickness $h_4 = \delta > 0$ just below the phreatic surface, for ease of application of numerical procedure. The third sub-layer reduces by a value $h_3 - \delta$ in this zone. The steady-state pollutant concentration profile is plotted in Figure 5.21. Note that the total fluid volume flux is higher in this case compared to that in Figure 5.20 because of higher gradient of mean dynamic hydraulic heads $\bar{H}_i$. Also, the pollutant concentration starts building in the aquifer well

before the start of the "zone of contact" of the polluted stream and the top sub-layer because there is only stream to aquifer flow in this example. The plateau of pollutant concentration is quite flat here compared to the that in Figure 5.20.

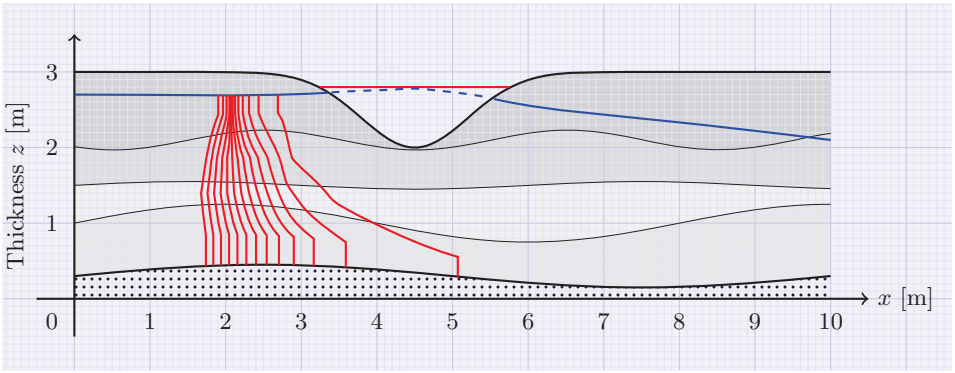

Figure 5.21: The pollutant concentration contours in a layered phreatic aquifer with a transverse running stream at the top. The contour levels are $10^{-2.5(0.2)-0.1}$ [kg m^{-3}].

5.4 Site data

An experiment was conducted to observe to observe transport of the contamination of groundwater in a phreatic sand aquifer at the Canadian Forces Base in Borden, Ontario [22]. The aquifer was fairly homogeneous with mean value of hydraulic conductivity $\kappa = 7 \times 10^{-5}$ [m s^{-1}] which is equal to 7.157×10^{-12} [m^2] when density of the groundwater ρ is 1000 [kg m^{-3}], the gravitational acceleration g is 9.8 [m s^{-2}] and the dynamic viscosity of the groundwater μ is 1.002×10^{-3} [kg m^{-1} s^{-1}]. The total porosity ϕ_{tot} of the aquifer was measured to be 0.33 [-] and the hydraulic head gradient dH/dx in the direction of flow was -0.0043 [-]. With these parameters, the tracer velocity is 0.079 [m day^{-1}] which is slightly less than the observed tracer velocity which was 0.091 [m day^{-1}]. This was probably because of a slightly lower effective porosity ϕ [-] of the aquifer.

There were a total of nine tracer injection wells in the aquifer and a 12 [m^3] solution of several tracers such as chloride ion, carbon tetrachloride, etc., was injected over a 14.75 [hr] period. The injected mass of chloride ion was 10.7 [kg]. The longitudinal dispersivity was estimated to be 0.49 [m] [18].

The whole aquifer is assumed homogeneous and two-dimensional transport model (5.16) is applied. By using the known parameters and varying the effective porosity ϕ and the horizontal dispersivity α_T, this transport problem is simulated for chloride and the resultant concentration profiles are plotted after the same times of release on the right side of Figure 5.22. It was found that the $\phi = 0.28$ [-] and $\alpha_T = 0.05$ [m]. The aquifer is considered totally homogeneous and fluid velocity is assumed uniform and unidirectional over the year. Since, in [22], the data was normalised with respect to the maximum concentration, Figure 5.22 shows such normalised values. The simulated results match closely with the concentration data.

The observed concentration of the chloride after 1, 85, 464 and 647 [days] in groundwater is shown in left side of Figure 5.22 [22].

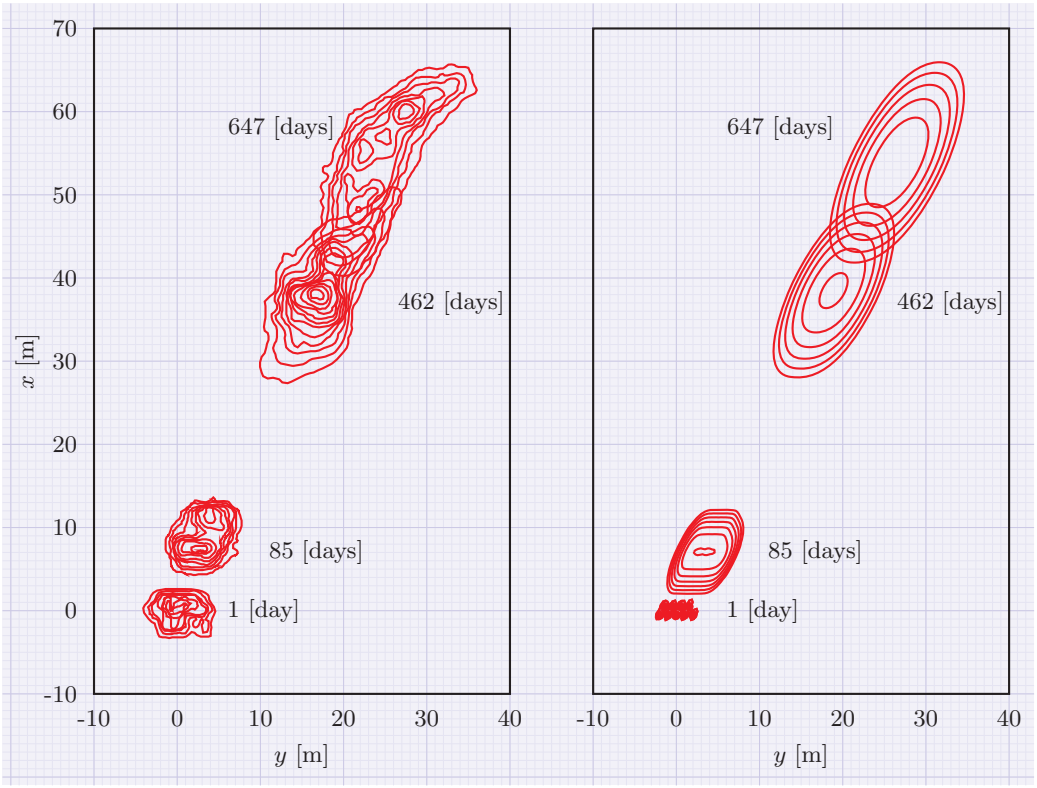

Figure 5.22: (Left) Vertically averaged concentration profile of the chloride ion, 1,85,462, and 647 days after injection (from [22]). (Right) Simulated vertically averaged concentration of the chloride ion at the same times after the release.

6

Pollutant Remediation

Groundwater pollution is a major hazard in areas where groundwater is the sole source of drinking water. Some contaminants are unpleasant and others are even toxic. The pollutants may enter into groundwater through various sources, such as, wastes of chemical industries, excessive use of fertilizers and agrochemicals, sewage water and hydrologic cycle.

The remediation of pollutants from groundwater is a challenge in itself. The contaminants flow along groundwater through complex pathways in porous aquifers. Sometimes, contaminants from multiple sources may enter in groundwater and interact with each other to produce new complex compounds and hence complicating the remediation strategy. Complete clean-up of groundwater is not possible, however, a good strategy could be devised to harvest maximum possible cleansing of groundwater. There are many strategies in place for remediation of contaminants in groundwater.

One of the strategies is "pump-and-treat" [33], in which contaminated water is pumped out of the aquifer and treated to remove contaminants and is allowed to re-enter the aquifer by either recharging through wells or adding in surface water. The drawback of the strategy is that it is not cost effective. Another strategy is using "sorptive barriers" or "permeable reactive barriers" installed directly in the aquifer perpendicular to the flow of groundwater [33]. Again, this strategy is not very cost effective. Remediation by green plants or "phytoremediation" [15] is a non-invasive strategy. It is cost effective, provides sequestering of carbon, gives an aesthetic look, is more environmentally friendly and has technical advantages over traditional engineering solutions. This method is, however, only useful when contaminants are near to surface

and are relatively non-leachable and do not pose high risk to the health of plants to grow.

In Situ Chemical Oxidation (ISCO) [23] is emerging as a popular technology in which strong chemical oxidizers are introduced directly in the porous medium to destroy contaminants present in groundwater. Most commonly used remediating oxidants are permanganate, Fenton's reagent, persulphate and ozone. ISCO can be used to remediate certain organic substances present in groundwater such as chlorinated solvents and gasoline-related compounds which are released from industrial sources.

The models presented in this Chapter are for an ISCO remediation strategy. The oxidants are released directly in the aquifer at the optimum location to get the best possible reduction of the contaminants. In the case of steady release of the pollutants, the optimal location for the release of remedial agent is exactly where the pollutant is injected. For the time-dependant case, the optimal location for the release of remedial agent is always where the pollutant concentration is maximum at that time. The kinetics of the oxidation reaction is typically of second order [20].

6.1 One-dimensional homogeneous aquifers

If $\bar{c}_P(x,t)$ [kg m^{-3}] is the mean concentration of pollutant in groundwater averaged over the thickness of the aquifer and $\bar{c}_R(x,t)$ [kg m^{-3}] is the mean concentration of the removal agent, then their rates of change of concentrations with position x and time t are given by

$$\begin{aligned}
\phi h\frac{\partial \bar{c}_P}{\partial t} &= -q_x\frac{\partial \bar{c}_P}{\partial x} - \phi\frac{\partial}{\partial x}\left[hD_{Px}\left(-\frac{\partial \bar{c}_P}{\partial x}\right)\right] + \phi h f_P(x,t) - \phi h k_1 \bar{c}_P \bar{c}_R \\
\phi h\frac{\partial \bar{c}_R}{\partial t} &= -q_x\frac{\partial \bar{c}_R}{\partial x} - \phi\frac{\partial}{\partial x}\left[hD_{Rx}\left(-\frac{\partial \bar{c}_R}{\partial x}\right)\right] + \phi h f_R(x,t) - \phi h k_2 \bar{c}_P \bar{c}_R, \quad (6.1)
\end{aligned}$$

where k_1 and k_2 [(kg m^{-3})$^{-1}$ s^{-1}] are the second order rates of removal of pollutant and pollutant removing agent, respectively. Also, D_{Px} and D_{Rx} are the coefficients of dispersion of the pollutant and the pollutant removing agent, respectively. The rates of molecular diffusion of the pollutant and the removing agent may generally be different from each other. However, the coefficients of dispersion for both the pollutant and the pollutant removing agent are almost the same. This is because the coefficient of dispersion in porous media is the sum of the coefficient of molecular diffusion of

the solutes in water and the coefficient of mechanical dispersion, and the coefficient of molecular diffusion is generally very small as compared to the coefficient of mechanical dispersion. Therefore, the coefficients of dispersion D_{Px} and D_{Rx} can be replaced with $D_x = \alpha_L \bar{U}_x = \alpha_L q_x/(\phi h)$. Suppose $f_P(x,t) = q_P \delta(x - x_1)$ and $f_R(x,t) = q_R \delta(x - x_2)$ are plane sources for the pollutant and the removing agent acting on $x = x_0$ and $x = x_1$ with constant rates q_P and q_R [kg m^{-2} s^{-1}] respectively. Then, the coupled system (6.1) for a homogeneous aquifer becomes

$$\begin{aligned} \frac{\partial \bar{c}_P}{\partial t} &= -\bar{U}_x \frac{\partial \bar{c}_P}{\partial x} + \alpha_L \bar{U}_x \frac{\partial^2 \bar{c}_P}{\partial x^2} + q_P \delta(x - x_1) - k_1 \bar{c}_P \bar{c}_R \\ \frac{\partial \bar{c}_R}{\partial t} &= -\bar{U}_x \frac{\partial \bar{c}_R}{\partial x} + \alpha_L \bar{U}_x \frac{\partial^2 \bar{c}_R}{\partial x^2} + q_R \delta(x - x_2) - k_2 \bar{c}_P \bar{c}_R, \end{aligned} \tag{6.2}$$

where $\bar{U}_x = q_x/(\phi h)$ is the interstitial velocity.

6.1.1 Illustration

Consider a homogeneous aquifer with thickness varying only in one horizontal direction (say x). Suppose, pollutant q_P [kg m^{-2} day^{-1}] is being injected steadily at x_1 and a pollutant removing agent q_R [kg m^{-2} day^{-1}] is being released downstream at x_2 (both as plane sources).

The steady-state numerical solution for the non-linear coupled system (6.2) for the data shown in Table 6.1 is plotted in Figure 6.1.

Parameters	**Values**	**Units**
thickness $h(x)$	$1 + 0.3\cos x$	[m]
total volumetric flux q_x	1	[m^2 day^{-1}]
porosity ϕ	0.1	[-]
longitudinal dispersivity α_L	0.1	[m]
rate of pollution release q_P	1	[kg m^{-2} day^{-1}]
rate of pollution removing agent release q_R	1	[kg m^{-2} day^{-1}]
removal rate for pollution k_1	3	[$\left(\text{kg m}^{-3}\right)^{-1}$ day^{-1}]
removal rate for pollution removing agent k_2	1	[$\left(\text{kg m}^{-3}\right)^{-1}$ day^{-1}]

Table 6.1: Parameter values for the aquifer shown in Figure 6.1

The rate of the total mass of the pollutant that enters into the aquifer at its release point x_1 is $q_P \times h(x_1)$ per unit lateral width per day while the rate at which the mass of

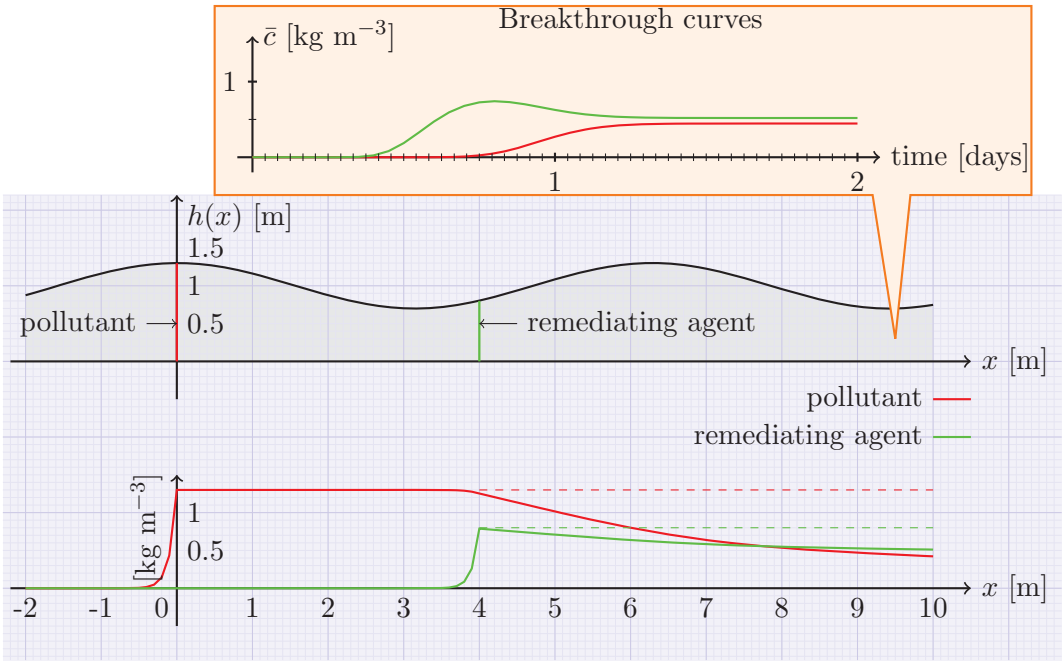

Figure 6.1: Variable thickness profile of the homogeneous aquifer with points of release x_1 and x_2 of the pollutant and the pollutant removing agent respectively (top) and steady-state concentrations of the pollutant in red and the pollutant removing agent in green (bottom). The separate graph for the point $x = 9.5$ [m] of the aquifer, shows breakthrough curves for the pollutant (red) and the remediating agent (green) mean concentrations at that point.

the remediating agent enters into the aquifer at x_2 is $q_R \times h(x_2)$ per day per unit lateral width of the aquifer. Therefore, the concentrations of the two chemicals are different at their steady levels when they are not interacting with each other (shown as dashed lines in Figure 6.1). The concentration of the pollutant upstream of its release point x_1 becomes steady at a level determined by the equilibrium of the upstream dispersion and downstream advection. The higher the ratio of dispersion to advection, the longer the tail of the concentration profile of the pollutant upstream of x_1. The concentration of the remediating agent upstream of its release point x_2 is determined by dispersion, advection and the decay rate constant of the remediating agent k_2 when it interacts with the pollutant. Higher values of k_2 mean more consumption of the remediating agent and hence the sharper the upstream tail of the remediating agent there. The curves shown in the separate window for $x = 9.5$ are breakthrough curves at that point for concentrations of both the remediating agent and the pollutant when release of both

the chemicals started at the same time $t = 0$. The red curve is concentration of the pollutant at $x = 9.5$ against time and green one is that of the remediating agent. The remediating chemical was released at x_2 which is ahead of the release point of pollutant x_1, so it arrived earlier at the "check point" i.e., $x = 9.5$ and hence its concentration rises to a maximum after about 18 hours of its release. But, then the pollutant started reaching there and the oxidation process started, reducing the concentration of the remediating agent at a rate of $k_2\bar{c}_P\bar{c}_R$ [kg m^{-3} day^{-1}]. In the zone where the oxidation process is taking place (where both the chemicals are present), the total concentration of each chemical stabilises to an equilibrium value determined by the advection rate, the relative rate of decay of the chemical and the dispersion rate. It is obvious from the breakthrough curves, that the equilibrium or the steady-state concentration profiles are achieved after approximately 1 day and 6 hours at $x = 9.5$. The concentrations of chemicals at this point are no longer time dependant but they do vary along x. The concentrations of the chemicals keep reducing downstream depending on their corresponding decay rates until one of them vanishes.

6.2 Two-dimensional homogeneous aquifers

The dispersion rate for both the pollutant and the pollutant remediating agent is the same and is given by (5.2) when the x-axis is aligned with the averaged direction of flow and the variations in the direction of flow are negligible. If the pollutant is being released steadily as a line source at (x_1, y_1) with a rate q_P [kg m^{-1} day^{-1}] and the remediating agent at (x_2, y_2) with a rate q_R [kg m^{-1} day^{-1}], the system of non-linear coupled partial differential equations for the concentration of the pollutant $P(x, y, t)$ and the concentration of the remediating agent $R(x, y, t)$ can be written as

$$\begin{aligned}
\phi h\frac{\partial \bar{c}_P}{\partial t} &= -q_x\frac{\partial \bar{c}_P}{\partial x} - q_y\frac{\partial \bar{c}_P}{\partial y} + \alpha_L\frac{\partial}{\partial x}\left(|\mathbf{q}|\,\frac{\partial \bar{c}_P}{\partial x}\right) + \alpha_T\frac{\partial}{\partial y}\left(|\mathbf{q}|\,\frac{\partial \bar{c}_P}{\partial y}\right) \\
&\quad +\phi h q_P\delta(x - x_1)\delta(y - y_1) - \phi h k_1\bar{c}_P\bar{c}_R \\
\phi h\frac{\partial \bar{c}_R}{\partial t} &= -q_x\frac{\partial \bar{c}_R}{\partial x} - q_y\frac{\partial \bar{c}_R}{\partial y} + \alpha_L\frac{\partial}{\partial x}\left(|\mathbf{q}|\,\frac{\partial \bar{c}_R}{\partial x}\right) + \alpha_T\frac{\partial}{\partial y}\left(|\mathbf{q}|\,\frac{\partial \bar{c}_R}{\partial y}\right) \\
&\quad +\phi h q_R\delta(x - x_2)\delta(y - y_2) - \phi h k_2\bar{c}_P\bar{c}_R. \qquad (6.3)
\end{aligned}$$

6.2.1 Illustration

Consider the aquifer shown in Figure 3.1 and assume a continuous injection of a strong oxidizer (a remediating agent) without a significant fluid component at (50,50). The steady injection rate for the dry remediating agent is $q_R = 20$ [kg m^{-1} day^{-1}]. Suppose that the aquifer is being recharged with contaminated water through the well at $(40, 50)$ with a rate F_I [(m^3 day^{-1}) m^{-1} = m^2 day^{-1}] and water is being pumped out from the pumping well at $(80, 30)$ with a rate F_W [(m^3 day^{-1}) m^{-1} = m^2 day^{-1}].

Suppose that the parameters for the fluid flow and the pollutant transport in this aquifer are the same as in Figure 5.4 then the steady-state concentration profile of the pollutant while it is transported and remediated, is plotted in Figure 6.2 for the parameter values listed in Table 6.2. The red, blue and green dots represent locations of the recharge well, the pumping well (or monitoring well) and the release point for the remediating agent, respectively.

Parameters	**Values**	**Units**
concentration of contaminant in injected water C_P	1	[kg m^{-3}]
rate of release of pollutant removing agent q_R	10	[kg m^{-1} day^{-1}]
degradation rate coefficient for pollution k_1	5	[$\left(\text{kg m}^{-3}\right)^{-1}$ day^{-1}]
degradation rate coefficient for pollution removing agent k_2	1	[$\left(\text{kg m}^{-3}\right)^{-1}$ day^{-1}]

Table 6.2: Parameter values used for the simulation in Figure 6.2. All other parameters are the same as in Figure 5.4

The contours are plotted on a logarithmic scale $10^{-3,-2.7,-2.4,\cdots,0}$ [kg m^{-3}] from the outer contour to the inner ones, respectively. The new breakthrough curve at the pumping well at (80,30) is plotted in solid red in the separate graph in Figure 6.2 (bottom). The dashed red curve is the breakthrough curve for the simulation without any added remediating agent. Another separate graph (Figure 6.2 (top)) at (95,50) shows breakthrough curves for the pollutant at that point. The dashed red curve is the concentration of the pollutant at that point when there was no remediating agent being released and the solid one is the breakthrough curve when the remediating agent was being released with q_R rate.

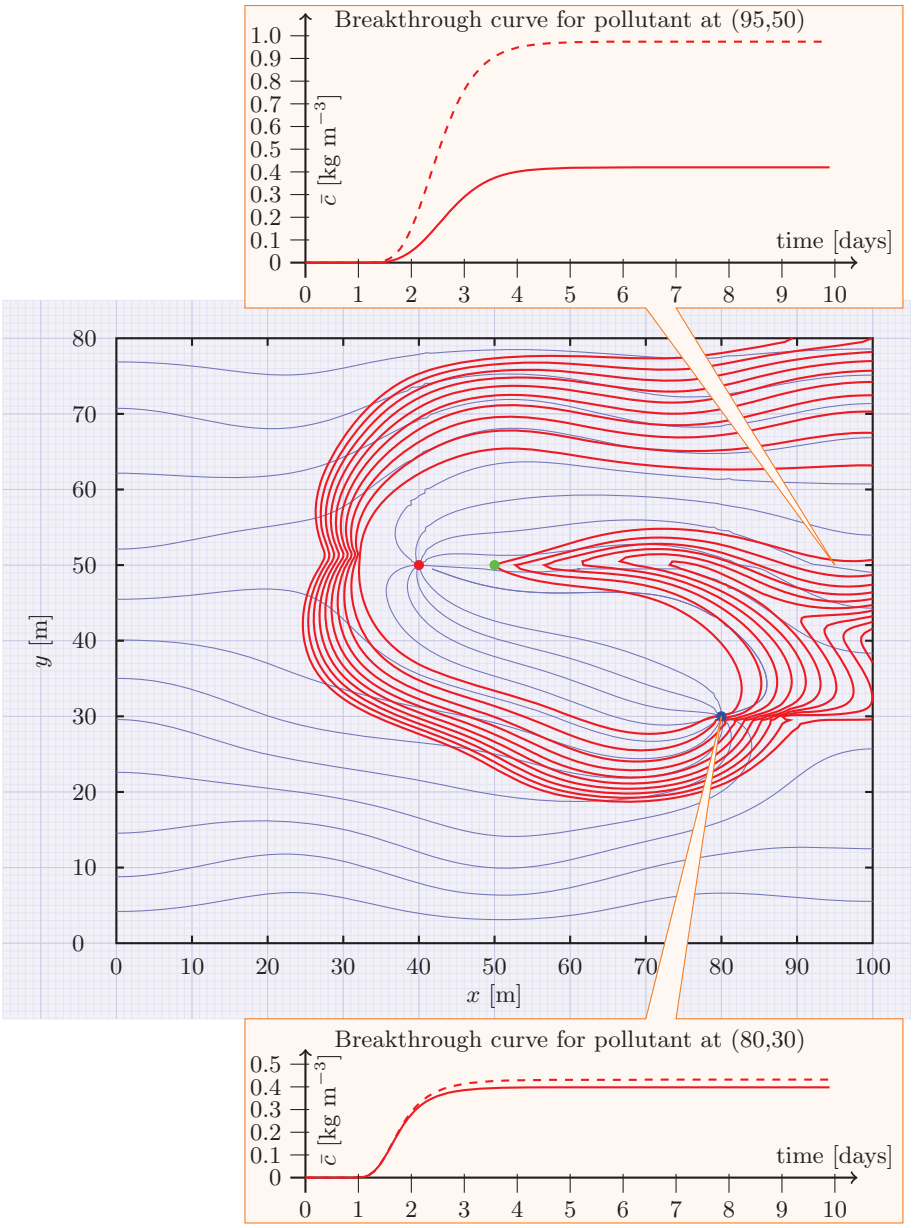

Figure 6.2: Steady-state pollution concentration when water in the recharge well is contaminated with concentration $C_P = 1$ [kg m^{-3}] and the contaminant is being remediated by remediating agent that is being released continuously at (50,50) with a rate $q_R = 10$ [kr m^{-1} day^{-1}] (all parameters are the same as in Figure 5.4). The contours are plotted at $10^{-3(0.3)0}$ [kg m^{-3}] from the outer contour to the inner ones. The two separate graphs (above and below) show the breakthrough curves for the pollutant concentration at (95,50) and (80,30).

One can notice that there is a larger difference in the removed steady concentration at (95,50) than that at the monitoring well at (80,30). As discussed before, the fluid speed between the recharge and the pumping well is much more as compared to that in rest of the aquifer. This does not allow the remediating agent to wipe out the pollutant for long enough. Whereas, the fluid carrying the remediating agent moves relatively slowly from the injection point of the remediating agent to (95,50) and hence there is more opportunity for the remediating agent to deoxidize the pollutant.

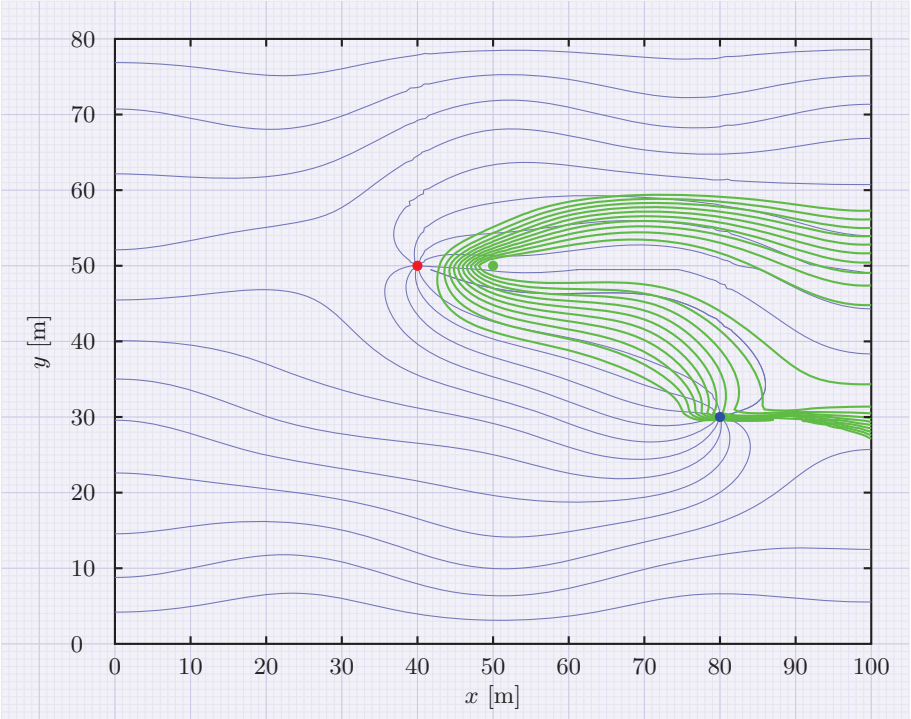

Figure 6.3: Steady-state concentration of the remediating agent when water in the recharge well is contaminated with concentration $C_P = 1$ [kg m^{-3}] and the remediating agent is being used up to break down the contaminant. The remediating agent is being released at (50,50). The contours are plotted at $10^{-3(0.3)0}$ [kg m^{-3}] from the outer contour to the inner ones. Note that no water is being added at (50,50).

Figure 6.3 shows the concentration profile of the remediating agent when it is being advected with the fluid, being dispersed in all directions and being used up to remove the pollutant. One can observe that the pollutant from the recharge well disperses more than the remediating agent from its injection point. This is because the fluid dispersing from the recharge well advects the pollutant along with it whereas the remediating

agent does not have any fluid with it to alter the background fluid flow. Some of the remediating agent is also pumped out from the pumping well. Thus in this case, the pumped out water contains concentrations of both the pollutant and the remediating agent.

6.3 Multi-layered aquifers

Suppose, $\mathbf{q}(x,y) = (q_x(x,y), q_y(x,y))$ is the total volume flux vector of the fluid per unit width of the whole aquifer and $\mathbf{q}_i(x,y) = (q_{xi}(x,y), q_{yi}(x,y))$ is that in the ith sub-layer. The concentrations of the pollutant $\bar{c}_{Pi}(x,y,t)$ and the remediating agent $\bar{c}_{Ri}(x,y,t)$ in the ith sub-layer of the multilayer aquifer composed of N sedimentary sub-layers, satisfy

$$
\begin{aligned}
\phi_i h_i \frac{\partial \bar{c}_{Pi}}{\partial t} &= \frac{\partial}{\partial x}\left(-q_{x_i}\bar{c}_{Pi} + \alpha_{Li}|\mathbf{q}_i|\frac{\partial \bar{c}_{Pi}}{\partial x}\right) + \frac{\partial}{\partial y}\left(-q_{y_i}\bar{c}_{Pi} + \alpha_{Ti}|\mathbf{q}_i|\frac{\partial \bar{c}_{Pi}}{\partial y}\right) \\
&\quad + \left(\tau_{i-1} + \frac{1+\mathrm{sgn}(r_{i-1})}{2}r_{i-1}\right)\bar{c}_{Pi-1} + \left(-\tau_{i-1} + \frac{1-\mathrm{sgn}(r_{i-1})}{2}r_{i-1}\right)\bar{c}_{Pi} \\
&\quad + \left(-\tau_i - \frac{1+\mathrm{sgn}(r_i)}{2}r_i\right)\bar{c}_{Pi} + \left(\tau_i - \frac{1-\mathrm{sgn}(r_i)}{2}r_i\right)\bar{c}_{Pi+1} \\
&\quad + \phi_i h_i f_{Pi} - \phi_i h_i k_1 \bar{c}_{Pi}\bar{c}_{Ri} \\
\phi_i h_i \frac{\partial \bar{c}_{Ri}}{\partial t} &= \frac{\partial}{\partial x}\left(-q_{x_i}\bar{c}_{Ri} + \alpha_{Li}|\mathbf{q}_i|\frac{\partial \bar{c}_{Ri}}{\partial x}\right) + \frac{\partial}{\partial y}\left(-q_{y_i}\bar{c}_{Ri} + \alpha_{Ti}|\mathbf{q}_i|\frac{\partial \bar{c}_{Ri}}{\partial y}\right) \\
&\quad + \left(\tau_{i-1} + \frac{1+\mathrm{sgn}(r_{i-1})}{2}r_{i-1}\right)\bar{c}_{Ri-1} + \left(-\tau_{i-1} + \frac{1-\mathrm{sgn}(r_{i-1})}{2}r_{i-1}\right)\bar{c}_{Ri} \\
&\quad + \left(-\tau_i - \frac{1+\mathrm{sgn}(r_i)}{2}r_i\right)\bar{c}_{Ri} + \left(\tau_i - \frac{1-\mathrm{sgn}(r_i)}{2}r_i\right)\bar{c}_{Ri+1} \\
&\quad + \phi_i h_i f_{Ri} - \phi_i h_i k_2 \bar{c}_{Pi}\bar{c}_{Ri} \quad \text{for} \quad 1 \le i \le N,
\end{aligned} \tag{6.4}
$$

where ϕ [-] is the porosity of the solid matrix in the ith sub-layer, α_{Li} and α_{Ti} [m] are respectively the longitudinal and the transverse dispersivities, and $r_i(x,y)$ [(m^3 s^{-1}) m^2 = m s^{-1}] is the directed interlayer fluid flux from ith sub-layer to the i+1th sub-layer normal to the layer interface. The interlayer dispersive transfer coefficient between the ith and the $i+1$th sub-layer $\tau_i(x,y)$ [m s^{-1}] is estimated by (5.7) for internal sub-layer boundaries and $\tau_0 = \tau_N = 0$ at the base and the top of the aquifer. The functions $f_{Pi}(x,y,t)$ and $f_{Ri}(x,y,t)$ [kg m^{-3} s^{-1}] are respectively source terms for pollutant and removing agent at the point (x,y) of the ith sub-layer averaged over the layer

thickness. For a point source of pollutant at (x_0, y_0) in the ith sub-layer that is released instantaneously at $t = t_0$, the pollutant source function f_{P_i} becomes $Q_{P_i}\delta(x-x_0)\delta(y-y_0)\delta(t-t_0)$, where Q_{P_i} [kg m^{-1}] is the mass of the pollutant released instantaneously at (x_0, y_0) at time $t = t_0$ in the ith sub-layer. Similarly, for a continuously released point source, the pollutant source function would be $q_{p_i}\delta(x - x_0)\delta(y - y_0)$, where q_{P_i} [kg m^{-1} s^{-1}] is the rate of mass flow of the pollutant released continuously at (x_0, y_0) in the ith sub-layer. The second order removal constants k_1 and k_2 are respectively the rates of removal of pollutant and remediating agent when they interact with each other chemically. It is noted that as the pollutant and the remediating agent are transported in a similar way, the equations for the two substances only differ in their last two terms: the source term and the interaction term.

6.3.1 Illustration

Consider again the multi-layered phreatic aquifer discussed in Sections 4.3.2 and 5.3.4 and assume that a remediating agent is being released in the top (4th) sub-layer at $x = 6$ [m] with a steady rate $q_{R4} = 0.1$ [kg m^{-1} hr^{-1}] with no significant fluid entering along with it. As an illustration, the decay rates for the pollutant and the remediating agent k_1 and k_2, respectively are taken as $k_1 = 1$ and $k_2 = 2$ [(kg m^{-3})$^{-1}$ hr^{-1}]. The rest of the flow and transport parameters are the same as were taken in Sections 4.3.2 and 5.3.4. As the pollutant enters into the aquifer and advects along the fluid and disperses in all directions, the remediating agent that is being released in the top sub-layer interacts with it. Hence, both the pollutant and the remediating agent decay with the rates k_1 and k_2 in this reaction. The resultant concentration profile of the pollutant is shown in Figure 6.4 as a contour plot. One can compare the concentration plot of this remediated pollutant to the one in Figure 5.20 that was not being remediated.

A separate sub-graph in Figure 6.4 shows the breakthrough curve at the downstream end in the top sub-layer of the aquifer. The solid red curve shows the concentration of the pollutant in the 4th sub-layer at the downstream end plotted against time when it is being remediated with the remediating agent. While the dashed red curve is the pollutant concentration if it was not being remediated (e.g., in Section 5.3.4). The total remediation at a point of the aquifer depends on how far both the chemicals have travelled together, how high were both the concentrations, and the decay rate of the pollutant when it reacts with the remediating agent. Therefore, the concentrations of

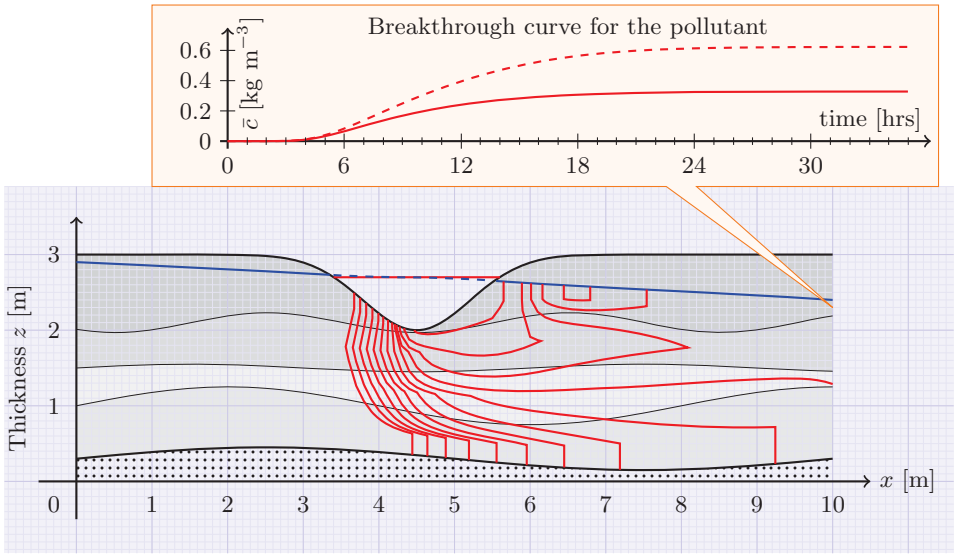

Figure 6.4: The pollutant concentration contours in a layered phreatic aquifer with a transverse running stream at the top. The pollutant is being remediated with a remediation agent that is being released continuously at $x = 6$ [m] with a rate q_R. The contour levels are $10^{-2.5(0.2)-0.1}$ [kg m^{-3}]. The separate graph (above) shows the breakthrough curve for the pollutant concentration at $x = 10$ [m] in the 4th sub-layer.

the two chemicals become lower and lower as one travels downstream until one of the chemicals is completely used up.

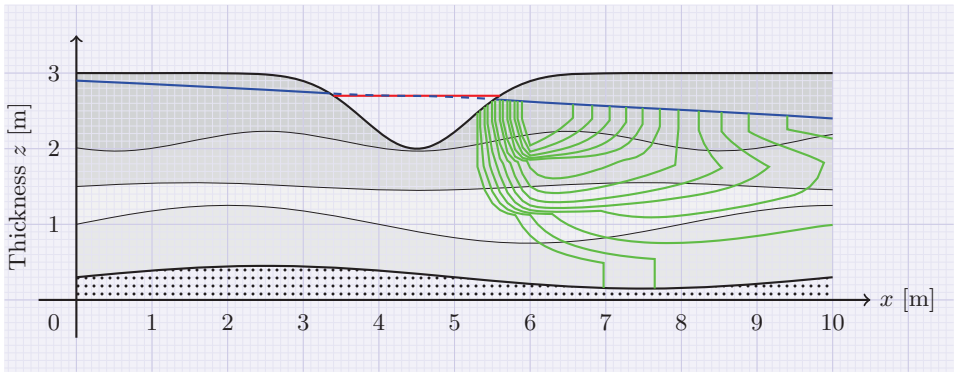

Figure 6.5: The concentration of remediating agent in the layered phreatic aquifer with a transverse running contaminated stream at the top. The remediating agent is being released steadily at $x = 6$ [m] with a rate q_R. The contour levels are $10^{-2.5(0.2)-0.1}$ [kg m^{-3}].

The concentration of the remediating agent in the aquifer in this simulation as it

reacts with the pollutant, is shown in Figure 6.5. The remediating agent advects along with the background fluid flow, disperses in all directions and reacts with the pollutant to neutralize it and in this process the remediating agent is depleted as it is used up in this reaction.

6.4 Location of oxidizer release to achieve optimum remediation

Consider a confined aquifer of uniform thickness that is composed of three parallel layers of equal thicknesses (Figure 6.6) and where a layer of sand and gravel (permeability $K = 10^{-9}$ [m^2]) is sandwiched in two layers of clean sand ($K = 10^{-10}$ [m^2]) [7]. Here, only dispersive transfer of species occurs across the layer interfaces. Fluid speed in the middle layer is higher than that in the outer layers. Each layer is further discretized in five sub-layers for the model. An instantaneous pollutant release (1 [kg]) is made within a sub-layer in the transverse y-direction, as is shown with a red rectangle. The fluid volume flux per unit width of the whole aquifer is 10 [m^2 day^{-1}] here. The pollutant advects, disperses horizontally and vertically and as a result of this vertical dispersion, it enters into the more permeable middle layer. It advects with higher speed in the middle layer and some of it disperses vertically back into the top layer. The resultant pollutant concentration profile after 10 days is shown in the top plot of Figure 6.6. The scenario is simulated again when 1 kg mass of remediating agent is released 5 m downstream (shown as a green rectangle) in the same sub-layer after two days of pollutant release. The resultant concentration profiles of the pollutant and the remediating agent are shown in the bottom two plots of Figure 6.6, respectively. The concentrations in all three plots are contoured at an equally spaced logarithmic scale $10^{-4,-3.725,-3.450,\cdots,-0.150}$ [kg m^{-3}].

Figure 6.7 shows pollutant concentration profiles after 15 [days] of pollutant release when remediating agent is released at positions one sub-layer higher, one sub-layer lower, 2 [m] upstream and 2 [m] downstream from the previous position. The lengths and heights of the aquifer shown here are not drawn on the same scale. The contours in each graph of concentration are plotted on an equally spaced logarithmic scale $10^{-4,-3.725,-3.450,\cdots,-0.150}$ [kg m^{-3}]. The resultant mass of the pollutant alleviated, flowed out of the aquifer and still present in the aquifer is also shown in each case.

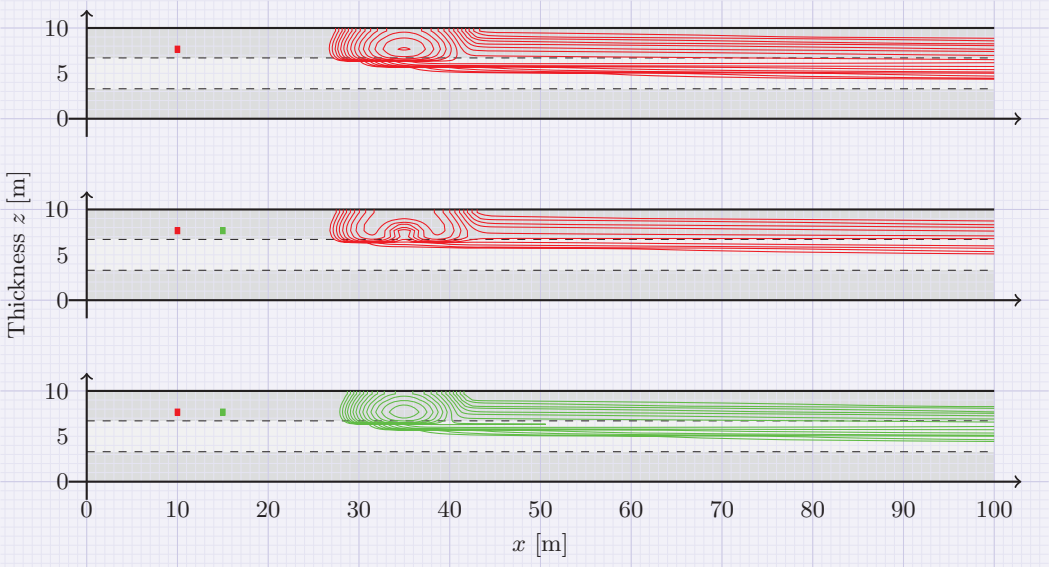

Figure 6.6: Concentration of solutes after 10 [days] of pollutant release at the position marked as a red rectangle. The remediation agent is injected downstream after 2 [days] of pollutant release at the position marked as a green rectangle. 1 Top: pollutant when there is no removal agent released, 2 Middle: pollutant when it is reacting with the remediating agent, 3 Bottom: remediating agent when it is reacting with the pollutant.

While, there is no easy way to clear all the released pollutant from the aquifer, a strategy could be devised to achieve maximum possible remediation. In this case, when the remediating agent is released two days after the release of pollution, the maximum remediation is obtained by injecting the remediating agent exactly at the centre of the plume of pollutant.

The upper plot in each of the simulations, shows total pollutant mass present in the aquifer (red), mass that is removed from the aquifer by the remediating agent (green) and the mass that has flowed out of the downstream boundary of the aquifer (blue), all plotted against time. In each case, the sum of all these masses is equal to the released mass (1 [kg]) of the pollutant. The lower of the pair of plots in the upper right corner of the Figure 6.7 shows the concentration of pollutant when there was no remediating agent released and the upper one is a plot for the total pollutant mass in the aquifer and mass that has flowed out of the downstream boundary both plotted against time. Their sum is also equal to the total injected mass of the pollutant.

While the optimum point for maximum remediation in continuous pollutant injec-

tion case is exactly where the pollutant is injected, it needs to be determined for the case of instantaneous pollutant injection. In time-dependant instantaneous case, it is always where the pollutant has maximum concentration at that time. This can be determined by numerical solution of the pollutant transport problem for general (real) aquifers.

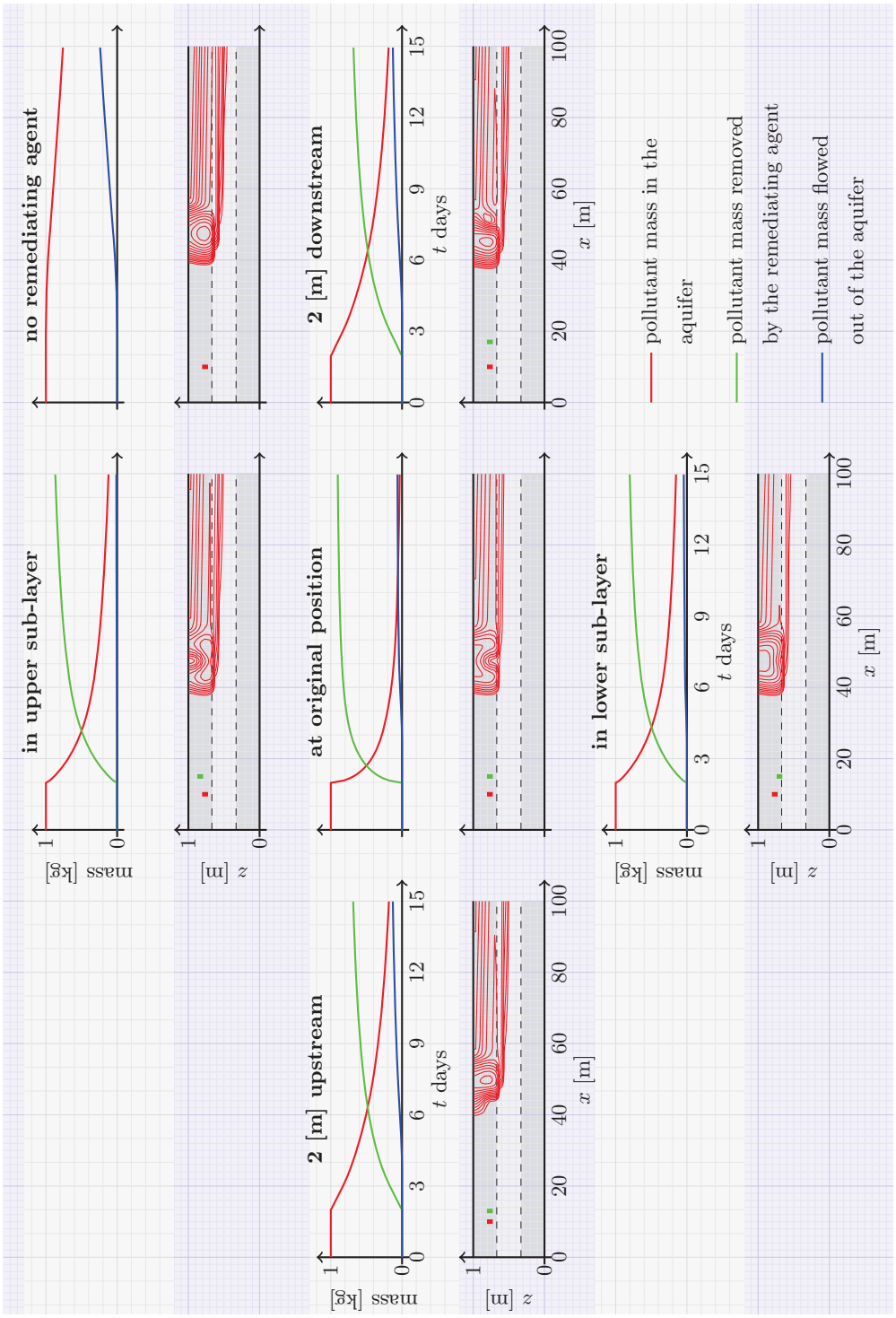

Figure 6.7: A comparison of the remediating effect when remediating agent is injected after two days of pollutant release at the different positions indicated by green rectangles in each case.

7

Summary and Discussion

7.1 Summary

In this thesis, some simplified models have been presented for predicting pollutant concentration transported by groundwater flow within homogeneous or layered aquifers. The vertical discretization based on the natural layering of the geological structures simplifies the problem from a full-scale three-dimensional modelling of fluid flow and transport in each sub-layer to their two-dimensional averages. By solving fluid flow and transport models in each of the sub-layers and by matching the transfers at the sub-layer interfaces, the three-dimensional naturally-discretized (simplified) models have been developed. The models can be used for any layered three-dimensional aquifer. The examples presented were chosen to be two-dimensional for better demonstration purpose.

Even if the sub-layers are not well defined, the aquifer can still be discretized vertically in the best possible way so that physical properties in each of the sub-layers do not vary extensively in the vertical direction at each horizontal point.

Fluid flow models presented in this thesis for both the confined and unconfined aquifers are based on the assumptions:

- The lateral extent of the aquifer is much larger than the thicknesses of sub-layers.
- The groundwater is single-phase(liquid) and at low pressure and temperature.
- The slopes of sub-layer interfaces are not extreme.

- The groundwater is incompressible and isothermal.
- The groundwater flow is steady.
- The porous media is rigid and non-deformable over time.
- The scale of modelling is large so that small scale factors such as wettability, capillary action, etc., are negligible.

The scope of this thesis is to exploit natural layering of the geological structures for vertical discretization. The horizontal extent of the aquifers is generally much larger than the thicknesses of the sublayers. The thesis deals with shallow water aquifers, where water is under low pressure and they are not very hot. Thus the water is generally in liquid phase only. Also, in such conditions, the assumption of incompressibility is also practical. The aquifers are usually located over a scale of kilometres, therefore, the effects of wettability and capillary action are also practically negligible.

It is convenient to use hydraulic head $\bar{H}$ instead of mean dynamic pressure in phreatic aquifers. The groundwater flow models for the aquifers where dominant flow is horizontal, i.e., where there is no fluid injection or withdrawal in one of the sub-layers, etc., assume a constant mean dynamic pressure $\bar{P}$ or hydraulic head $\bar{H}$ with an error which is of the order of square of sub-layer interface slopes. If withdrawal or injection is in all the sub-layers of the aquifer at one horizontal point, then the $\bar{P}$ or $\bar{H}$ will still be assumed constant vertically with the same error.

For the aquifers where injection or withdrawal is in one of the sub-layers of the aquifer, the $\bar{P}$ or $\bar{H}$ may be assumed different in each sub-layer of the aquifer. The system of coupled PDE's in $\bar{P}_i$ or $\bar{H}_i$ can then be solved with suitable boundary conditions.

The transport models presented in this thesis are based on the following assumptions:

- The tracer or pollutant is dissolvable, and it has negligible adsorption properties.
- The slopes of the sub-layer interfaces in the aquifer are small.

The presented remediation models are for the remediation strategy called In Situ Chemical Oxidation (ISCO) and the reaction between the pollutant and the remediating agent is of second order here. The exact order depends on the nature of chemicals

involved in the reaction. Similarly, the removal rates of the pollutant and the remediating agent used are only for illustrative purposes.

7.2 Further research

Some suggestions for future research following this thesis include:

- Include transient groundwater flow and extend the idea of simplified modelling based on naturally-layered aquifers to include more effects, such as storativity of the aquifer, specific storage of the aquifer, adsorption of pollutant, etc.
- To devise a strategy for predicting the layered structure of the aquifer by reading tracer/pollutant break through curve at the downstream.
- To model multi-phase transient fluid flows and reactive and sorptive solute transport. In this case, the permeability of the solid matrix should also change.
- To develop the model of an ISCO remediation strategy in transient and multi-phase fluid flows.

7.3 Publications and presentations

The author has presented material from this thesis st a number of conferences, and was recipient of the best paper presenter prize at IIMS Postgraduate Students' Conference, Massey University, Auckland, twice in 2010 and 2011. Some material from this thesis has been published in different conference proceedings ([3], [2], [4], [6],[5]).

References

[1] Brian Adams, Roger Calow, John Chilton, Ben Klinck, Adrian Lawrence, Brian Morris, and Nick Robins. Groundwater and its susceptibility to degradation: A global assessment of the problem and options for management. Technical Report Early Warning and Assessment Report Series, RS. 03-3, United Nations Environment Programme, Nairobi, Kenya, June 2003. 1

[2] Amjad Ali, Robert McKibbin, and Winston L. Sweatman. Fluid flow and solute transport in unevenly-stratified ground-water aquifers. In Kambiz Vafai, editor, *Proceedings of Porous Media and its Applications in Science, Engineering, and Industry, Fourth International Conference (ICPM4), Potsdam, Germany, June 17–22, 2012*, volume 1453, pages 11–16. American Institute of Physics, 2012. 2, 12, 103

[3] Amjad Ali, Robert McKibbin, and Winston L. Sweatman. Simplified modelling of pollutant transport in stratified groundwater aquifers. In R. Seppelt, A.A. Voinov, S. Lange, and D. Bankamp, editors, *Proceedings of International Environmental Modelling and Software Society (iEMSs) 2012 International Congress on Environmental Modelling and Software Managing Resources of a Limited Planet, Sixth Biennial Meeting, Leipzig, Germany*, pages 2739–2746, 2012. 2, 12, 103

[4] Amjad Ali, Robert McKibbin, and Winston L. Sweatman. Tracer transport: Appearing or disappearing sub-layer in a groundwater aquifer. In Gordon Mallinson, editor, *Proceedings of The 23rd International Symposium on Transport Phenomena, The University of Auckland, New Zealand, 19-22 November, 2012*, 2012. 2, 12, 38, 103

[5] Amjad Ali, Robert McKibbin, and Winston L. Sweatman. A simplified model for transport in aquifers. In Kambiz Vafai, editor, *Proceedings of the 5th International Conference on Porous media and its Applications in Science and Engineering (ICPM5), June 22-27, 2014, Kona, Hawaii*, 2014. 2, 12, 103

[6] Amjad Ali, Winston L. Sweatman, and Robert McKibbin. Pollutant transport and its alleviation in groundwater aquifers. In Magnus Fontes, Michael Günther, and Nicole Marheineke, editors, *Proceedings of Progress in Industrial Mathematics at ECMI 2012, Mathematics in Industry*, volume 19. Springer Berlin Heidelberg, 2012. 2, 12, 103

[7] Amjad Ali, Winston L. Sweatman, and Robert McKibbin. Pollutant transport and remediation in layered groundwater aquifers. Poster from New Zealand Mathematical Society Colloquium, Massey University, Palmerston North, 2012. 96

[8] Mary P. Anderson. Movement of contaminants in groundwater: Groundwater transport – advection and dispersion. In *Groundwater Contamination*, chapter 2, pages 37 – 45. National Academy Press, Washington D. C., 1984. 11

[9] Mary P. Anderson and John A. Cherry. Using models to simulate the movement of contaminants through groundwater flow systems. *C R C Critical Reviews in Environmental Control*, 9(2):97–156, 1979. 1

[10] George E. Andrews, Richard Askey, and Ranjan Roy. *Special Functions*. Cambridge University Press, United Kingdom, 1999. 65

[11] Jacob Bear. *Dynamics of fluid in porous media*. Dover, New York, 1972. 1, 7, 9, 57

[12] Jacob Bear and Yehuda Bachmat. *Introduction to modeling of transport phenomena in porous media*. Kluwer, Dordrecht, Holland, 1991. 7, 57

[13] Jacob Bear and Arnold Verruijt. *Modeling Groundwater flow and pollution*. D. Reidel, Dordrecht, Holland, 1978. 1, 10, 11, 32, 57

[14] Miroslav Černik, Kurt Barmettler, Daniel Grolimund, Werner Rohr, Michal Borkovec, and Hans Sticher. Cation transport in natural porous media on laboratory scale: multicomponent effects. *Journal of Contaminant Hydrology*, 16:319–337, 1994. 12

[15] Scott D. Cunningham and William R. Berti. Remediation of contaminated soils with green plants: An overview. *In Vitro Cellular Developmental Biology*, 29:207–212, October 1993. 85

[16] Henry P. G. Darcy. Les fontaines publiques de la ville de dijon. Technical report, Victor Dalmont, Paris, 1856. 7

[17] Jules Dupuit. *Estudes Thèoriques et Pratiques sur le mouvement des Eaux dans les canaux dècouverts et à travers les terrains permèables*. Dunod, Paris, 2nd edition, 1863. 10

[18] David L. Freyberg. A natural gradient experiment on solute transport in a sand aquifer: 2. Spatial moments and the advection and dispersion of nonreactive tracers. *Water Resources Research*, 22:2031–2046, December 1986. 83

[19] Ronald N. Horne and Fernando Rodriguez. Dispersion in tracer flow in fractured geothermal systems. *Geophys. Res. Lett.*, 10(4):289–292, 1983. 11

[20] C. M. Kao, K. D. Huang, J. Y. Wang, T. Y. Chen, and H. Y. Chien. Application of potassium permanganate as an oxidant for in situ oxidation of trichloroethylene-contaminated groundwater: A laboratory and kinetics study. *Journal of Hazardous Materials*, 153:919–927, 2008. 86

[21] Joseph Kestin, Mordechai Sokolov, and William A. Wakeham. Viscosity of liquid water in the range -8°C to 150°C. *J. Phys. Chem. Ref. Data*, 7(3):941–948, 1978. 9

[22] D. M. Mackay, D. L. Freyberg, P. V Roberts, and J. A. Cherry. A natural gradient experiment on solute transport in a sand aquifer: 1. Approach and overview of plume movement. *Water Resources Research*, 22:2017–2029, December 1986. 83, 84

[23] L. K. MacKinnon and N. R. Thomson. Laboratory-scale in situ chemical oxidation of a perchloroethylene pool using permanganate. *Journal of Contaminant Hydrology*, 56:49–74, May 2002. 86

[24] Robert McKibbin. Groundwater pollutant transport: transforming layered models to dynamical systems. *An. St. Univ. Ovidius Constanta, Ser. Mat*, 17(3):183–196, October 2009. 2, 11, 12

[25] Robert McKibbin. Some aspects of modelling pollution transport in groundwater aquifers. In L. H. Weiranto and S.R. Pudjaprasetya, editors, *Proceedings of CIAM 2010, Conference on Industrial and Applied Mathematics 6-8 July 2010, Institut Teknologi Bandung, Indonesia*, 2010. 2, 11, 12, 53, 54, 58

[26] Karsten Pruess. TOUGH: Suite of simulators for nonisothermal multiphase flow and transport in fractured porous media. `http://esd.lbl.gov/research/projects/tough/`, 1983. 2

[27] A. Raoof, H. M. Nick, S. M. Hassanizadeh, and C. J. Spiers. PoreFlow: A complex pore-network model for simulation of reactive transport in variably saturated porous media. *Coumputers & Geosciences*, 61:160–174, December 2013. 2

[28] Marta Scott and Carl Hanson. Risk maps of nitrate in Canterbury groundwater. Technical Report R13/44, Environment Canterbury Regional Council, Christchurch, New Zealand, June 2013. 1

[29] Ioannis P Stavroulakis and Stepan A Tersian. *Partial Differential Equations*. World Scientific Publishing Co. Pte. Ltd., Singapore, second edition, 2004. 55, 64

[30] Onno A. van Herwaarden. Spread of pollution by dispersive groundwater flow. *SIAM Journal of Applied Mathematics*, 54(1):26–41, 1994. 11

[31] Trevor Webb, Allan Hewitt, Linda Lilburne, Malcolm McLeod, and Murray Close. Mapping of vulnerability of nitrate and phosphorus leaching, microbial bypass flow, and soil runoff potential for two areas of Canterbury. Technical Report R10/125, Environment Canterbury Regional Council, Christchurch, New Zealand, June 2010. 1

[32] Warren W. Wood. A geochemical method of determining dispersivity in regional groundwater systems. *Journal of Hydrology*, 54:209–224, 1981. 12

[33] P. Wycisk, H. Weiss, A. Kaschl, S. Heidrich, and K. Sommerwerk. Groundwater pollution and remediation options for multisource contaminated aquifers (bitterfeld/wolfen, germany). *Texicology Letters*, 140-141:343–351, 2003. 85